LAPPEENRANTA-LAHTI UNIVERSITY OF TECHNOLOGY
School of Energy Systems
Degree Programme in Electrical Engineering

Pietu Kinnunen

IMPACT OF GRID CODE ON DESIGN OF A DIRECTLY GRID-CONNECTED PERMANENT MAGNET GENERATOR

Examiners: Professor Juha Pyrhönen
D.Sc. Asko Parviainen

ABSTRACT

Lappeenranta-Lahti University of Technology
LUT School of Energy Systems
Electrical Engineering

Pietu Kinnunen
Impact of grid code on design of a directly grid-connected permanent magnet generator
Master's thesis.
26.2.2021
97 pages, 39 figures, 14 tables and 2 appendices

Examiners: Professor Juha Pyrhönen
D.Sc. Asko Parviainen

Keywords: direct-on-line, electrical machine design, generator, grid code, hydropower, permanent magnet, simulation

In this thesis the design characteristics of a direct-on-line (DOL) permanent magnet synchronous generator (PMSG) are investigated with respect to the European Union Commission Regulation (EU) 2016/631. The design characteristics are described by lumped parameters which can be regarded as a guideline or a goal for machine design. An overview of the Regulation is given, requirements that potentially cause constraints for the design are identified and necessary simulation scenarios are sorted out. A suitable simulation tool is created using MATLAB® and Simulink® and validated by reproducing the current waveform obtained from an incident in which a permanent magnet generator was connected to the grid in a phase opposition. The main results of this thesis are produced by simulations based on the findings in the overview of the Regulation.

It was found out that the voltage control requirements largely limit the practical usability of DOL PMSGs to the powerplant category B and below. The most interesting issue in the Regulation was identified as the fault-ride-through (FRT) requirement which states that generators in categories B, C and D should be capable of remaining grid connected and retaining synchronism in a specific type of fault. It was considered that the FRT capability would be beneficial also in category A. The fault-ride-through scenario was simulated repeatedly while varying the machine parameters and it was inspected whether the synchronism could be restored or not. Three different reference machines were included in the study. The sensitivity of the FRT performance to the different parameters was evaluated and suitable ranges for the parameters and general trends in the effects of the parameters were searched. It was found out that with a DOL PMSG it seems very difficult to achieve the FRT performance according to the regulation without a temporary pole slip. However, restoring synchronism is still possible because of the damper winding. Based on the simulations, assuming that the temporary pole slip can be tolerated, it was concluded that the most effective ways to improve the probability of restoring synchronism in the event of FRT with a DOL PMSG are minimizing the stator leakage inductance and focusing on finding optimal values for the damper winding resistances. Also, minimizing the damper winding leakage inductances is beneficial and inverse saliency may be preferred.

TIIVISTELMÄ

Lappeenrannan-Lahden teknillinen yliopisto
LUT School of Energy Systems
Sähkötekniikka

Pietu Kinnunen
Verkkosääntöjen vaikutus suoraan verkkoon liitetyn kestomagneettitahtigeneraattorin suunnitteluun
Diplomityö
26.2.2021
97 sivua, 39 kuvaa, 14 taulukkoa ja 2 liitettä

Tarkastajat: Professori Juha Pyrhönen
TkT Asko Parviainen

Hakusanat: generaattori, kestomagneetti, simulaatio, suoraan verkkoon liitetty, sähkökoneen suunnittelu, verkkosääntö, vesivoima

Diplomityössä tarkastellaan suoraan verkkoon liitettävän kestomagneettitahtigeneraattorin suunnittelulähtökohtia verraten asetukseen (EU) 2016/631. Suunnittelulähtökohtia edustavat tässä työssä sijaiskytkennän parametrit, joita voidaan pitää ohjeistavana tavoitteena koneen suunnittelussa. Työssä tehdään yleiskatsaus asetukseen, eritellään asetuksen vaatimukset, jotka voivat aiheuttaa rajoitteita koneen suunnitteluun ja selvitetään tarvittavat simulaatioskenaariot. Tarvittaviin simulaatioihin sopiva työkalu luodaan MATLAB®- ja Simulink®-ympäristössä ja validoidaan jäljentämällä virran aaltomuoto, joka oli mitattu tapauksessa, jossa generaattori kytkettiin verkkoon vaiheoppositiossa. Työn päätulokset on tuotettu simulaatioilla, jotka perustuvat asetuksesta tehtyihin havaintoihin.

Asetuksen yleiskatsauksessa todettiin, että jännitteensäätövaatimukset rajoittavat suoraan verkkoon liitettävien kestomagneettigeneraattorien soveltuvuuden käytännössä katsoen voimalaitosluokkaan B ja sen alapuolelle. Asetuksen kiinnostavimmaksi vaatimukseksi katsottiin lähivikakestoisuusvaatimus (vian läpiajo), jonka mukaan generaattorien luokissa B, C ja D tulee pystyä pysymään liitettynä verkkoon ja säilyttämään tahtikäyttö asetuksessa määritellyn kaltaisen vian ilmetessä. Lähivikakestoisuutta voidaan pitää hyödyllisenä myös luokassa A. Vian läpiajoa simuloitiin toistuvasti samalla muuttaen koneen parametrejä ja tarkastettiin, pystytäänkö tahtikäyttö palauttamaan vai ei. Tutkimuksessa käytettiin kolmea erilaista referenssikonetta. Vian läpiajon suorituskyvyn herkkyyttä eri parametreihin arvioitiin ja etsittiin soveltuvia vaihteluvälejä parametreille sekä yleisiä suuntauksia liittyen parametrien vaikutuksiin. Simulaatioista selvisi, että asetuksen mukaisen lähivikakestoisuuden saavuttaminen suoraan verkkoon liitettävällä kestomagneettigeneraattorilla vaikuttaa olevan hyvin haastavaa ilman hetkellistä navan luiskahdusta. Tahtikäytön palauttaminen on kuitenkin mahdollista vaimennuskäämityksen ansiosta. Työn johtopäätöksenä todettiin simulaatioihin perustuen, että tehokkaimmat keinot tahtikäytön palauttamiseksi vian läpiajossa ovat staattorin hajainduktanssin minimointi ja keskittyminen optimaalisten vaimennuskäämityksen resistanssiarvojen etsimiseen olettaen, että hetkellinen navan luiskahdus voidaan sietää. Myös vaimennuskäämityksen hajainduktanssien minimointi on hyödyllistä ja käänteinen tahti-induktanssisuhde voi olla eduksi.

TABLE OF CONTENTS

LIST OF SYMBOLS AND ABBREVIATIONS

A	cross sectional area, linear current density
$\boldsymbol{B}$	magnetic flux density
$\boldsymbol{D}$	electric flux density
D	friction coefficient
E	electromotive force, energy
$\boldsymbol{E}$	electric field strength
$\boldsymbol{F}$	force
f	frequency
H	inertia constant
$\boldsymbol{H}$	magnetic field strength
$\boldsymbol{I}^*$	complex conjugate of current
I	current
i_s''	sub-transient short circuit current
J	moment of inertia
$\boldsymbol{J}$	current density
K	stiffness coefficient
k	thermal exponent scale factor, time parameter scale factor, winding factor
L	inductance
l	length
l'	equivalent length
m	number of phases
N	number of turns
n	rotational speed
$\boldsymbol{n}$	unit vector
P	active power
p	number of pole pairs
Q	charge, reactive power
R	resistance
r	radius
S	apparent power, surface area
T	temperature, torque
t	time

U	voltage
$\overleftrightarrow{\boldsymbol{T}}$	Maxwell stress tensor
V	volume
X	symbol for a variable in general, reactance
X_{d}''	sub-transient reactance
X_{d}'	transient reactance
Z	impedance

α	temperature coefficient
γ	angle between magnetizing current and d-axis
δ	Kroneker delta function, load-angle
ε	permittivity
θ	rotor position angle
μ	permability
ρ	electrical resistivity
σ	conductivity
σ_{F}	stress
τ	relative time
τ''	sub-transient time constant
Φ	magnetic flux
φ	phase angle difference of current and voltage
ψ	flux linkage
Ω	mechanical angular velocity
ω	angular velocity

ACER	Agency for the Cooperation of Energy Regulators
AC	alternating current
DOL	direct-on-line
DC	direct current
DSO	distribution system operator
EESM	electrically excited synchronous machine
ENTSO-E	European Network of Transmission System Operators
EU	European Union

FC	frequency converter
FEA	finite element analysis
FEM	finite element method
FRT	fault ride through
FSM	frequency sensitive mode
HESM	hybrid excited permanent magnet synchronous machine
IEC	International Electrotechnical Commission
IEEE	Institute of Electrical and Electronics Engineers
IEA	International Energy Agency
IM	induction machine
LFSM-O	limited frequency sensitive mode – overfrequency
LFSM-U	limited frequency sensitive mode – underfrequency
PCC	point of common coupling
PID	proportional-integral-derivative
PM	permanent magnet
PMSM	permanent magnet synchronous machine
PMSG	permanent magnet synchronous generator
PPM	power park module
PSH	pumped-storage hydropower
pu.	per unit
PV	photovoltaic
PWM	pulse width modulation
RoCoF	rate of change of frequency
SM	synchronous machine
TSO	transmission system operator
VLH	very low head
VSD	variable speed drive

Subscripts

b	base
c	coupling
D	direct axis damper winding
d	direct axis
e	electromagnetic

g	generator
i	index of array, index of summation
k	kinetic, short circuit
n	column index, nominal, normal, rated,
m	magnetization. row index
Q	quadrature axis damper winding
q	quadrature axis
r	rotor
t	turbine
s	stator, synchronous
w	winding
x	x-axis
y	y-axis
z	z-axis

σ	leakage

AC	alternating current
Al	aluminium
Cu	copper
DC	direct current
LL	line-to-line
mech	mechanical
min	minimum
ph	phase
PM	permanent magnet
pu.	per unit
rec	recovery
res	resonance
ret	retained
run	runaway
sh	shaft
ssc	sustained short circuit
tan	tangential

th	thermal
tot	total
turb	turbine
0	initial, vacuum, zero-sequence

1. INTRODUCTION

New generators installed in EU countries must fulfil the European Union Commission Regulation (EU) 2016/631 and derived national regulations such as VJV2018 in Finland, which establish a network code on requirements for the grid connection of generators. The operation of a new powerplant versus regulation requirements must be validated with appropriate simulations before grid connection is allowed. In this thesis the design characteristics of direct-on-line (DOL) permanent magnet synchronous machines (PMSM) intended for small scale (≤ 10 MW) hydropower are investigated with respect to the Regulation.

1.1 Objectives, research methods and structure of the thesis

The target of the thesis is to give an overview of the Regulation (EU) 2016/631, derive machine design criteria based on the regulation and develop a related simulation tool that can be used to demonstrate a given machine performance. Regarding the design criteria, especially damper winding parameters are of interest as the damper winding has a rather decisive impact on the transient behaviour of a machine.

PMSM designs in general are obviously already quite widely studied. However, the DOL permanent magnet synchronous generators (PMSG) in particular, are not very common and more research results about their performance and behaviour are desirable. Also, the Regulation (EU) 2016/631 is quite new and it should be investigated with respect to the product validation and possible product refinement needs. Providing the simulation results and design criteria form most of the scientific contribution of this thesis.

Firstly, the role of hydropower in modern electric power systems is evaluated briefly and the status of electric drives and machines in hydropower is discussed. The working principle and construction of the radial-flux inner-rotor PMSM are introduced, and the fundamentals of torque production are studied to give perspective to the modelling approach and the analysis of the simulations. Secondly, an overview of the Regulation (EU) 2016/631 is given. Requirements that potentially cause constraints for the DOL PMSG design are identified and necessary simulation scenarios are sorted out. Thirdly, a suitable simulation tool is made with MATLAB® and Simulink®, validated and demonstrated with scenarios based on the findings in the Regulation overview. Possible ranges and optimal values for the parameters and general trends are searched for with the simulations. The effects of the machine design

characteristics on the machine performance in the simulations are discussed along with a parameter sensitivity analysis.

1.2 Electrical machines and drives in hydropower as part of electric power systems

Most of electricity is generated by using direct-on-line generators even though their share is decreasing because more and more variable speed drives (VSD) are applied and because of the rapidly emerging PV-energy. Figure 1.1 shows the worldwide electricity generation capacity in 2000-2020 and IEA's Stated Policies Scenario prediction in 2020-2040, which tries to illustrate what are the consequences of today's policy intentions that have been announced (IEA, 2019).

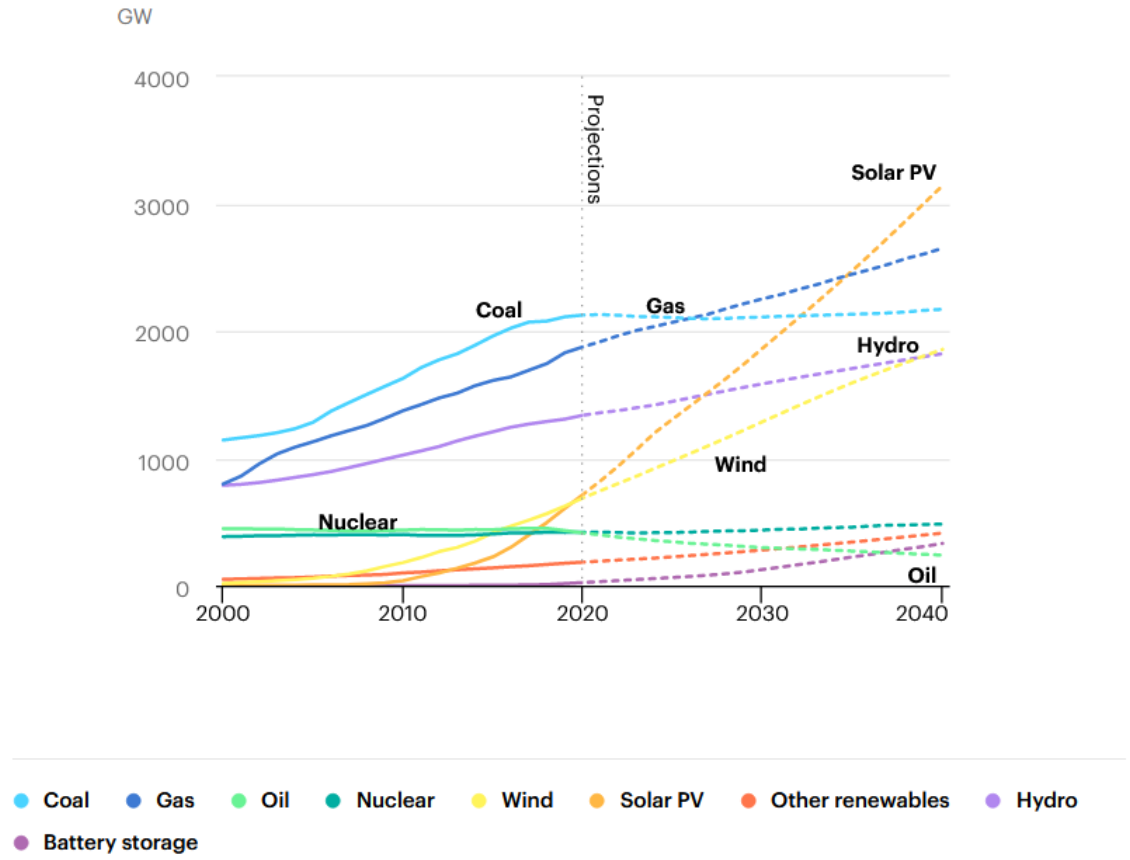

Figure 1.1 Installed electric power generation capacity by energy source and IEA's Stated Policies Scenario predictions, 2000-2040 (adapted from IEA, 2019).

It can be seen in figure that solar PV and wind are predicted to have a major share of electricity production in the future. This bodes challenges to grid frequency stability not only because of uneven production of wind and solar, but also because of lack of synchronous inertia. In the power grid, generation and load must be equal within hundreds of millisec-

onds. Otherwise, the rotational speed of the connected generators and thus also the grid frequency will fluctuate as the rotational energy of the system is changed. This can be illustrated as follow: The rotational kinetic energy E_K is generally given as

$$E_\mathrm{k} = \frac{1}{2} J \Omega^2, \tag{1.1}$$

where J is the moment of inertia of the synchronous machine and Ω the mechanical angular velocity. The dynamic behaviour of the machine when the damping is neglected, can be described as

$$J \frac{\mathrm{d}\Omega}{\mathrm{d}t} = \sum T = T_\mathrm{mech} + T_\mathrm{em}, \tag{1.2}$$

where T_mech and T_em are the mechanical and electromagnetic torques applied to the shaft. Here the angular velocity and the torques can be treated similarly as scalars as they have two possible directions which are opposing each other. The kinetic rotational power is

$$P_\mathrm{k} = \Omega T \tag{1.3}$$

so, the relation between power unbalance and angular acceleration can be seen by multiplying equation (1.2) with Ω. When losses are neglected it is obtained that

$$J \Omega \frac{\mathrm{d}\Omega}{\mathrm{d}t} = P_\mathrm{mech} - P_\mathrm{e}, \tag{1.4}$$

where P_mech is the mechanical power and P_e the electrical power. This can be further developed by introducing an inertia constant H defined by the rotational energy E_k and apparent power of the generator S_g as

$$H\ [\mathrm{Ws/VA}] = \frac{E_\mathrm{k}}{S_\mathrm{g}}, \tag{1.5}$$

which is in aggregated systems

$$H_\mathrm{sys} = \frac{\sum_i H_i S_{\mathrm{g},i}}{\sum_i S_{\mathrm{g},i}}. \tag{1.6}$$

Substituting equations (1.1) and (1.5) to equation (1.4), a per-unit presentation is obtained:

$$\frac{2H}{\Omega} \frac{\mathrm{d}\Omega}{\mathrm{d}t} = P_\mathrm{mech,p.u} - P_\mathrm{e,p.u}. \tag{1.7}$$

The system rate of change of frequency (*RoCoF*) depends on the inertia and the power difference as follows

$$RoCoF\ [\mathrm{Hz/s}] = \frac{\Delta P_{\mathrm{p.u}} f_{\mathrm{s}}}{2H_{\mathrm{sys}}}, \tag{1.8}$$

$$[\mathrm{Hz/s}] = \frac{\left[\frac{\mathrm{W}}{\mathrm{VA}}\right]\cdot[\mathrm{Hz}]}{\left[\frac{\mathrm{Ws}}{\mathrm{VA}}\right]}, \tag{1.9}$$

where f_{s} is the nominal electrical frequency. Non-synchronous power plants or storages do not inherently contribute to the grid inertia, but the inertial response of a synchronous powerplant can still be emulated via a control mode called synthetic inertia. However, the synthetic inertia requires a grid frequency measurement and some processing time to react to the grid frequency changes. The control loop delay is typically around a few tens of milliseconds (Chown G. et al., 2017). When there is an unbalance in power between generation and load, the *RoCoF* can be very high during the reaction time if there are only few synchronous generators, and therefore low inertia, in the grid. (Peltoniemi P., 2017), (Zaidi A. & Cheng Q., 2018)

Hydropower is a renewable energy source that does not suffer from the frequency stability related issues similarly as wind and solar because the power input can be controlled with the water flow rate without losing energy resources to some extent depending on the powerplant type and the reservoir size. Moreover, if the generator is directly grid connected, it provides synchronous inertia to the grid. Hydropower plants also have a possibility to be used as energy storages depending on the water reservoir type and plant official licensing. In pumped-storage hydropower (PSH) plants excess solar and wind energy can be stored in the potential energy of the water by pumping water from the downstream outlet back to the reservoir. Furthermore, DOL permanent magnet synchronous machine hydropower plants are potential candidates to be designed to have a black start functionality as no electricity is needed for a converter or magnetization. However, grid forming often requires voltage control capability, which the DOL PMSM does not offer inherently. Although, if relatively large voltage variation (e.g. 80 … 120 %) is temporarily allowed, a PM generator may alone create an island grid if its prime mover is speed controlled. Power plants with black start capabilities are necessary when considering grid power restoration after a black-out. Therefore, a black start readiness should be regarded as a value adding feature as black start services are usually recognized by grid operator tariffs. (Koritarov V. et al., 2014)

The biggest disadvantage of hydropower is the local environmental damage, especially to river ecosystems because e.g. functional fish ladders have often been avoided in building the

dam. On the other hand, hydropower can be helpful in a flood mitigation. Another disadvantage is the rainfall dependency of the resource availability resulting in different annual availability of hydro power. In addition, in many cases the flow rate during flood times e.g. in Finland in spring times when snow is melting may cause the mean maximum flow (MHQ) to be very large compared to the mean flow (MQ). Dimensioning of the turbine system may therefore be difficult. The advantages are still often considered to overweight the disadvantages and therefore it is likely that hydropower retains its significant role in electricity production also in the future while moving towards a carbon neutral energy sector. However, the fish-ladder problem needs a generally acceptable and economic enough solution. Other alternatives include utilization of novel technologies such as very-low-head (VLH) turbines or two-sided Archimedes screws to enable fish passage through powerplant. However, economical feasibility of such systems is limited. In Europe, the growth of hydropower is somewhat limited by the fact that the majority of potential capacity has already been utilized. That said, there is still some new installation potential left and a significant part of the growth comes from the improved energy efficiency as a result of modernisation of existing power plants. (Hydropower Europe, 2020)

Generators can be connected to the grid directly or using a four-quadrant power electronic converter first rectifying the generator power and then supplying the power to the network. The rotation speed of a synchronous electrical machine is defined as

$$n = \frac{f}{p}, \tag{1.10}$$

where f is the electrical frequency and p is the pole pair number. When directly connected, the machine operates on a fixed grid frequency, whereas by using a frequency converter (FC) the frequency can be adjusted and therefore the speed can be easily controlled. Before the grid connection, the direct-on-line machine has to be synchronized to the grid frequency, while with the FC connection this is not necessary, as the machine is decoupled from the grid frequency via the DC-link of the converter.

Variable speed drives have become common also in electricity generation as a result of the development of modern power electronics. Some of the key benefits of VSDs compared to DOL generators are advanced active and reactive power control, simple and smooth start-up and process optimization capabilities, which can lead to an optimal overall efficiency.

However, the power-electronic four-guadrant drive system has a lower efficiency than a DOL-system at the rated point. The maximum efficiency of the four-guadrant frequency converter is in the range of 97 % and additional losses will be generated also in the generator when in PWM control. All in all, we can assume that there will be about 4 % unit lower energy gain in a VSD drive compared to a DOL drive when operating at the rated point. Therefore, a direct-on-line drive is a compelling choice in systems where one fixed speed is sufficient.

If an energy conversion system can operate optimally most of the time with a grid frequency, the converter only offers reduced efficiency at a significantly higher investment cost. A frequency converter has also potential to cause a system failure by failing itself or by introducing electromagnetic compatibility issues such as overvoltages and bearing currents (Korhonen J., 2012). Moreover, a frequency converter supplying power to the grid creates additional harmonic distortion to the grid voltage because of a pulse width modulation (PWM). Although, in fairness the harmonic distortion, frequency converter induced bearing currents and overvoltages can be mitigated by taking them into account in converter, control, filtering, cable and machine designs. Furthermore, with a clever control using a frequency converter, mechanical vibrations, which can for instance also cause bearing degradation, can be reduced.

Large power plants usually have a synchronous machine (SM) as a generator because an electrically excited synchronous machine (EESM) offers high power and good reactive power control capabilities as a result of controllable field winding current. In comparison, the major disadvantage of asynchronous generators is that they draw reactive magnetizing power from the grid unless a compensating device is used. The magnetization through the stator also means that a black start is not feasible and the capability of feeding fault current in a short circuit is poor. The efficiencies of a comparable induction machine and an EESM are typically in the same range. However, the efficiency of the EESM can be improved by replacing the field winding with permanent magnets which removes the losses created in electrical excitation. Additional benefit of a PMSM is a simple brushless construction. Therefore, a permanent magnet synchronous machine can be a very compelling machine type choice for small scale ($\leq$ 10 MW) hydropower. It should be noted though that the permanent magnet (PM) material can increase the cost compared to an electrical excitation, PM flux cannot be controlled and there is a risk of demagnetization. If reactive power control is

desired with a DOL PMSM, the use of separate compensator devices such as static synchronous compensators, capacitors, reactors and tap changing transformers is needed because of the uncontrollable magnetization. Therefore, the applicability is somewhat limited at high powers, where the reactive power control requirements are very prominent. Moreover, without strict space limitations a very large EESM efficiency can already approach 99 %, and in that case sacrificing the controllable field excitation for minimally better efficiency with potentially higher cost is usually not the best solution as a whole. If a top tier efficiency is still desired and controllable field excitation is needed, a less common hybrid excited permanent magnet synchronous machine (HESM) can be used (Kamiev K., 2013). The HESM aims to combine the benefits of EESM and PMSM but it also combines the disadvantages. The main drawback of the hybrid excitation is a high investment cost, especially if a brushless excitation is required.

Another advantage of the PMSM is that it is a well suitable machine type for a direct-drive technology. Typically, in low-head hydropower operation, the rotational speed of an electrical machine must be relatively low. To achieve a high power, therefore, a high torque is required. As shown in equation (1.9) a low speed requires a high pole pair number or a low electrical frequency. With a PMSM the number of poles can be designed high without major issues such as poor power factor because of low magnetizing inductance similarly as in the case of an induction machine (IM) or bulkiness in the case of a comparable EESM. A gearless drivetrain can reduce mechanical losses, improve controllability, possibly save space, and simplify the drive train, thus making it more reliable. However, a direct-drive machine needs to be larger for the sake of high torque than a higher speed counterpart with a speed reduction gear. Also, low-speed PM machine drives are prone to suffer from a considerable cogging torque, which causes potentially harmful vibration and speed fluctuation (Wu D. & Zhu Z., 2015). This set-back can be, however eliminated by implementing proper design features, such as skew and shaped rotor poles into machine electrical design.

To conclude, hydropower is an important renewable electrical energy resource especially from the grid reliability point of view when considering the grid integration of wind and solar power. Hydropower still has growth potential, and the permanent magnet synchronous machines are used when targeting maximum efficiency. Efficiency is a very significant factor in an investment in its entirety given that hydropower plants typically have a relatively

long lifetime, typically around 30-50 years. DOL synchronous generators still serve a purpose because of their synchronous inertia and in many cases, they can be more reliable and feasible in a techno-economical sense than a VSD. It should still be noted in a context of this thesis that the optimal electrical machine designs for DOL or frequency converter connection are not exactly the same. For example, with a DOL machine the damper winding is often essential and with an FC connection it can be even harmful.

1.3 Background physics of electromagnetic torque production

In this thesis, a simulation tool based on the lumped parameter model of a PMSM is created and the main results are based on the simulations carried out with the tool. It is useful to understand some of the related background physics so that the significance of the simplifications of the lumped parameter modelling can be evaluated at least to some extent.

Electromagnetic torque production and design of a rotating electrical machine are based on the Maxwell's equations, Lorentz force and constitutive relations. Fundamental general equations governing physical laws of classical electromagnetism were presented in a complete form in 1860's by James Maxwell. In modern literature the Maxwell's equations are typically written in differential form derived by Oliver Heaviside as

$$\nabla \times \boldsymbol{H} = \boldsymbol{J} + \frac{\partial \boldsymbol{D}}{\partial t}, \tag{1.11}$$

$$\nabla \times \boldsymbol{E} = -\frac{\partial \boldsymbol{B}}{\partial t}, \tag{1.12}$$

$$\nabla \cdot \boldsymbol{B} = 0, \tag{1.13}$$

$$\nabla \cdot \boldsymbol{D} = \rho, \tag{1.14}$$

and the force experienced by a charged particle Q [As] moving in electric and magnetic fields at a velocity $\boldsymbol{v}$ [m/s] is given in a form derived by Hendrik Lorentz as

$$\boldsymbol{F} = Q(\boldsymbol{E} + \boldsymbol{v} \times \boldsymbol{B}). \tag{1.15}$$

Equation (1.11) known as Ampére's law descibing how current density $\boldsymbol{J}$ [A/m^2] and changing electric flux density $\boldsymbol{D}$ [As/m^2] produce magnetic field around them is used to calculate magnetic potential differences and required current linkage for specific field strenght in a magnetic circuit. The displacement current term $\frac{\partial \boldsymbol{D}}{\partial t}$, which is Maxwell's contribution can usually be neglected at frequencies occuring in electrical machines.

Equation (1.12) known as Faraday's induction law states that a changing magnetic flux density creates an electric field $\boldsymbol{E}$ [V/m] around it. It is used to calcute induced voltages. Equation (1.13) is Gauss's law for magnetic field and it states that the divergence of magnetic flux density $\boldsymbol{B}$ [Vs/m^2] is zero, meaning that a magnetic flux forms always closed loops with no starting or end point. Equation (1.14) is Gauss's law for electric field and it states that an electric flux flows always from a positive charge to a negative charge. It can be used to calcute stresses in insulation. The Lorentz force (1.15) is the principle of force and torque production. (Pyrhönen J. et al., 2014)

To solve the Maxwell's equations in practical problems, constitutive relations and necessary boundary conditions are used. Also, the integral forms of the equations are often employed. The constitutive equations describing material properties are

$$\boldsymbol{D} = \varepsilon \boldsymbol{E}\,, \tag{1.16}$$

$$\boldsymbol{B} = \mu \boldsymbol{H}\,, \tag{1.17}$$

$$\boldsymbol{J} = \sigma \boldsymbol{E}\,, \tag{1.18}$$

where ε [As/(Vm)] is permittivity μ [Vs/(Am)] permeability and σ [1/(Ωm)] conductivity, which are not necessarily constants and not even scalars but may have different values in different directions in a material. In other words, the material properties can be tensorial in nature. Equation (1.18) is known as the Ohm's law in its microscopic form.

The Lorentz force is often not practical in complex problems as such, and therefore an equivalent method based on the Maxwell stress tensor is commonly used for the electromagnetic force calculation. The Maxwell stress tensor can be derived from the Lorentz force and the Maxwell's equations leading to its definition for magnetic fields written as (using index notation)

$$\overleftrightarrow{\boldsymbol{T}} = T_{\mathrm{mn}} = \frac{1}{\mu_0}\left(B_{\mathrm{m}}B_{\mathrm{n}} - \frac{1}{2}\delta_{\mathrm{mn}}B_k^2\right), \tag{1.19}$$

where subscripts m and n are row and column indices of the tensor, $B_k^2 = \sum_k B_k^2 = B_{\mathrm{x}}^2 + B_{\mathrm{y}}^2 + B_{\mathrm{z}}^2$ and δ_{mn} is the Kroneker delta function $\delta_{\mathrm{mn}} = 1$ if $\mathrm{m} = \mathrm{n}$ and $\delta_{\mathrm{mn}} = 0$ if $\mathrm{m} \neq \mathrm{n}$ (Woodson, H. and Melcher, J., 1968). Deriving the elements according to (1.20) yields a following matrix in cartesian xyz-coordinate system:

$$T_{\mathrm{mn}} = \frac{1}{\mu_0}\begin{bmatrix} T_{\mathrm{xx}} & T_{\mathrm{xy}} & T_{\mathrm{xz}} \\ T_{\mathrm{yx}} & T_{\mathrm{yy}} & T_{\mathrm{yz}} \\ T_{\mathrm{zx}} & T_{\mathrm{zy}} & T_{\mathrm{zz}} \end{bmatrix} = \frac{1}{\mu_0}\begin{bmatrix} B_{\mathrm{x}}^2 - \frac{B_k^2}{2} & B_{\mathrm{x}}B_{\mathrm{y}} & B_{\mathrm{x}}B_{\mathrm{z}} \\ B_{\mathrm{y}}B_{\mathrm{x}} & B_{\mathrm{y}}^2 - \frac{B_k^2}{2} & B_{\mathrm{y}}B_z \\ B_{\mathrm{z}}B_{\mathrm{x}} & B_{\mathrm{z}}B_{\mathrm{y}} & B_z^2 - \frac{B_k^2}{2} \end{bmatrix}, \tag{1.20}$$

where diagonal elements are pressure stress components and the others are shear stress components. If a rotor of an electrical machine is considered a cylinder coinciding with the *z*-axis and variations along the *z*-axis are ignored, the stress tensor can be simplified as

$$T_{\mathrm{mn}} = \frac{1}{\mu_0}(B_{\mathrm{m}}B_{\mathrm{n}} - \frac{1}{2}\delta_{\mathrm{mn}}B_k^2) = \frac{1}{\mu_0}(B_{\mathrm{m}}B_{\mathrm{n}} - \frac{1}{2}\delta_{\mathrm{mn}}({B_{\mathrm{x}}}^2 + {B_{\mathrm{y}}}^2), \tag{1.21}$$

$$= \frac{1}{\mu_0}\begin{bmatrix} B_{\mathrm{x}}^2 - \frac{{B_{\mathrm{x}}}^2+{B_{\mathrm{y}}}^2}{2} & B_{\mathrm{x}}B_{\mathrm{y}} & 0 \\ B_{\mathrm{y}}B_{\mathrm{x}} & B_{\mathrm{y}}^2 - \frac{{B_{\mathrm{x}}}^2+{B_{\mathrm{y}}}^2}{2} & 0 \\ 0 & 0 & -\frac{1}{2}({B_{\mathrm{x}}}^2 + {B_{\mathrm{y}}}^2) \end{bmatrix}$$

$$= \begin{bmatrix} \frac{1}{2}\mu_0({H_{\mathrm{x}}}^2 - {H_{\mathrm{y}}}^2) & \mu_0 H_{\mathrm{x}}H_{\mathrm{y}} & 0 \\ \mu_0 H_{\mathrm{x}}H_{\mathrm{y}} & \frac{1}{2}\mu_0({H_{\mathrm{y}}}^2 - {H_{\mathrm{x}}}^2) & 0 \\ 0 & 0 & -\frac{1}{2}\mu_0({H_{\mathrm{x}}}^2 + {H_{\mathrm{y}}}^2) \end{bmatrix}.$$

The total force on the rotor can be calculated in principle by integrating a product of the Maxwell stress tensor and an unit vector $\boldsymbol{n}$ normal to the surface along the rotor surface:

$$\boldsymbol{F} = \oiint_S \overleftrightarrow{\boldsymbol{T}} \cdot \boldsymbol{n}\mathrm{d}S, \tag{1.22}$$

where $\mathrm{d}S$ is a differential surface element (Woodson H. & Melcher J., 1968). The matrix-vector multiplication gives a vector of force per unit area on a surface with parallel and perpendicular components to the unit vector. Therefore, the integral over an area yields the total force. The tangential component of the force creates torque which could be calculated by adding a cross product of the lever arm, that is the rotor radius, to the integral.

In the case of equation (1.21), the axial component is always zero. The direction of the unit vector determines which component of the magnetic field strength is normal and which is tangential in the xyz-coordinate system and so the stress components can be expressed as:

$$\sigma_{F\mathrm{n}} = \frac{1}{2}\mu_0({H_{\mathrm{n}}}^2 - {H_{\mathrm{tan}}}^2), \tag{1.23}$$

$$\sigma_{F\mathrm{tan}} = \mu_0 H_{\mathrm{n}}H_{\mathrm{tan}} = B_{\mathrm{n}}A, \tag{1.24}$$

where A [A/m] is the linear current density. Using an average tangential stress on the rotor surafce a toque estimate is given as

$$T = \sigma_{F\tan} r_{\mathrm{r}} S_{\mathrm{r}} = \sigma_{F\tan} 2\pi r^2 l' = \sigma_{F\tan} 2V_{\mathrm{r}}, \tag{1.25}$$

where r_{r} is the rotor radius, S_{r} the roror surface area, l' the equivalent rotor length and V_{r} the rotor volume (Pyrhönen J. et al., 2014). The tangential stress can be used as a guideline for a machine size dimensioning for a desired torque. The flux density B_{n} in equation (1.24) is limited by the stator core material saturation or by the permanent magnet flux production capability, so the torque can be increased by increasing the rotor radius or the linear current density. An approximate efficiency goal can be taken into account with given frequency and pole pair number when evaluating the machine size as the linear current density is linked to the copper losses in the stator winding while the machine volume is linked to the iron losses, the copper losses being typically the most dominant source of losses in machines incorporating low line frequncy.

The Maxwell stress tensor force is suitable for numerical methods such as finite element analysis (FEA), where the integration is made over a flux solution of a meshed geometry. However, it should be recognized that the integration is sensitive to the field discontinuity at the boundary of the magnetized object when a surface is close to the object, and when a surafce is far from the object, numerical errors become larger (Freschi F. and Repetto M., 2013). Therefore, measures to mitigate the inaccuracies are necessary and it is also often worth ensuring that the results agree with analytical calculations. Alternatively to Maxwell stress tensor based methods, a Coulomb's virtual work could be utilized as a basis in FEA (Pyrhönen et al., 2014). In any case, the FEA can become quite laborious and computationally heavy. Therefore, it is not necessarily best suited for tasks such as determining suitable lumped parameter values through an extensive testing where a lighter dynamic model can produce useful information. The parameter values can be thought as a rough design goal. The FEA is most useful for example in refining and validating an analytical design, studying subtle topics such as air gap flux density harmonic content or in some cases substituting real-world tests if they are not possible or feasible.

1.4 PMSM working principle and basic construction

A synchronous machine consists of two main parts; a stator and a rotor with an airgap in between. The parts can be aligned axially or radially with the rotor being either the outer or

inner part. In the stator a rotating magnetic field is created most commonly with a three-phase winding. In an SM that is called an armature winding. The simplest three-phase winding that produces a rotating field can be made by placing three coils with a position diffenrce of 120° degrees in six stator slots so that the sides of each coil are on the opposite slots making the arrangement as evenly distributed as possible. When the winding is supplied with a sinusoidal three-phase voltage with an 120° phase shift, the created current density produces a magnetic field strength according to the Ampére's law, and its peak value travels around the periphery because each coil reaches its peak current density periodically one after the other as a function of time. This arrengement with six phase zones produces one pole pair. More pole pairs can be created by adding more phase zones, i.e. dividing the phase windings into sections and routing them for example so that there is 12 phase zones. This would produce two pole pairs and require 12 slots as a minimum. It is, however, common that each phase zone occupies more than one slot as that way the machine properties can be enchanced. Different stator winding topologies offer various and significant design optimization possibilities, for example in flux leakage optimization and minimizing harmonic distortion.

In the rotor the same number of pole pairs is created as in the stator, but with a stationary magnetic field. This can be achieved with a field winding supplied with direct current for example through slip rings and brushes or using permanent magnets. It should be noted though that a tooth-coil stator winding arrangement (number of slots per pole and phase < 0.5) can operate with different numbers of poles depending on the rotor pole pair number as far as the stator is capable of properly linking the air gap flux. As the north and south poles of the rotating stator field are aligned with the south and north poles of the stationary rotor field, the poles gets locked in a sense because even a slightest deviation from that alignment produces a tangential magnetic field strength component and therefore torque according to the Maxwell stress tensor force, and so the rotor starts to rotate in synchronism with the stator field. Mechanical forces are counteracting with the electromagnetic forces preventing the stator from collapsing or rotating. Because of the rotor inertia, synchronization is not possible if the stator field is rotating too fast, which can be the case in DOL machines. Self-synchronization is still achievable with a help of a damper winding which produces torque in a same principle as a squirrel cage rotor of an asynchronous machine. In fact, the damper winding is quite essential with salient pole SMs and PMSMs even if the machine is accelerated to the synchronous speed before grid connection as without suitable amount of

damping the machine would slip out of synchronism quite easily in DOL operation. Other conductive parts than actual damper bars in the rotor can also provide some damping as a result of induced eddy currents but that is often not enough.

The details of the machine construction obviously depend on the machine type and design choices, but some general basics of inner rotor radial flux machine are addressed next. The stator frame forms the body that supports the machine. It also provides ducting for cooling and acts as a heat dissipation surface. The frame can be made of cast iron, for example. The stator core provides magnetic path, cooling and support for the stator winding. It is made of highly permeable material that does not allow excessive eddy currents. Typically this is achieved with laminated silicon steel providing the magnetic flux a low reluctance path. The laminations effectively minimize eddy current losses. The silicon steel is a soft magnetic material, meaning it has a narrow hysteresis loop area, and therefore low hysteresis losses. The silicon also decreases conductivity which helps in mitigating eddy current losses. The eddy current and especially hysteresis losses in the rotor core are not as prominent as in the stator because there are no AC carrying windings, but the core may still be made of the same laminated silicon steel. In the case of a PMSM, the rotor provides support and cooling for permanent magnets which may be surface mounted or embedded using various possible topologies that offer different advantages. The magnets may be segmented to decrease the eddy currents in the magnets which improves efficiency and prevents permanent-magnet overheating. The magnets may also be skewed, which can reduce the airgap flux harmonic distortion but also increase flux leakages. The rotor can also be equipped with flux barriers creating saliency if the increase of reluctance torque is desired. The damper bars of the DOL PMSM, which can be made of aluminium or copper can be slotted in the rotor. The rotor is attached to the shaft which can be made of fabricated or forged steel bar. The shaft lies on top of bearings which are in bearing brackets. The brackets are attached to the stator frame completing the basic structure. (Kirkpatric J., 1992)

2. COMMISSION REGULATION (EU) 2016/631 – AN OVERVIEW

Grid codes are documents that define rules and requirements for grid connection of generators. The main objective of grid codes is to ensure safe, reliable and efficient operation of generators and to provide knowledge regarding grid phenomena. Grid codes also contribute to fairness and competitiveness of electricity markets. In the European Union (EU) the common grid codes are created by European Network of Transmission System Operators for Electricity (ENTSO-E) with collaboration of Agency for the Cooperation of Energy Regulators (ACER). After the Commission approval the codes become regulations. The Regulation (EU) 2016/631 includes general requirements and regional requirements for different synchronous areas. In addition, national grid codes are defined by relevant transmission system operators (TSO). For example, in Finland national grid codes, which are compatible with the Commission Regulation, are adopted and modified to Finland by Fingrid. In addition, distribution system operators (DSO) are allowed to make necessary local additions. In this chapter an overview of the Regulation (EU) 2016/631 is given. The focus is mainly on topics that affect DOL machine design criteria.

2.1 Scope of application and significance

The Regulation has been approved and published on 14.4.2016 and it entered into force on 17.5.2016. The Regulation was set to apply from three years after publication. The date of effect was 27.4.2019. The Regulation is binding and applicable in all EU countries.

The requirements apply to new power-generating modules which are considered significant, and to existing power-generating modules of type C or D that are substantially modified. Also, after a proposal of a relevant TSO, a regulatory authority or a Member State can make an existing power-generating module subject to the requirements. PSH power plants must fulfil all the relevant requirements both during generating and pumping. The Regulation does not apply to power-generating modules that are connected to non-synchronously operating island grids, modules designed for temporary usage or storage devices other than PSH. Power-generating modules are generally considered existing if it has been already connected to the grid on 27.4.2019 or a final contract for the purchase of the plant has been concluded after two years of that date at the latest.

The Regulation sets requirements based on the power plant connection and its significance. Power plants are divided into synchronous power-generating modules and power park modules (PPM). Synchronous power-generating modules mean simply generators that are directly grid connected and power park modules mean asynchronously or through a power electronic converter connected electricity generating units with a single connection point. The significance is determined by categorizing power plants into types A, B, C and D having varying definitions based on region, nominal connection point voltage and nominal active power. Voltage and maximum capacity thresholds that relevant TSOs can propose for each type are represented in Table 2.1.

Table 2.1 Connection point voltage thresholds and limits for maximum capacity thresholds that relevant TSOs can propose for power-generating modules. It should be noted that the Regulation was published before the Brexit (modified from the (EU) 2016/631).

Synchronous area	**A**	**B**	**C**	**D**
Continental Europe	0.8 kW and < 110 kV	1 MW and < 110 kV	50 MW and < 110 kV	75 MW or ≥ 110 kV
Great Britain	0.8 kW and < 110 kV	1 MW and < 110 kV	50 MW and < 110 kV	75 MW or ≥ 110 kV
Nordic Countries	0.8 kW and < 110 kV	1.5 MW and < 110 kV	10 MW and < 110 kV	30 MW or ≥ 110 kV
Ireland and Northern Ireland	0.8 kW and < 110 kV	0.1 MW and < 110 kV	5 MW and < 110 kV	10 MW or ≥ 110 kV
Baltic Countries	0.8 kW and < 110 kV	0.5 MW and < 110 kV	10 MW and < 110 kV	15 MW or ≥ 110 kV

For example, in Nordic countries a 10 MW generator with a nominal connection point voltage of 20 kV is of type C and with 110 kV it would be of type D. Power-generating modules under 0.8 kW and 110 kV are not considered significant enough. Generally, the higher the alphabetical order, the bigger is the impact of the power-generating module on the characteristics of the grid, and therefore the more requirements it is subject to. The regional differences in capacity threshold limits are because of differences in grid strengths. The weaker the grid, the more significant a new power-generating module is in that region. The factors that contribute to the grid strength are for example short circuit impedance, amount of inertia, transmission capacity and grid topology.

2.2 Frequency stability

The grid frequency is the same throughout the whole system and it is proportional to active power. Consequently, the power balance is maintained on a system level by scheduling generation and load with price signals in electricity markets and the mismatch after the scheduling is corrected with frequency balancing services. Every significant synchronous generator prime mover must be able to contribute to frequency stability with the features listed in Table 2.2.

Table 2.2 Requirements that affect frequency stability for different synchronous generator categories. A feature is marked with X if it is required (modified from the reference Peltoniemi, 2020).

Requirement	Type A	Type B	Type C	Type D
Frequency ranges	X	X	X	X
LFSM-O	X	X	X	X
RoCoF withstand	X	X	X	X
Constant output at target active power	X	X	X	X
Maximum active power reduction at underfrequency	X	X	X	X
Automatic connection	X	X	X	X
Ceasing of active power output within five second using a logic interface and possibility for remote switch on/off	X	X		
Active power reduction using a logic interface and possibility for remote operation		X		
Active power controllability and control range in line with the instructions specified by the system operator or TSO			X	X
Disconnection of load (e.g. a pump-storage) because of underfrequency			X	X
Frequency restoration control			X	X
Frequency sensitive mode			X	X
LFSM-U			X	X
Monitoring of frequency response			X	X

Automatic connection is allowed unless otherwise specified by the relevant system operator in coordination with the relevant TSO. The TSO defines the frequency ranges, delay time and maximum rate of increase of active power under which the automatic connection is allowed.

2.2.1 Frequency sensitive mode – droop-control

The frequency balancing is carried out with a droop-control where the output power of a generator is controlled proportionally to the grid frequency:

$$Droop\ [\%] = 100 \cdot \frac{\frac{|\Delta f| - |\Delta f_1|}{f_\mathrm{n}}}{\frac{\Delta P}{P_\mathrm{n}}}, \tag{2.1}$$

where Δf is the frequency deviation in the network, $\Delta f_1 = \pm 0.2 \ldots 0.5$ Hz the dead band, $f_\mathrm{n} = 50$ Hz the nominal grid frequency, ΔP the change in active power output and P_n the rated active power. The droop is realized in the governor control of the DOL generator prime mover. The droop setting shall be between 2 % and 12 % and activated as fast as possible (< 2 s) when the frequency deviation exceeds the set dead band threshold. For example, considering a generator with $P_\mathrm{n} = 10$ MW, a typical dead band in the Nordic region of 0.5 Hz, $\Delta f = 0.6$ Hz and a droop setting of 5 % the change in active power is

$$\Delta P = \frac{100}{Droop} \frac{|\Delta f| - |\Delta f_1|}{f_\mathrm{n}} P_\mathrm{n} = \frac{100}{5} \cdot \frac{0.6\ \mathrm{Hz} - 0.5\ \mathrm{Hz}}{50} \cdot 10\ \mathrm{MW} = 0.4\ \mathrm{MW}.$$

With the limited frequency sensitive mode – overfrequency (LFSM-O) the power is reduced by 0.4 MW and with the limited frequency sensitive mode – udnerfrequency (LFSM-U), it is increased. LFSM-U is only required with types C and D.

In the regulation, the frequency sensitive mode (FSM) is distinguished from LFSM-O and LFSM-U. The parameters and their ranges for FSM (types C and D) are given in Figure 2.1 and Table 2.3.

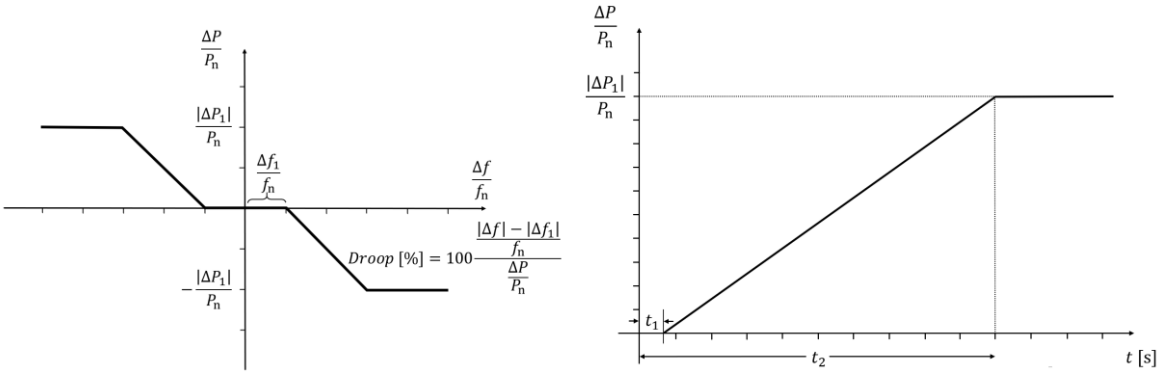

Figure 2.1 On the left active power frequency response in frequency sensitive mode when the frequency response insensitivity is zero. In reality, the droop slope has discrete levels. On the right active power frequency response slope as a function of time. (modified from the (EU) 2016/631)

Table 2.3 Active power frequency response parameters with regard to Figure 2.1. (modified from the (EU) 2016/631)

Parameters	**Ranges**
Active power range related to nominal capacity $\frac{\lvert\Delta P_1\rvert}{P_\mathrm{n}}$	1.5 … 10 %
Frequency response insensitivity $\frac{\lvert\Delta f_i\rvert}{f_\mathrm{n}}$	0.02 … 0.06 %
Frequency response deadband Δf_1	0 … 0.5 Hz
Droop	2 … 12 %
For power-generating modules with inertia, the maximum admissible initial delay t_1 unless longer time is justifiable	2 s
Maximum admissible full activation time t_2, unless longer activation times are allowed by the relevant TSO for reasons of system stability	30 s

In comparison with LFSM-O and LFSM-U, in the FSM power ranges, insensitivity and full activation time are introduced and the deadband can be zero. Also, it is said in the Regulation that a power-generating module shall be capable of providing full active power frequency response for a period of between 15 and 30 minutes as specified by the relevant TSO. As no more than nominal power is required, this is more of an energy resource rationing issue than an electrical machine design issue.

The full activation time in combination with the droop setting should be considered as they can possibly determine the required maximum torque slope. However, the limiting factor here is more likely to be in the prime mover and its control rather than in the generator design. Maximum steady state torque value would be more relevant from the generator design point view as that would define d- and q-axis inductance values with a given inductance ratio according to the load angle equation.

2.2.2 Maximum active power reduction at underfrequency

The Regulation sets boundaries in which the relevant TSO shall specify admissible active power reduction with falling frequency. The boundaries are shown in Figure 2.2.

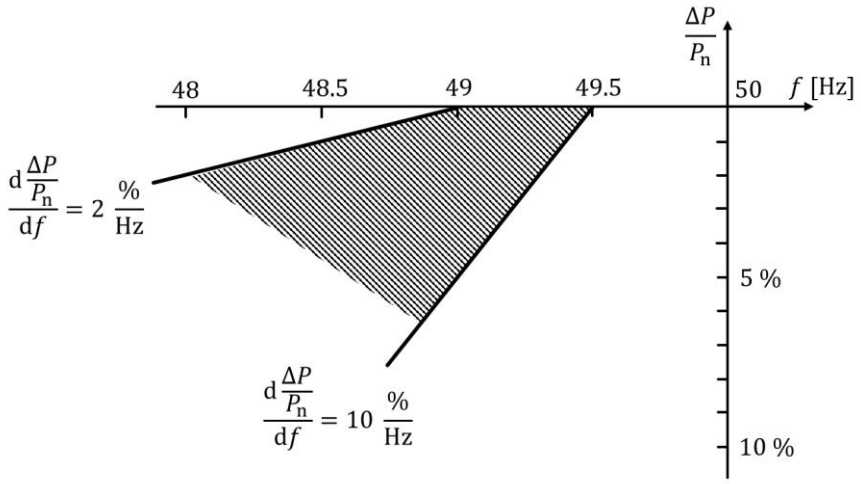

Figure 2.2 The maximum active power reduction boundaries at underfrequency. Below 49 Hz a reduction rate of 2 % of the nominal power per 1 Hz drop is allowed at maximum, and below 49.5 Hz 10 % respectively. (Modified from the (EU) 2016/631)

The boundaries are not particularly relevant for types C and D as they are subject to LFSM-U requirements. Types A and B are allowed to reduce active power even at underfrequency, whether for technical or economic reasons. The boundaries ensure that the reduction remains at least moderate and underfrequency situation will not become uncontrollable. This requirement may concern mostly the turbine design and control system.

2.2.3 Frequency ranges

In Table 2.4 an example of required operation time periods for different frequency ranges is given. Wider ranges, longer times or combined voltage and frequency deviation requirements are possible with an agreement between the relevant system operator and the power plant owner in coordination with the relevant TSO. Also, a generator must withstand a rate of change of frequency up to the value (e.g. 2 Hz/s) specified by the relevant TSO and stay connected, unless disconnection was triggered by an appropriate RoCoF-type loss of mains protection.

Table 2.4 An example of minimum operational times with different frequency ranges without disconnection (recreated from the (EU) 2016/631).

Synchronous area	Frequency range	Time period for operation
Continental Europe	47.5 Hz … 48.5 Hz	To be specified by each TSO, but not less than 30 minutes
	48.5 Hz … 49.0 Hz	To be specified by each TSO, but not less than the period for 47.5 Hz … 48.5 Hz
	49.0 Hz … 51.0 Hz	Unlimited
	51.0 Hz … 51.5 Hz	30 minutes
Nordic Countries	47.5 Hz … 48.5 Hz	30 minutes
	48.5 Hz … 49.0 Hz	To be specified by each TSO, but not less than 30 minutes
	49.0 Hz … 51.0 Hz	Unlimited
	51.0 Hz … 51.5 Hz	30 minutes

From the generator design point of view the operation times alone in Table 2.4 are not overly significant as long as it is made sure that the frequencies or their harmonics do not excite any harmful oscillations. At underfrequencies slight overtorques can occur with type C and D generators as nominal power can be required. Also, the operation point of a DOL PMSG moves towards under-excited condition as the emf decreases because of the slower speed. At over frequencies higher emf is induced and the operation point moves towards over-excited condition. The load angle stays roughly the same if the active power is held constant. However, at least with the existing small-scale hydropower plants it seems to be common that the turbine is not controlled and therefore the active power and load angle vary with the frequency slightly.

2.3 Voltage stability

The grid voltage is a local quantity, and it is controlled with the reactive power. The relation between voltage and reactive power can be shown with the load angle equation. The load angle equation can be derived from Figure 2.3, in which a power transfer in a simplified transmission line is illustrated.

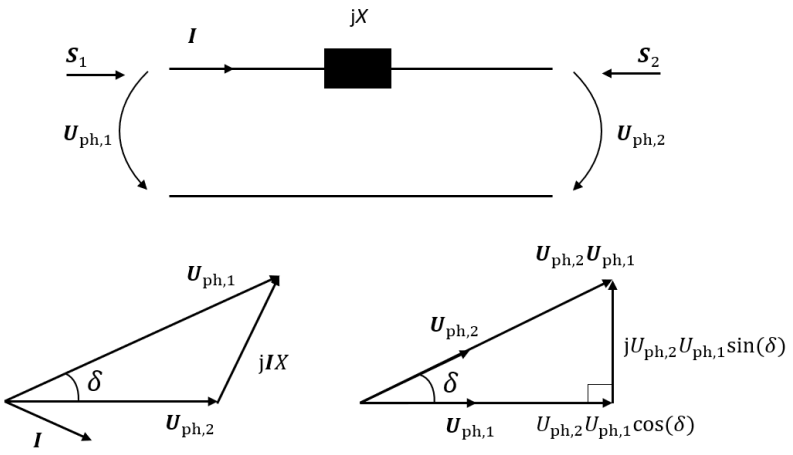

Figure 2.3 Power transfer in a simplified transmission line when resistance and capacitance are neglected.

In figure $U_{\mathrm{ph},1}\angle\delta = U_{\mathrm{ph},2}\angle 0° + \mathrm{j}\boldsymbol{I}X$, so the apparent power $\boldsymbol{S}_2$ in a three-phase system is therefore

$$\boldsymbol{S}_2 = 3\boldsymbol{U}_{\mathrm{ph},2}\boldsymbol{I}^* = 3(U_{\mathrm{ph},2}\angle 0°)\cdot\frac{U_{\mathrm{ph},1}\angle -\delta - U_{\mathrm{ph},2}\angle 0°}{-\mathrm{j}X} \tag{2.2}$$

$$= 3\left(\frac{U_{\mathrm{ph},1}\angle -\delta \cdot U_{\mathrm{ph},2}\angle 0°}{-\mathrm{j}X} + \frac{-U_{\mathrm{ph},2}^2\angle 0°}{-\mathrm{j}X}\right) = 3\left(\frac{U_{\mathrm{ph},1}U_{\mathrm{ph},2}\angle -\delta}{-\mathrm{j}X} - \mathrm{j}\frac{U_{\mathrm{ph},2}^2\angle 0°}{X}\right),$$

where $\boldsymbol{U}_{\mathrm{ph},1}$ is the source phase voltage, $\boldsymbol{I}^*$ the complex conjugate of current, $\boldsymbol{U}_{\mathrm{ph},2}$ the receiving end voltage and δ the load angle. By considering the trigonometry, the simplified (neglected resistance) load angle equation is obtained:

$$\boldsymbol{S}_2 = 3\left(\frac{U_{\mathrm{ph},1}U_{\mathrm{ph},2}\cos(\delta) - \mathrm{j}U_{\mathrm{ph}1}U_{\mathrm{ph},2}\sin(\delta)}{-\mathrm{j}X} - \mathrm{j}\frac{U_{\mathrm{ph},2}^2\angle 0°}{X}\right) \tag{2.3}$$

$$= 3\left(\frac{U_{\mathrm{ph},1}U_{\mathrm{ph},2}}{X}\sin(\delta) + \mathrm{j}\left(\frac{U_{\mathrm{ph},1}U_{\mathrm{ph},2}}{X}\cos(\delta) - \frac{U_{\mathrm{ph},2}^2}{X}\right)\right),$$

in which the first term is active power and the second term reactive power. When a transmission line is at no-load, the load angle is zero and no active power is transmitted. It should be noted that in the load angle equation of a synchronous generator, where the source is the permanent magnet or field excitation induced electromotive force (emf), the reactance is the synchronous reactance and the receiving end voltage is the terminal voltage, also the power arising from the magnetic saliency of the rotor should be taken into account.

The per-unit presentations for active and reactive powers in equation (2.3) are

$$P = \frac{U_1 U_2}{X}\sin(\delta), \tag{2.4}$$

$$Q = \frac{U_1 U_2}{X}\cos(\delta) - \frac{U_2^2}{X}. \tag{2.5}$$

By taking partial derivatives with respect to the voltage and the load angle

$$\frac{\partial P}{\partial U_2} = \frac{U_1}{X}\sin(\delta), \tag{2.6}$$

$$\frac{\partial P}{\partial \delta} = \frac{U_1 U_2}{X}\cos(\delta), \tag{2.7}$$

$$\frac{\partial Q}{\partial U_2} = \frac{U_1}{X}\cos(\delta) - \frac{2U_2}{X}, \tag{2.8}$$

$$\frac{\partial Q}{\partial \delta} = \frac{U_1 U_{,2}}{X}\sin(\delta), \tag{2.9}$$

it can be seen that the active power is heavily load angle dependent (with small $\delta, \sin(\delta) \approx \delta$) and the reactive power is heavily voltage dependent (with small $\delta, \cos(\delta) \approx 1$), as the load angle is typically small in transmission lines. To analyse voltage stability and further illustrate the voltage and power relations in transmission lines, so called nose curves can be presented, Figure 2.4. Nose curves can be plotted by eliminating δ in (2.4) and (2.5) and solving $U_2 \geq 0$ (Rincón R. et al., 2016):

$$U_2 = \left(\frac{U_1^2}{2} - XQ \pm \left(\frac{U_1^4}{4} - X^2P^2 - XU_1^2Q\right)^{\frac{1}{2}}\right)^{\frac{1}{2}}. \tag{2.10}$$

The nose curves show the load voltage as a function of loadability. The real solutions above the voltage collapse- or “nose” point are stable and solutions below that are unstable. At the unstable region, the current is high and the power does not behave in a presumable manner, i.e. an attempt to increase load by lowering impedance decreases power as the voltage is pulled down rapidly.

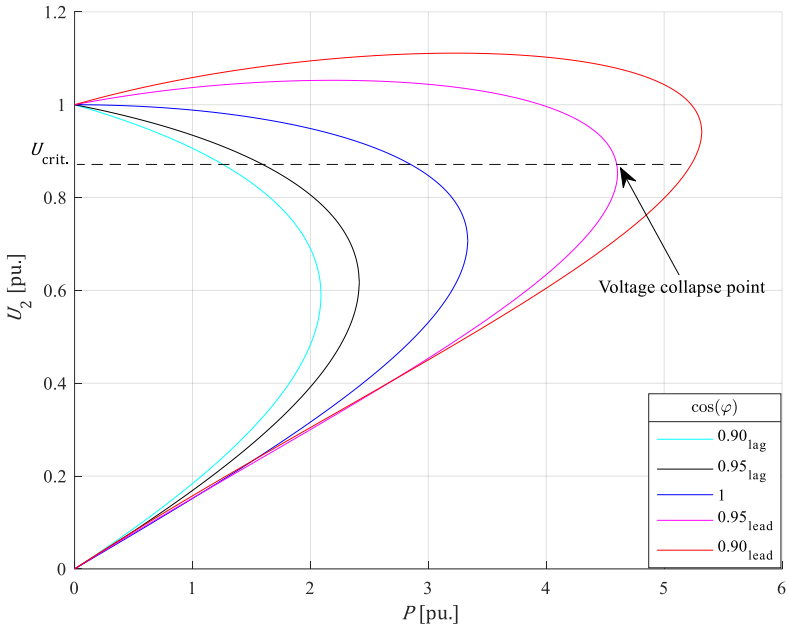

Figure 2.4 Nose curves with different power factors. The $U_{crit.}$ is the voltage value at the collapse point where the maximum loadability is achieved.

In Figure 2.4 the nose curves are plotted with different power factors. It can be seen, that supplying reactive power supports voltage. With a leading power factor, a higher load can be achieved before the voltage collapses compared to a lagging power factor.

In Table 2.5 the requirements regarding voltage stability are listed.

Table 2.5 Requirements that affect voltage stability for different synchronous generator categories. A feature is marked with "X" if it is required and with "/" if it is required with some annotation. (modified from the reference Peltoniemi P., 2020).

Requirement	Type A	Type B	Type C	Type D
High/low voltage disconnection			X	/
Voltage ranges with time periods				X
Voltage control system (simple)		X	X	
Reactive power capability (simple)		/		
Reactive power capability at maximum (nominal) active power			X	X
Reactive power capability below maximum (nominal) active power			X	X
Voltage control system				X

Disconnection with over- and undervoltage values specified by the relevant system operator and the TSO is required for type C modules. Type D must also fulfil the operation times with different voltage ranges with which the disconnection values must not contradict. For type

B reactive power capability is specified by the relevant system operator, but the Regulation does not address that feature any further. The voltage control system for types B and C means an automatic permanent excitation control system that can provide a stable constant terminal voltage over the entire operating range. However, it appears that in practice powerplants in category B without automatic excitation control may be accepted for use. For type D the voltage control system is more strictly regulated: The voltage control specifications shall be agreed between the power plant owner and the relevant system operator, in coordination with the relevant TSO, and the control system shall include bandwidth limitation of the output signal, an underexcitation limiter, an overexcitation limiter, a stator current limiter and possibly a power system stabilizer functionality. The reactive power capability at and below maximum active power for types C and D are specified with *U-Q/P* -profiles.

2.3.1 *U-Q/P* -profile

Figure 2.5 with Table 2.6 shows the boundaries in which the relevant system operator in coordination with the relevant TSO shall specify the reactive power capability requirements for types C and D synchronous power-generating modules at the point of common coupling (PCC). The inner envelope may also be of other shape than rectangular. Operation at every possible point in the diagram is required both at and below the nominal active power.

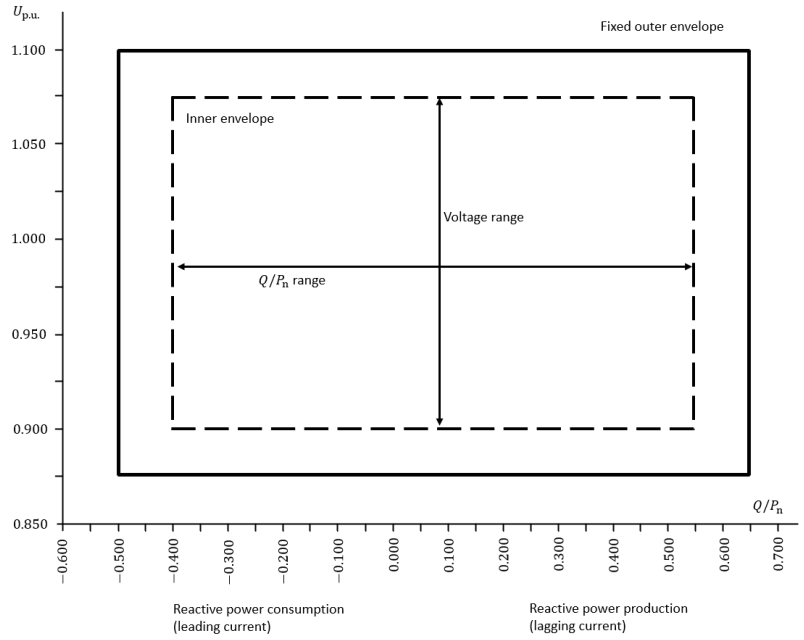

Figure 2.5 Voltage-reactive power profile of a synchronous power-generating module. The example parameters for the inner envelope are in Table 2.6. Positive power value means here that the power is flowing to the grid. Therefore, lagging power factor produces reactive power. (modified from the (EU) 2016/631)

Table 2.6 An example of maximum parameter values for the inner envelope in Figure 2.5 (recreated from the (EU) 2016/631).

Synchronous area	Maximum range of Q/P_{n}	Maximum range of steady-state voltage level in p.u.
Continental Europe	0.95	0.225
Nordic	0.95	0.150

For example, a Q/P_{n} range of 0.95 could be specified as –0.4…0.55 and a voltage range of 0.225 as 0.875…1.1. As the requirements apply at the PCC, it should be possible to fulfil them also with PMSGs by using separate compensator devices. In the electrical machine design process, the *U-Q/P* -profile may affect the continuous overvoltage withstand requirement and settling of starting values; apparent power and power factor.

2.3.2 Voltage ranges

The minimum operation times without disconnection for different voltage ranges are represented in Table 2.7. The requirement applies for type D power-generating modules. The times can be specified to be shorter by the relevant TSO in the case of simultaneous overvoltage and underfrequency or simultaneous undervoltage and overfrequency. Wider ranges or longer times are possible with an agreement between the relevant system operator and the power plant owner in coordination with the relevant TSO.

Table 2.7 An example of minimum operational times with different voltage ranges without disconnection (recreated from the (EU) 2016/631).

Synchronous area	Voltage range [pu.]	Time period for operation
Continental Europe	0.85 … 0.90	60 minutes
	0.90 … 1.05	Unlimited
	1.05 … 1.10	To be specified by each TSO, but not less than 20 minutes and not more than 60 minutes
Nordic	0.90 … 1.05	Unlimited
	1.05 … 1.10	To be specified by each TSO, but not more than 60 minutes

The voltage ranges with operation times alone are not likely to affect electrical machine design very significantly. The insulation should be dimensioned to withstand the required overvoltages and the cooling should be appropriate for slight overcurrents that can occur.

2.4 Robustness – fault-ride-through

The requirements regarding robustness concerns generators of type B, C and D, Table 2.8.

Table 2.8 Requirements that affect robustness for different synchronous generator categories. A feature is marked with X if it is required (modified from the reference Peltoniemi P., 2020).

Requirement	Type A	Type B	Type C	Type D
Fault-ride-through capability		X	X	X
Remain connected during grid auto reclosures			X	X
Steady-state stability during power oscillations at any *P*-*Q* diagram operation point			X	X
Post fault active power recovery within time specified by the relevant TSO		X	X	X

The requirements include fault-ride-through capability limits to be specified by the relevant TSO within the ranges shown in Figure 2.6 and Table 2.9. Also, the relevant TSO shall specify and publish pre- and post-fault minimum short circuit capacity in MVA, voltage and active and reactive power operating point of the power-generating module at the connection point. In the Regulation only a symmetrical short circuit (all phases shorted) is considered and fault-ride-through capabilities in asymmetrical faults shall be specified by each TSO.

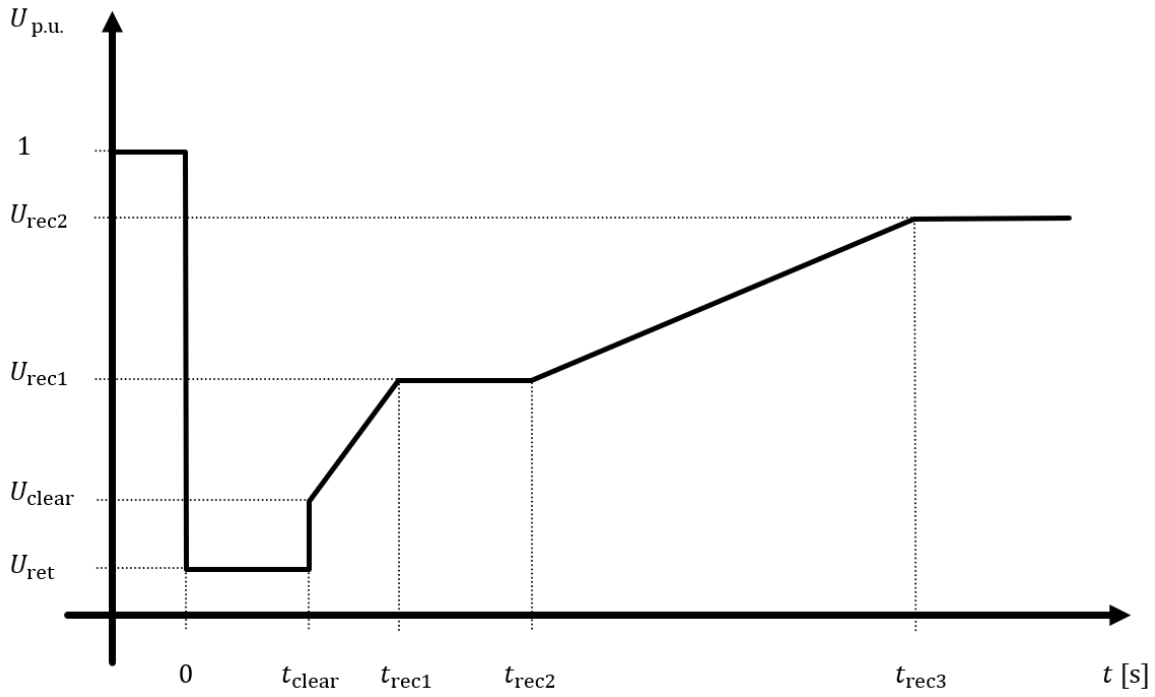

Figure 2.6 Fault-ride-through profile of a power-generating module. A per-unit line-to-line voltage as a function of time during a symmetrical fault. (modified from the (EU) 2016/631)

Table 2.9 Fault-ride-through parameters with regard to the Figure 2.6 for different synchronous generator categories. U_{ret} is the retained voltage at the connection point during a fault, U_{clear} is the lower voltage limit at fault clearance, U_{rec1} and U_{rec2} are the lower voltage limits after the clearance, t_{clear} is the time instance for fault clearance and t_{rec1}, t_{rec2} and t_{rec3} are time instances for the voltage limits. (modified from the (EU) 2016/631)

Voltage parameter (p.u.)	**Types B and C**	**Type D**	**Time parameter [s]**	**Types B and C**	**Type D**
U_{ret}	0.05 … 0.3	0	t_{clear}	0.14 … 0.15 (or 0.14 … 0.25 if system protection and secure operation so require)	0.14 … 0.15 (or 0.14 … 0.25 if system protection and secure operation so require)
U_{clear}	0.7 … 0.9	0.25	t_{rec1}	t_{clear}	t_{clear} … 0.45
U_{rec1}	U_{clear}	0.5 … 0.7	t_{rec2}	t_{rec1}… 0.7	t_{rec1} … 0.7
U_{rec2}	0.85 … 0.9 and ≥ U_{clear}	0.85 … 0.9	t_{rec3}	t_{rec2} … 1.5	t_{rec2} … 1.5

The fault-ride-through profile can form significant criteria for generator design as the generator has a great impact on the power plant fault-ride-through performance. The generator should be capable of retaining synchronism and currents and torque should be admissible during the fault.

The requirement to remain connected during auto reclosures concerns mainly the protection devices but could also concern transient stability. The steady-state stability during power oscillations means that the generator should maintain a stable load angle and be capable of damping the oscillations. However, the Regulation does not give any definitions for the oscillations in this case and therefore, no direct design criteria for the damper winding can be given based on this requirement. The post fault active power recovery time and power value is entirely defined by the relevant TSO and it can potentially determine the required maximum torque slope.

The short-circuit capacity at the connection point can be expressed as

$$S_{\mathrm{k}} = \frac{U_{\mathrm{LL}}^2}{Z_{\mathrm{k}}} = \sqrt{3} U_{\mathrm{LL}} I_{\mathrm{k3}}, \tag{2.11}$$

where U_{LL} is the line-to-line voltage, Z_{k} short circuit impedance including generator, transformer and cable impedances and I_{k3} short circuit current in a three phase short circuit. Large short ciruit currents may result in an irreversible PM demagnetization with PMSMs

bcause of strong opposing armature reaction at the beginning of the short circuit (Kamiev K., 2013). The short-circuit capacity at the connection point specified by the TSO may set limits for the machine inductances. Also, the permanent magnets must be appropriately protected to withstand the short circuits without damage.

2.5 System restoration – reconnection, island operation and black start

The system restoration requirements are represented in Table 2.10.

Table 2.10 Requirements regarding system restoration for different synchronous generator categories. A feature is marked with X if it is required.

Requirement	Type A	Type B	Type C	Type D
Black start readiness if requested by the relevant TSO			X	X
Island operation capability if required by the relevant system operator in coordination with the TSO			X	X
Quick re-synchronisation			X	X
Additional synchronization rules				X

The black start capability is not mandatory on behalf of the Regulation, but a Member State can still introduce obligatory rules regarding the black start. Also, a power plant owner must give a quotation for black start services if asked by the relevant TSO. The black start means starting from shutdown without any external electricity supply. With a PMSG this is relatively easy as the magnetic flux is always present. However, it is required that the synchronization in black starts is possible within the frequency and voltage (type D) ranges shown in Table 2.7 and Table 2.4 and within a time frame specified by the relevant system operator in coordination with the relevant TSO. Also, automatic voltage control, LFSM-O, LFSM-U and parallel operation capability within one island are required with black start capable power plants. For type D the synchronization capability with the frequency ranges is required even if the plant is not black start capable and the power plant owner must agree with the relevant system operator voltage, frequency, phase angle range, phase sequence and deviation of voltage and frequency settings for synchronization.

The island operation means that part of the network is operating in isolation from the synchronous area. An island cannot be connected back to the grid if it has too large frequency, phase, or voltage deviations. Islands typically have quite poor properties in terms of fre-

quency and voltage stability, which causes safety and protection issues and possibly destruction of devices connected to the grid. Also, island operation may cause dangerous situations where a live wire is thought to be voltage free. Therefore, islanding is often prevented in distributed generation with anti-islanding functions. It may still be needed in system restoration, so the Regulation states that types C and D must be capable of taking part in island operation if required by the relevant system operator in coordination with the relevant TSO. During island operation frequency and voltage (type D) ranges are as in Table 2.7 and Table 2.4, LFSM-O, LFSM-U, FSM and active power reduction as much as technically feasible (at least 55 % of nominal) are required and the island operation detection should not be based only on the system operator's switchgear position signals.

The quick re-synchronisation capability for types C and D means that in a case of disconnection the re-synchronisation is carried out in line with the protection strategy agreed between the powerplant owner and the relevant system operator in coordination with the relevant TSO. If a minimum re-synchronisation time is greater than 15 minutes the power plant must be designed to trip to houseload operation. The minimum operation time for houseload is specified by the relevant system operator in coordination with the relevant TSO. The houseload means that a powerplant is running and supplying power for the devices in the plant but not to the grid. The point is that from houseload the reconnection to the grid is faster than from shutdown.

The synchronization time and ranges set quite clear performance requirements that are dependent on the electrical machine design, especially on the damper winding properties. With regard to the island operation, PMSGs without additional compensator device would have to be heavily overdimensioned and are not very well suited for the purpose to begin with. In island operation a controllable internal voltage is essential because grid voltage level depends on the generator characteristics and the power factor is affected heavily by the load. (Kamiev K., 2013), (Kinnunen J., 2007)

2.6 Compliance simulations

For power plant types B, C and D compliance simulations and tests are required to be performed by the power plant owner. Alternatively, compliance can be demonstrated with equipment certificates issued by an authorised certifier. The required simulation scenarios

to prove compliance with the relevant requirement are represented in Table 2.11 and descriptions of the simulations are in Table 2.12.

Table 2.11 Required compliance simulations for different synchronous generator categories. A scenario is marked with X if it is required.

Scenario	Type A	Type B	Type C	Type D
LFSM-O response		X	X	X
Fault-ride-through capability		X	X	X
Post fault active power recovery		X	X	X
LFSM-U response			X	X
FSM response			X	X
Island operation			X	X
Reactive power capability			X	X
Power oscillations damping control				X

Table 2.12 Compliance simulation specifications for synchronous power plants in the Regulation.

Scenario	Possible execution	Success conditions
LFSM-O response	- Frequency deviation signals are injected into the control system references. - High frequency steps and ramps reaching minimum regulating level are used, taking into account the droop settings and the deadband.	- The results comply with the requirements in chapter 2.2.1.
Fault-ride-through capability	- Capability to ride through faults as discussed in the chapter 2.4. - Fault-ride-through profile is injected as a reference to the generator model.	- The results comply with the requirements in chapter 2.4. - Synchronism is retained and currents are within acceptable range
Post fault active power recovery	- Active power recovery is checked in the fault-ride-through simulation.	- The required active power value is recovered in time specified by the relevant TSO.
LFSM-U response	- Frequency deviation signals are injected into the control system references. - Low frequency steps and ramps reaching max. capacity are used, taking into account the droop settings and the deadband.	- The results comply with the requirements in chapter 2.2.1.
FSM response	- Frequency deviation signals are injected into the control system references. - Frequency steps and ramps big enough to trigger the whole active power frequency response range are used, taking into account the droop settings and the deadband.	- The results comply with the requirements in chapter 2.2.1.
Island operation	- Same as FSM response but in an island condition	- The results comply with the requirements in chapter 2.5.
Reactive power capability	- Leading and lagging reactive power capability is demonstrated - Voltage reference that triggers max. reactive power response is injected to reactive power control at active power levels of min., max. and in between.	- The results comply with the requirements in chapter 2.3.
Power oscillations damping control	- Damping control performance is demonstrated. - Sudden load changes are simulated, and damping performance is inspected. - The PSS function is tuned so that it improves damping compared to automatic voltage regulator alone.	- The PSS function damps power oscillations specified by the relevant TSO - A sudden load reduction from 1 p.u. to 0.6 p.u. does not lead to undamped oscillations

The frequency control modes concern mainly the prime mover and its control. Examining a PMSG model behaviour under such scenarios is almost trivial from the perspective of this thesis. Also, the reactive power control or island operation are not relevant with a pure PMSG as it is not intended for such use cases. Furthermore, with regard to the power oscillations damping control, the PSS function is not of interest with PMSGs. Therefore, the primary focus with the simulations carried out in this thesis is the fault-ride-through capability. Even though the damping performance simulation is specifically for the type D in the Regulation, the capability to dampen oscillations with other types is obviously also necessary and embedded in the requirements to maintain stable operation.

2.7 Summary

The Regulation is written from a TSO's perspective in Europe and it does not directly address features such as efficiency and harmonic distortion that should also be considered in a generator design in general. More requirements in addition to the ones in the (EU) 2016/631 can be found for example from the standards issued by international organizations such as IEEE, IEC and CENELEC as well as from national standards. With all the technical requirements on top of financial issues the generator design is inevitably a certain type of multi-objective optimization task. Moreover, the optimization can be somewhat site specific as grid properties affect the DOL machine performance.

The requirements found in the Regulation that may have some potential to cause constraints for a DOL PMSG design are:

- The fault-ride-through profile (B, C and D), Table 2.9. Fault-ride-through performance could be affected with system inertia and settling of inductance and resistance values.
- The steady-state stability during power oscillations (C and D) means that the generator should maintain stable load angle and be capable of damping the oscillations, chapter 2.4.
- The post fault active power recovery time and power value (B, C and D) defined by the relevant TSO can potentially determine the required maximum torque slope, chapter 2.4.

- The short-circuit capacity at the connection point specified by the TSO may set limits for the machine inductances. Also, measures to protect permanent magnets could be necessary, chapter 2.4.
- *U-Q/P* -profile ((B), C and D) may affect the overvoltage withstand requirement for insulation and settling of starting values; apparent power and power factor. Figure 2.5.
- Synchronization in black starts within the frequency and voltage ranges shown in Table 2.4 and Table 2.7 and within a time frame specified by the relevant system operator (C, D) sets performance requirements which can be achieved with damper winding design. For type D the above is valid even if it is not labelled as black start capable. Also, phase angle range and deviation of voltage and frequency settings for synchronization must be separately considered, chapter 2.5.
- The voltage ranges (D) may affect the overvoltage withstand requirement for insulation and the cooling should be appropriate for slight overcurrents that can occur, Table 2.7.
- The frequency ranges may slightly affect overcurrent withstand requirements, Table 2.4. At underfrequencies slight overtorques occur as nominal active power can be required (C and D).
- The island or houseload operation (C, D) mean that a generator should be capable of operating when the grid properties change greatly, chapter 2.5.

The reactive power, voltage control and possible island operation requirements limit the practical usability of DOL PMSGs to category B and below. However, additional compensator device may be needed in category B. In categories C and D regular SGs are likely more appealing. There are no significant requirements in category A to which special attention should be paid in the machine design, but in category B the fault-ride-through capability is required. Therefore, the main simulations carried out in this thesis focus on the FRT, which seems the most demanding, the least well known and probably the most difficult requirement to achieve. The fault-ride-through capability is not required in category A, but it would be a benefit nevertheless.

3. SIMULATION MODEL

In this chapter the created simulation model is documented, and the limitations of the model are discussed. Two-axis theory is used as a basis, so no machine design data (dimensions etc.) is necessary. The model is created from the scratch using MATLAB® and Simulink®. The simulation tool development was part of the goals of the thesis, and therefore some functionalities of the model that are not used in the simulations of this thesis are also introduced and discussed. Pictures of main parts of the model are presented in Appendix 1.

A synchronous machine model can be built in terms of time constants or in terms of lumped parameters in circuit-model form. Here the lumped parameter approach is an obvious choice as the lumped parameters hold clearer physical significance with respect to the machine design when the parameters are varied across a wide range. It is also perhaps easier to include more details when using the lumped parameter circuit-model.

3.1 Reference frames and coordinate transformations

It is sensible to build the model in a reference frame which produces the simplest equations. Synchronous machines may have different properties in direct (d) and quadrature (q) magnetic axes which must be taken into account. With an orthogonal dq coordinate system the equations can easily be written separately for d-axis and q-axis without rotor position dependent terms. In a rotor reference frame, the axes rotate along with the rotor, and therefore all the electric and magnetic quantities are constants at steady state in the case of an SM. For these reasons, the rotor reference frame is commonly used in SM models and is also used in this thesis.

Phase quantities of a three-phase system (L1, L2, L3) in a stationary reference frame can be converted to the rotor reference frame by applying a transformation based on R. H. Park's original work as follows:

$$\begin{bmatrix} X_{\mathrm{d}} \\ X_{\mathrm{q}} \\ X_0 \end{bmatrix} = \frac{2}{3} \begin{bmatrix} \cos(\theta) & \cos(\theta - \frac{2\pi}{3}) & \cos(\theta + \frac{2\pi}{3}) \\ -\sin(\theta) & -\sin(\theta - \frac{2\pi}{3}) & -\sin(\theta + \frac{2\pi}{3}) \\ \frac{1}{2} & \frac{1}{2} & \frac{1}{2} \end{bmatrix} \begin{bmatrix} X_{\mathrm{L1}} \\ X_{\mathrm{L2}} \\ X_{\mathrm{L3}} \end{bmatrix}, \tag{3.1}$$

and inversely

$$\begin{bmatrix} X_{\mathrm{L1}} \\ X_{\mathrm{L2}} \\ X_{\mathrm{L3}} \end{bmatrix} = \begin{bmatrix} \cos(\theta) & -\sin(\theta) & 1 \\ \cos(\theta - \frac{2\pi}{3}) & -\sin(\theta - \frac{2\pi}{3}) & 1 \\ \cos(\theta + \frac{2\pi}{3}) & -\sin(\theta + \frac{2\pi}{3}) & 1 \end{bmatrix} \begin{bmatrix} X_{\mathrm{d}} \\ X_{\mathrm{q}} \\ X_0 \end{bmatrix}, \tag{3.2}$$

where X represents a quantity that is converted and θ is the position angle. The transformation may have slightly different forms depending on the locations of the axes and how the magnitudes are desired to be scaled. Also, the variables may, of course, be laid out in a different order in the equation. Here the q-axis is 90 ° ahead of the d-axis, the θ is the angle between d-axis and the phase L1 and the d-axis is initially aligned with the phase L1. The X_0 is a zero-sequence component that is zero in a balanced system. The factor $\frac{2}{3}$ is used to make the amplitudes of dq-vectors the same as that of the phase quantities at balanced steady state. Consequently, a $\frac{3}{2}$ factor must be used in three-phase power and torque calculations with dq variables. With equation (3.1) the reference frame speed can in principle be arbitrarily defined. In the rotor reference frame, the position angle θ is

$$\theta_{\mathrm{r}} = \int \omega_{\mathrm{r}} \mathrm{d}t = \int p\Omega_{\mathrm{r}} \mathrm{d}t, \tag{3.3}$$

where ω_r is the electrical rotor angular velocity, p the number of pole pairs and Ω_{r} the mechanical rotor angular velocity. Therefore, the axes do not rotate at synchronous speed during transients in this reference frame. Setting the reference frame speed to zero would yield a transformation referred as Clarke's transformation, which converts the phase variables into αβ0 components in a stationary reference frame. (Krause P. et al., 2017)

3.2 Per-unit system

The model is built using SI units. However, some of the results are presented with per-unit values for easier comparison between machines with different rated values. The used base values are the following:

$$\omega_{\mathrm{b}} = 2\pi f_{\mathrm{n}},$$

$$U_{\mathrm{b}} = \sqrt{2}\frac{U_{\mathrm{LL,n}}}{\sqrt{3}},$$

$$I_{\mathrm{b}} = \sqrt{2} I_{\mathrm{n}},$$

$$Z_{\mathrm{b}} = \frac{U_{\mathrm{b}}}{I_{\mathrm{b}}},$$

$$L_{\mathrm{b}} = \frac{Z_{\mathrm{b}}}{\omega_{\mathrm{b}}},$$

$$\psi_\mathrm{b} = \frac{U_\mathrm{b}}{\omega_\mathrm{b}},$$

$$S_\mathrm{b} = \sqrt{3} U_\mathrm{LL,n} I_\mathrm{n},$$

$$T_\mathrm{b} = \frac{p3 I_\mathrm{b} U_\mathrm{b}}{2\omega_\mathrm{b}},$$

$$J_\mathrm{b} = \frac{p T_\mathrm{b}}{\omega_\mathrm{b}^2}.$$

The per-unit values are obtained by dividing the actual values with the base values.

If the model is desired to be operating with the per-unit values, the factors $\frac{3}{2}$ and $\frac{p3}{2}$ must be omitted from the power and torque equations in the model, because they are already taken into account in the base value definitions. Also, mechanical and electrical angular velocities of the rotor should be set to equal with the above mentioned definitions. In other words, all the machines are treated as if the number of pole pairs were unity and the actual number of pole pair value is taken into account in the torque and moment of inertia base values. The friction and the shaft stifness must also be scaled so that the resulting torque components are in per-unit. The friction torque can be scaled using $\frac{1}{\frac{pT_\mathrm{b}}{\omega_\mathrm{b}}}$ as a gain and the torque component corresponding to the angular displacement caused by the shaft twisting using $\frac{1}{pT_\mathrm{b}}$ respectively. Finally, the relative time $\tau = \omega_\mathrm{b} t$ must be used in order to calculate the differential equations correctly.

3.3 Generator model

The generator model is the core part of the simulation tool. The equivalent circuits with the positive reference current and voltage directions are shown in Figure 3.1.

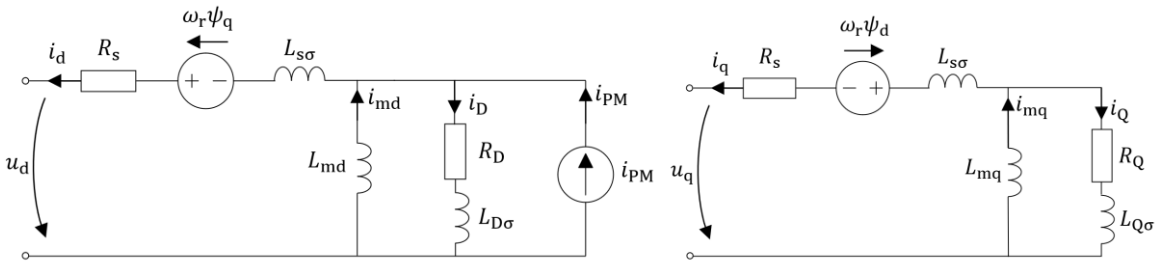

Figure 3.1 Equivalent circuits for d- and q-axes (modified from the reference Kinnunen J., 2007). Corresponding vector diagrams are shown in Figure 3.6. Positive currents are according to generator logic from machine towards the grid.

The equivalent circuits have one damper circuit on the d- and q-axes. The damper circuits represent the damping bars in the rotor. In principle, additional damping circuits could be added to account for induced currents in other parts of the rotor if detailed information of the machine is available. On the d-axis, the magnetization effect of the permanent magnets is represented by a virtual current source i_{PM}. The $i_{\mathrm{d,q}}$ are the stator currents, R_{s} is the stator resistance, $\omega_{\mathrm{r}}\psi_{\mathrm{q}}$ and $\omega_{\mathrm{r}}\psi_{\mathrm{d}}$ are the induced emfs at steady state, $L_{\mathrm{s}\sigma}$ is the stator leakage, $L_{\mathrm{md,q}}$ are the magnetizing inductances, $R_{\mathrm{D,Q}}$ are the damper winding resistances, $L_{\mathrm{D,Q}\sigma}$ are the damper winding leakage inductances, $i_{\mathrm{D,Q}}$ are the damper winding currents, $i_{\mathrm{md}} = i_{\mathrm{PM}} + i_{\mathrm{D}} + i_{\mathrm{d}}$ is the d-axis magnetizing current and $i_{\mathrm{mq}} = i_{\mathrm{Q}} + i_{\mathrm{q}}$ is the q-axis magnetizing current. The iron losses are neglected, which is a common practice. The positive reference directions correspond to the generator logic, where the stator current flowing to the grid is positive and the stator emf matches the terminal voltage by the difference of the voltage drop of the stator resistance. Therefore, the ψ_{PM} must be to the negative d-axis direction and positive $i_{\mathrm{d,q}}$ and $i_{\mathrm{D,Q}}$ currents cause positive armature and damper reactions, that have a demagnetizing effect on the d-axis.

In comparable EESM models, the PM circuit is replaced with a field winding circuit and the Canay inductance, which accounts for unequal mutual inductances between armature, field and damper circuits on the d-axis, is sometimes used.

The stator and damper winding voltage equations in the rotor reference frame are

$$u_{\mathrm{d}} = -R_{\mathrm{s}} i_{\mathrm{d}} - \frac{\mathrm{d}\psi_{\mathrm{d}}}{\mathrm{d}t} + \omega_{\mathrm{r}}\psi_{\mathrm{q}} \,, \tag{3.4}$$

$$u_{\mathrm{q}} = -R_{\mathrm{s}} i_{\mathrm{q}} - \frac{\mathrm{d}\psi_{\mathrm{q}}}{\mathrm{d}t} - \omega_{\mathrm{r}}\psi_{\mathrm{d}} \,, \tag{3.5}$$

$$0 = R_{\mathrm{D}} i_{\mathrm{D}} + \frac{\mathrm{d}\psi_{\mathrm{D}}}{\mathrm{d}t} \,, \tag{3.6}$$

$$0 = R_{\mathrm{Q}} i_{\mathrm{Q}} + \frac{\mathrm{d}\psi_{\mathrm{Q}}}{\mathrm{d}t} \,, \tag{3.7}$$

where on the right side the first term is the resistive voltage drop, second term is the rate of change of the flux linkage (DC quantity) and the third term is the induced emf at steady state.

The flux linkages represented by the currents are:

$$\psi_{\mathrm{d}} = L_{\mathrm{d}} i_{\mathrm{d}} + L_{\mathrm{md}} i_{\mathrm{D}} - \psi_{\mathrm{PM}} \,, \tag{3.8}$$

$$\psi_{\mathrm{q}} = L_{\mathrm{q}} i_{\mathrm{q}} + L_{\mathrm{mq}} i_{\mathrm{Q}} \,, \tag{3.9}$$

$$\psi_{\mathrm{D}} = L_{\mathrm{md}} i_{\mathrm{d}} + L_{\mathrm{D}} i_{\mathrm{D}} - \psi_{\mathrm{PM}}, \tag{3.10}$$

$$\psi_{\mathrm{Q}} = L_{\mathrm{mq}} i_{\mathrm{q}} + L_{\mathrm{Q}} i_{\mathrm{Q}}, \tag{3.11}$$

$$\boldsymbol{\psi} = \mathbf{L} \cdot \mathbf{i} = \begin{bmatrix} \psi_{\mathrm{d}} \\ \psi_{\mathrm{q}} \\ \psi_{\mathrm{D}} \\ \psi_{\mathrm{Q}} \end{bmatrix} = \begin{bmatrix} L_{\mathrm{d}} & 0 & L_{\mathrm{md}} & 0 \\ 0 & L_{\mathrm{q}} & 0 & L_{\mathrm{mq}} \\ L_{\mathrm{md}} & 0 & L_{\mathrm{D}} & 0 \\ 0 & L_{\mathrm{mq}} & 0 & L_{\mathrm{Q}} \end{bmatrix} \begin{bmatrix} i_{\mathrm{d}} \\ i_{\mathrm{q}} \\ i_{\mathrm{D}} \\ i_{\mathrm{Q}} \end{bmatrix} + \begin{bmatrix} -\psi_{\mathrm{PM}} \\ 0 \\ -\psi_{\mathrm{PM}} \\ 0 \end{bmatrix}, \tag{3.12}$$

where

$$L_{\mathrm{d}} = L_{\mathrm{md}} + L_{\mathrm{s}\sigma}, \tag{3.13}$$

$$L_{\mathrm{q}} = L_{\mathrm{mq}} + L_{\mathrm{s}\sigma}, \tag{3.14}$$

$$L_{\mathrm{D}} = L_{\mathrm{md}} + L_{\mathrm{D}\sigma}, \tag{3.15}$$

$$L_{\mathrm{Q}} = L_{\mathrm{mq}} + L_{\mathrm{Q}\sigma}. \tag{3.16}$$

The currents can then be solved as follows:

$$\begin{bmatrix} i_{\mathrm{d}} \\ i_{\mathrm{q}} \\ i_{\mathrm{D}} \\ i_{\mathrm{Q}} \end{bmatrix} = \begin{bmatrix} L_{\mathrm{d}} & 0 & L_{\mathrm{md}} & 0 \\ 0 & L_{\mathrm{q}} & 0 & L_{\mathrm{mq}} \\ L_{\mathrm{md}} & 0 & L_{\mathrm{D}} & 0 \\ 0 & L_{\mathrm{mq}} & 0 & L_{\mathrm{Q}} \end{bmatrix}^{-1} \cdot \left(\begin{bmatrix} \psi_{\mathrm{d}} \\ \psi_{\mathrm{q}} \\ \psi_{\mathrm{D}} \\ \psi_{\mathrm{Q}} \end{bmatrix} - \begin{bmatrix} -\psi_{\mathrm{PM}} \\ 0 \\ -\psi_{\mathrm{PM}} \\ 0 \end{bmatrix} \right), \tag{3.17}$$

where the flux linkages are obtained by integrating the derivates in the voltage equations:

$$\psi_{\mathrm{d}} = \int -u_{\mathrm{d}} - R_{\mathrm{s}} i_{\mathrm{d}} + \omega_{\mathrm{r}} \psi_{\mathrm{q}} \mathrm{d}t, \tag{3.18}$$

$$\psi_{\mathrm{q}} = \int -u_{\mathrm{d}} - R_{\mathrm{s}} i_{\mathrm{d}} - \omega_{\mathrm{r}} \psi_{\mathrm{d}} \mathrm{d}t, \tag{3.19}$$

$$\psi_{\mathrm{D}} = \int -R_{\mathrm{D}} i_{\mathrm{D}} \mathrm{d}t, \tag{3.20}$$

$$\psi_{\mathrm{Q}} = \int -R_{\mathrm{Q}} i_{\mathrm{Q}} \mathrm{d}t. \tag{3.21}$$

The ψ_{PM} is given as an input value which corresponds to the rated permanent magnet induced emf (converted to the rotor reference frame) which is the stator emf at open stator condition:

$$e_{\mathrm{PM}} = \psi_{\mathrm{PM}} \omega_{\mathrm{n}}. \tag{3.22}$$

The absolute value of the electromagnetic torque is calculated as a cross product of the stator flux linkage and the stator current:

$$\boldsymbol{T}_{\mathrm{e}} = \frac{3}{2} p \boldsymbol{\psi}_{\mathrm{s}} \times \boldsymbol{i}_{\mathrm{s}}, \tag{3.23}$$

$$T_{\mathrm{e}} = \frac{3}{2} p(\psi_{\mathrm{d}} i_{\mathrm{q}} - \psi_{\mathrm{q}} i_{\mathrm{d}}). \tag{3.24}$$

The per-unit equations are similar but omitting the factor $\frac{3}{2}p$.

3.4 Mechanics

In the main simulations of this thesis a simple equation of motion with a stiff shaft is used:

$$\Omega = \int \frac{T_{\mathrm{turb}} + T_{\mathrm{e}} - D_{\mathrm{tot}}\Omega}{J_{\mathrm{tot}}} \mathrm{d}t, \tag{3.25}$$

where Ω is the mechanical angular velocity, T_{turb} is the torque produced by the prime mover, T_{e} is the electromagnetic torque, D_{tot} is the total system friction coefficient and J_{tot} is the total system moment of inertia. The T_{e} is positive because equation (3.24) yields a negative value in a generator operation. This idealized model is used in the simulations, because it eliminates the need to define shaft stiffness coeffisients for different machines. Also, analyzing the effect of electrical parameters becomes clearer without additional interference coming from the mechanics. In addition, it is easier to automate the parameter survey simulations when there is no oscillation in the mechanics possibly causing instability in the model.

With more specific simulations focusing on a single machine performance, a two mass model is more adequate than the first order system described in equation (3.25). The shaft flexibility and friction may have a quite significant impact on stability. Moreover, with a two mass model, the mechanical resonance frequency can be taken into consideration. The two mass model that can be used optionally in the simulation tool is presented in Figure 3.2.

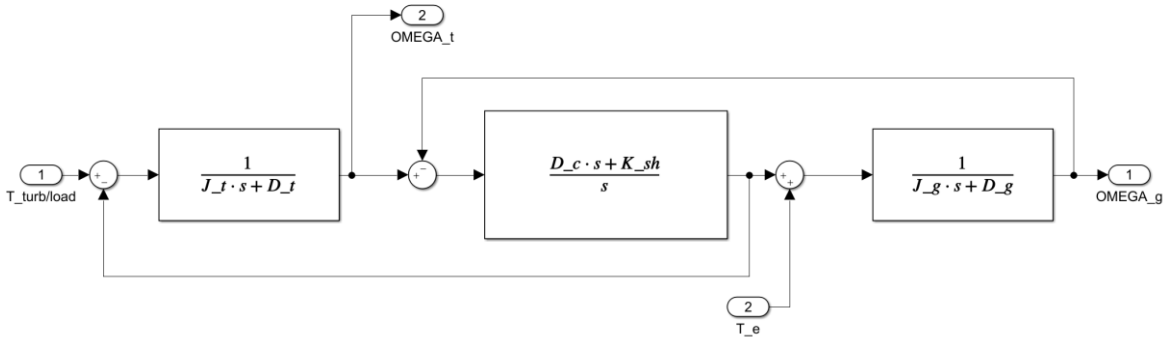

Figure 3.2 Two-mass model.

In the two mass model $J_{\mathrm{t,g}}$ and $D_{\mathrm{t,g}}$ are the moments of inertia and the friction coefficients [Nms/rad] of turbine and generator respectively, D_{c} is the friction coefficient of the

mechanical coupling and the K_{sh} is the shaft stiffness coefficient [Nm/rad]. According to the reference (Saarakkala S. & Hinkkanen M., 2015), the natural torsional resonant frequency is

$$f_{\mathrm{res}} = \frac{1}{2\pi}\sqrt{K_{\mathrm{sh}}\frac{J_{\mathrm{t}}+J_{\mathrm{g}}}{J_{\mathrm{t}}J_{\mathrm{g}}}}. \tag{3.26}$$

For example, with arbitrary values $K_{\mathrm{sh}} = 8 \cdot 10^7 [\mathrm{Nm/rad}]$, $J_{\mathrm{t}} = J_{\mathrm{g}} = 150\ [\mathrm{kgm^2}]$ and $D_{\mathrm{t}} = D_{\mathrm{g}} = D_{\mathrm{t}} = 3\ [\mathrm{Nms/rad}]$, it is obtained that $f_{\mathrm{res}} = 51.98$ Hz. Because of the damping, the actual resonant peak may shift slightly. The bode-diagram with the above mentioned parameters is presented in Figure 3.3, which shows that in this case the friction merely dampens the resonant peak and does not shift the peak almost at all.

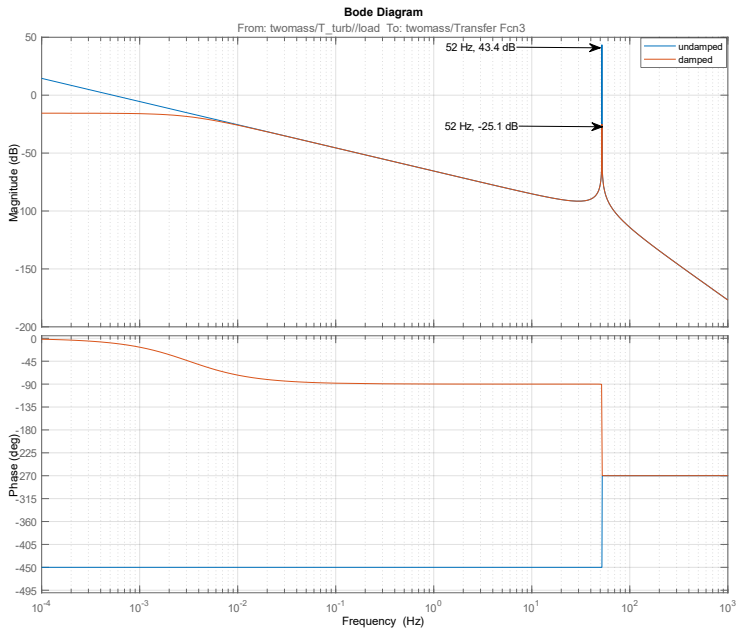

Figure 3.3 Bode-diagram of the two mass model. $K_{\mathrm{sh}} = 8 \cdot 10^7 [\mathrm{Nm/rad}]$, $J_{\mathrm{t}} = J_{\mathrm{g}} = 150\ [\mathrm{kgm^2}]$ and $D_{\mathrm{t}} = D_{\mathrm{g}} = D_{\mathrm{t}} = 3\ [\mathrm{Nms/rad}]$.

Without precise information on the friction caused by the bearings, air or water, the friction coefficients may be determined based on the friction losses which can be evaluated by subtracting the iron losses from the no-load losses. The shaft stiffness coefficient can be obtained by testing how much the shaft twist with a given torque or by calculating based on the shaft dimensions and material properties.

3.5 Grid model

The grid is modelled as an infinite bus, which should be appropriate given that the simulation tool is intended for the DOL PMSGs, which are typically not capable of affecting frequency

and voltage level of a rigid network very significantly (category B). The grid model has three phases with sinusoidal voltages, which are inputs of the generator model and initialized according to a given phase angle difference between the grid voltage and the generator emf before the generator is connected.

For an attempt to simulate island operation, the grid voltage should be generated based on the generator operating point and grid characteristics. The frequency could be set dependent on the power balance of the grid with a given total system inertia similarly as in equations (1.5 – 1.7). For the voltage level, a function that takes into account the load impedance and the generator operation point should be derived.

3.6 Prime mover and governor control

The prime mover characteristics and governor control are completely idealized. The turbine torque is given as an input value to the mechanical model. For frequency response simulations, guidelines for the governor control, water starting time and hammer effect can be found in the IEEE Guide (IEEE, 2011). It is assumed in this thesis that the governor control is not fast enough to give any response during grid connection, fault-ride-though or short-circuit before sustained short-circuit state. The turbine torque as a function of angular velocity resembles a straight line (Kim J. et al., 2017). Therefore, an ideal rough approximation may be given as follows:

$$T_{\mathrm{turb}} = \frac{-T_{\mathrm{n}}}{\Omega_{\mathrm{run}} - \Omega_{\mathrm{n}}} (\Omega - \Omega_{\mathrm{n}}) + T_{\mathrm{n}}, \tag{3.27}$$

Where Ω_{run} is the runaway angular velocity, Ω_{n} the rated angular velocity and T_{n} the rated torque. An example in which $\Omega_{\mathrm{run}} = 3\Omega_{\mathrm{n}}$ is shown in Figure 3.4. The runaway speed of three times the rated speed could be possible in the case of a Kaplan turbine.

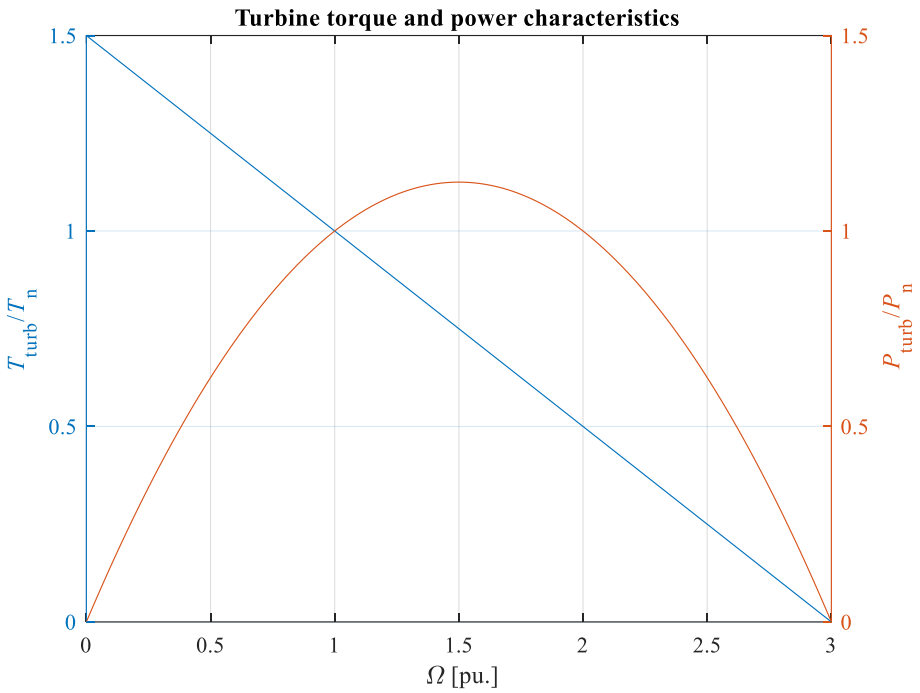

Figure 3.4 An example of idealized turbine torque and power characteristics.

3.7 Temperature dependencies

In the simulation tool, the resistance parameters and PM flux linkage can be adjusted according to the operating temperature. The temperature is estimated separately for stator and rotor based on the apparent power simply as follows:

$$T_{\mathrm{th,s}} = \left(\frac{|S|}{S_{\mathrm{n}}}\right)^{k_{\mathrm{th}}} \left(T_{\mathrm{th,n,s}} - T_{\mathrm{th,0,s}}\right) + T_{\mathrm{th,0,s}} \,, \tag{3.28}$$

$$T_{\mathrm{th,r}} = \left(\frac{|S|}{S_{\mathrm{n}}}\right)^{k_{\mathrm{th}}} \left(T_{\mathrm{th,n,r}} - T_{\mathrm{th,0,r}}\right) + T_{\mathrm{th,0,r}} \,, \tag{3.29}$$

where S is the momentary apparent power, $T_{\mathrm{th,n,s,r}}$ are the stator and rotor steady state temperatures at rated appararent power, $T_{\mathrm{th,0,s,r}}$ are the reference temperatures in which the parameters are defined and k_{th} is a factor that defines the warming characteristics. This approach was chosen because of its simplicity, and the manufacturer of the machines that are introduced in chapter 4. had had some experience in using such an estimate. As the copper losses are proportional to the square of the stator current, iron losses remain roughly constant at different loads and cooling performance might be tuned according to the load, an appropriate value for the k_{th} could be around 1.8. In the simulation tool, no time constants are defined for the temperature changes because the temperature time constants are typically very high (several hours) compared to the durations of the transient events such as grid connection, short circuit and fault-ride-through (a few hundred milliseconds). However, it

should be kept in mind that during e.g. a short circuit the heat generation in the stator may be several times the continuous thermal design value.

In the simulation tool the temperatures can be initialized as desired for the grid connection and updated whenever desired based on the apparent power and then set to a hold. For a more detailed thermal modeling, a thermal resistance and capacitance network approach could be used. However, that would require quite a lot machine specific information and more in-depth knowledge of the loss distribution.

DC resistance is generally defined as

$$R = \rho \frac{l}{A}, \tag{3.30}$$

Where ρ is the electrical resistivity [Ωm], l is the length of the conductor and A is the cross-sectional area of the conductor. From this point of view, the effect of thermal expansion is negligible, so the resitance values can be updated as follows:

$$R_{\mathrm{s}} = R_{T_0,\mathrm{s}}(1 + \alpha_{\mathrm{Cu}}(T_{\mathrm{th,s}} - T_{\mathrm{th},0,s})), \tag{3.31}$$

$$R_{\mathrm{D,Q}} = R_{T_0,\mathrm{r}}(1 + \alpha_{\mathrm{Al}}(T_{\mathrm{th,r}} - T_{0,\mathrm{r}})), \tag{3.32}$$

where $R_{T_0,s,\mathrm{r}}$ are the reference resistance values and $\alpha_{\mathrm{Cu,Al}}$ are the copper (0.0039 [1/°C]) and aluminum (0.0043 [1/°C]) temperature coefficients of resistance, assuming that the stator winding has copper conductors and damper bars are made of aluminum.

Characteristics of a common pemanent magnet material NdFeB NEOREM 576a is shown in Figure 3.5. The PM operation point depends on the external magnetic field strength H and temperature. The operation point should be kept on the right-hand side of the knee point, which marks the point of irreversible demagnetization (Parviainen A. et al., 2010).

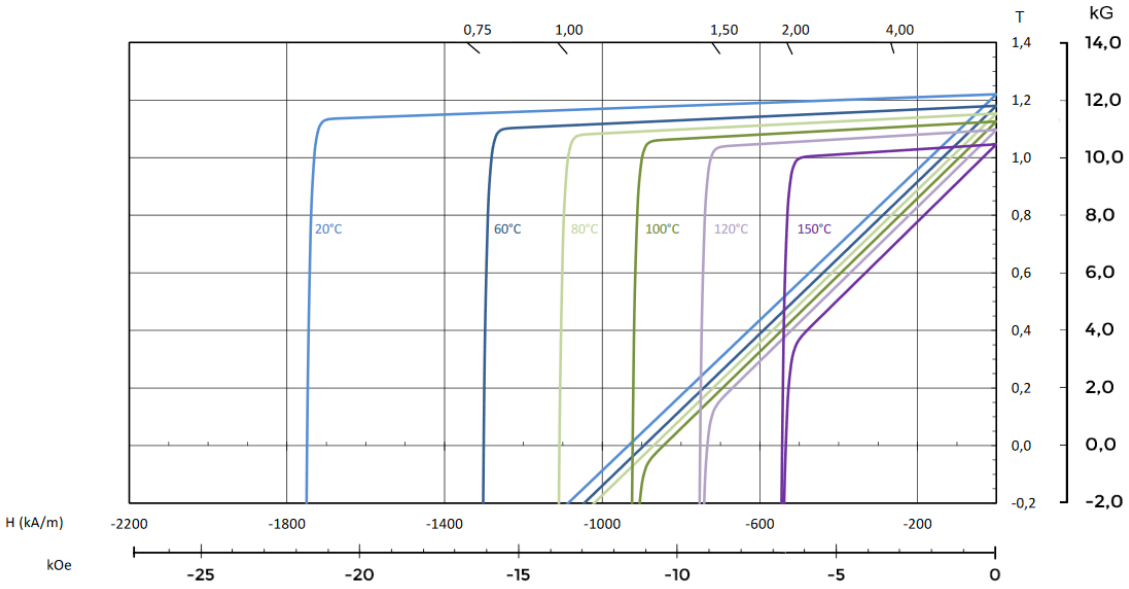

Figure 3.5 NdFeB NEOREM 576a pemanent magnet material demagnetization *J-H* and *B-H* curves at different temperatures (Neorem magnets Oy, 2019).

It can be seen that the magnetic field density *B* decreases somewhat linearly with increasing temperature. The flux linkage is generally given as

$$\psi = k_{\mathrm{w}} N \Phi = k_{\mathrm{w}} N \oiint_S \boldsymbol{B} \cdot \mathrm{d}\boldsymbol{S}, \tag{3.33}$$

where k_{w} is the winding factor, N is the number of turns in a winding, Φ is the magnetic flux, $\boldsymbol{B}$ is the magnetic flux density and $\boldsymbol{S}$ is the vector area the flux passes through. Therefore, the PM flux linkage temperature dependency is modelled in the simulation tool as follows:

$$\psi_{\mathrm{PM}} = \psi_{\mathrm{PM},T_0,\mathrm{r}} \left(1 - \alpha_{\mathrm{PM}} \left(T_{\mathrm{th,r}} - T_{0,\mathrm{r}}\right)\right), \tag{3.34}$$

where $\psi_{\mathrm{PM},T_0,\mathrm{r}}$ is the reference value and α_{PM} is the temperature coefficient based on Figure 3.5. (0.00114 [1/°C]).

3.8 Simulation tool operation

The generator model is driven with voltage and turbine torque references. The operation can be switched from generating to motoring by changing the direction of turbine/load torque (positive is generating). Initially, when the generator is not connected, the $u_{\mathrm{s,d}}$ is set to zero and the $u_{\mathrm{s,q}}$ to e_{PM} while the flux linkages are initialized as $\psi_{\mathrm{d}} = \psi_{\mathrm{D}} = -\psi_{\mathrm{PM}}$ and $\psi_{\mathrm{q}} = \psi_{\mathrm{Q}} = 0$, because the PM flux linkage is present and starts to induce voltage on the q-axis when the machine is accelerated. With this initialization, currents and flux linkage

derivatives become zeros, as they should when the stator is open. However, when the stator is opened while current is flowing in the stator, these initialized values are not valid anymore. This type of event has not yet been implemented in the simulation tool. Nevertheless, a three phase short circuit can be simulated by setting the terminal voltage to zero and the fault-ride-through by injecting the fault-ride-through profile.

The acceleration before grid connection is done with a PID-controller that outputs the turbine torque, which accelerates the generator to a desired speed. The PID is tuned very aggressively to speed up the simulation process. Unrealistic torque values are irrelevant when using the stiff shaft mechanical model. When the generator is connected, the turbine torque is set equal to the friction torque. After the synchronization, the turbine torque can be set as desired using steps or ramps or as described in equation (3.27).

3.8.1 State machine

The model can be operated manually or automatically. With the automation, desired scenarios can be simulated repeatedly in a loop. The automation is realized with a state machine structure. In the state machine, suitable conditions based on slip, load angle fluctuation, damper currents and angular velocity are used to detect steady state and a loss of synchronism.

3.8.2 Vector diagram

A vector diagram is useful for data visualization, which can be helpful in analysis. It can also be used as an indication that the model is working correctly. In the simulation tool the PMSG vector diagram can be plotted and animated. With the animation, a massive amount of simulation data can visualized quite compactly, for example for entertainment purposes. Vectordiagrams of an example PMSG are presented in Figure 3.6.

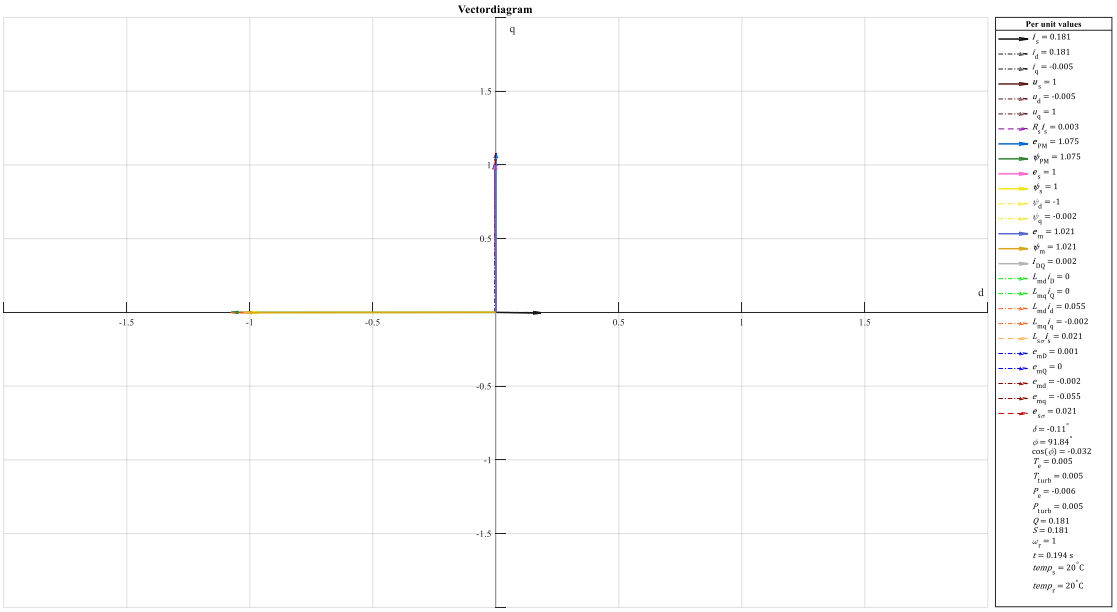
Vectordiagram
q
d
Per unit values
$I_s = 0.181$
$I_d = 0.181$
$I_q = -0.005$
$U_s = 1$
$U_d = -0.005$
$U_q = 1$
$R_s I_s = 0.003$
$e_{PM} = 1.075$
$\psi_{PM} = 1.075$
$e_s = 1$
$\psi_s = 1$
$\psi_d = -1$
$\psi_q = -0.002$
$e_m = 1.021$
$\psi_m = 1.021$
$I_{DQ} = 0.002$
$L_{md} i_D = 0$
$L_{mq} i_Q = 0$
$L_{md} I_d = 0.055$
$L_{mq} I_q = -0.002$
$L_{\sigma s} I_s = 0.021$
$e_{m0} = 0.001$
$e_{mQ} = 0$
$e_{md} = -0.002$
$e_{mq} = -0.055$
$e_{\sigma s} = 0.021$
$\delta = -0.11^{\circ}$
$\phi = 91.84^{\circ}$
$\cos(\phi) = -0.032$
$T_e = 0.005$
$T_{turb} = 0.005$
$P_e = -0.006$
$P_{turb} = 0.005$
$Q = 0.181$
$S = 0.181$
$\omega_r = 1$
$t = 0.194$ s
$temp_s = 20^{\circ}$C
$temp_r = 20^{\circ}$C

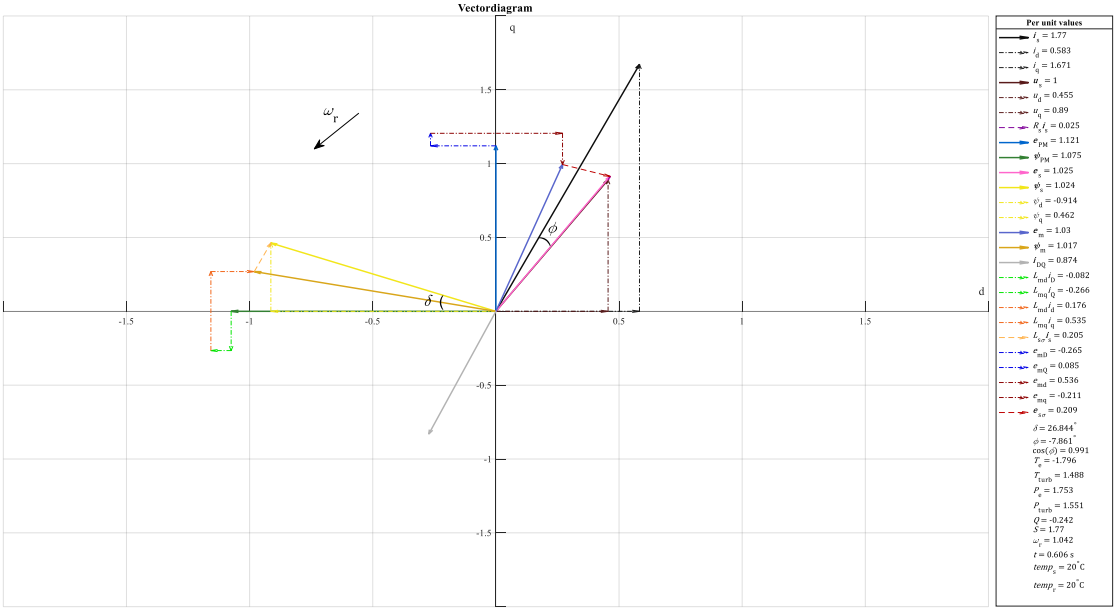
Vectordiagram
q
d
ω_r
ϕ
δ
Per unit values
$I_s = 1.77$
$I_d = 0.583$
$I_q = 1.671$
$U_s = 1$
$U_d = 0.455$
$U_q = 0.89$
$R_s I_s = 0.025$
$e_{PM} = 1.121$
$\psi_{PM} = 1.075$
$e_s = 1.025$
$\psi_s = 1.024$
$\psi_d = -0.914$
$\psi_q = 0.462$
$e_m = 1.03$
$\psi_m = 1.017$
$I_{DQ} = 0.874$
$L_{md} i_D = -0.082$
$L_{mq} i_Q = -0.266$
$L_{md} I_d = 0.176$
$L_{mq} I_q = 0.535$
$L_{\sigma s} I_s = 0.205$
$e_{m0} = -0.265$
$e_{mQ} = 0.085$
$e_{md} = 0.536$
$e_{mq} = -0.211$
$e_{\sigma s} = 0.209$
$\delta = 26.844^{\circ}$
$\phi = -7.861^{\circ}$
$\cos(\phi) = 0.991$
$T_e = -1.796$
$T_{turb} = 1.488$
$P_e = 1.753$
$P_{turb} = 1.551$
$Q = -0.242$
$S = 1.77$
$\omega_r = 1.042$
$t = 0.606$ s
$temp_s = 20^{\circ}$C
$temp_r = 20^{\circ}$C

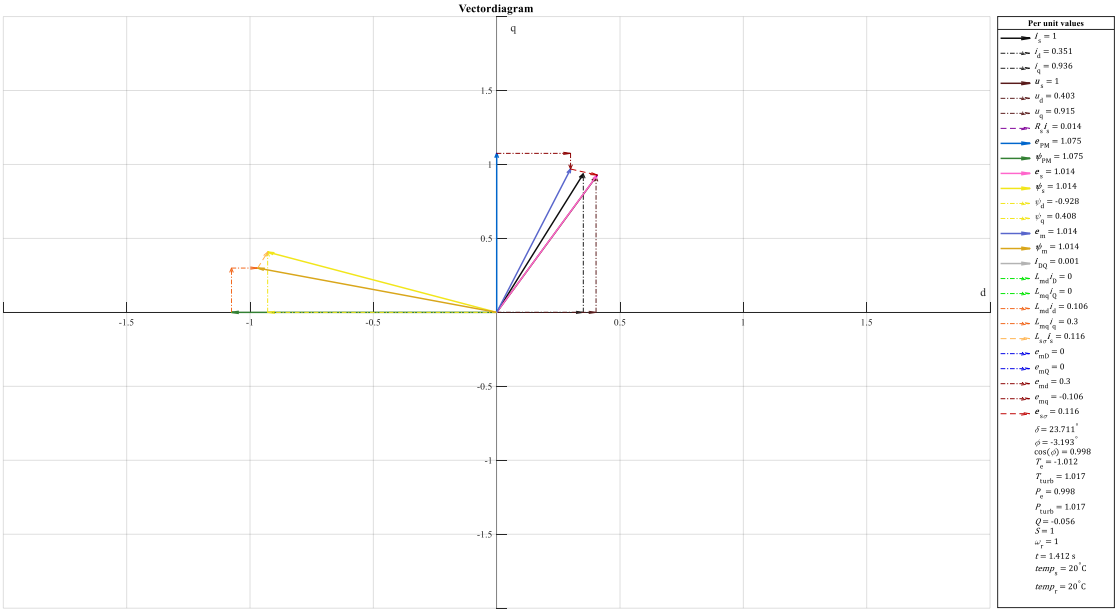
Vectordiagram
q
d
Per unit values
$I_s = 1$
$I_d = 0.351$
$I_q = 0.936$
$U_s = 1$
$U_d = 0.403$
$U_q = 0.915$
$R_s I_s = 0.014$
$e_{PM} = 1.075$
$\psi_{PM} = 1.075$
$e_s = 1.014$
$\psi_s = 1.014$
$\psi_d = -0.928$
$\psi_q = 0.408$
$e_m = 1.014$
$\psi_m = 1.014$
$I_{DQ} = 0.001$
$L_{md} i_D = 0$
$L_{mq} i_Q = 0$
$L_{md} I_d = 0.106$
$L_{mq} I_q = 0.3$
$L_{\sigma s} I_s = 0.116$
$e_{m0} = 0$
$e_{mQ} = 0$
$e_{md} = 0.3$
$e_{mq} = -0.106$
$e_{\sigma s} = 0.116$
$\delta = 23.711^{\circ}$
$\phi = -3.193^{\circ}$
$\cos(\phi) = 0.998$
$T_e = -1.012$
$T_{turb} = 1.017$
$P_e = 0.998$
$P_{turb} = 1.017$
$Q = -0.056$
$S = 1$
$\omega_r = 1$
$t = 1.412$ s
$temp_s = 20^{\circ}$C
$temp_r = 20^{\circ}$C

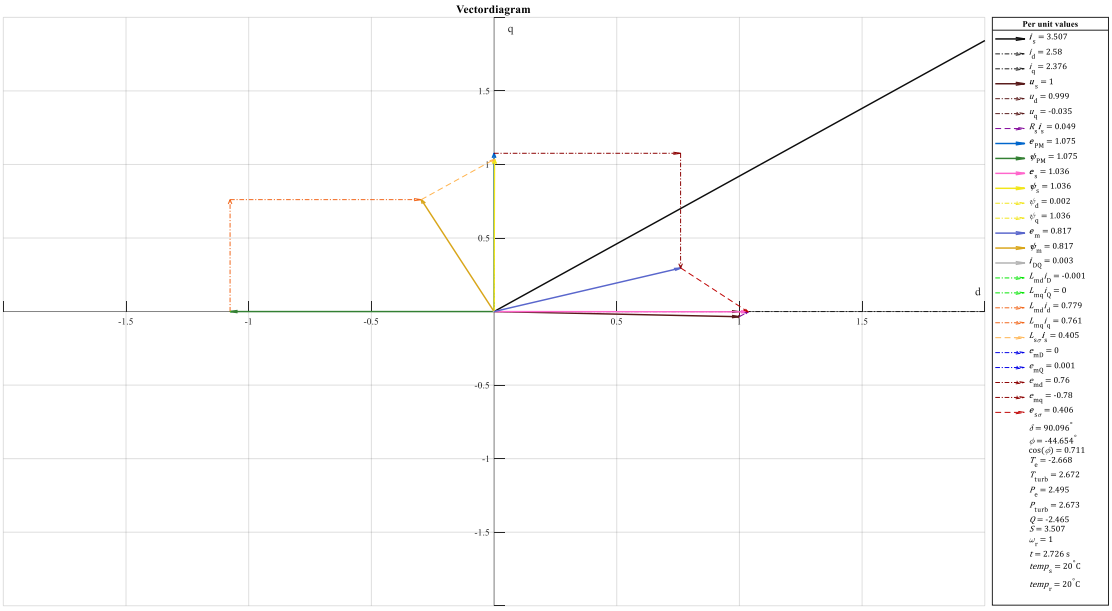

Figure 3.6 Vector diagrams of a PMSG from top to bottom no-load, transient, steady state near rated point and steady state near maximum load. Load-angle δ, the angle between current and voltage ϕ and angular velocity of the reference frame ω_r direction are marked in the transient figure.

Stator and PM flux linkages, stator and damper currents, stator voltage and torques are obtained directly from the core model for the vector diagram. Stator resistance voltage drop, damper and armature reactions and stator leakage flux linkage are calculated simply as shown in the legends. The electrical power is calculated as follows:

$$\boldsymbol{S} = \frac{3}{2}\left(i_\mathrm{d} - i_\mathrm{q}\mathrm{j}\right) \cdot \left(u_\mathrm{s,d} + u_\mathrm{s,q}\mathrm{j}\right), \tag{3.35}$$

and the stator emf

$$\boldsymbol{e}_\mathrm{s} = \left(\psi_\mathrm{q}\omega_\mathrm{r} - \frac{\mathrm{d}\psi_\mathrm{d}}{\mathrm{d}t}\right) + \left(-\psi_\mathrm{d}\omega_\mathrm{r} - \frac{\mathrm{d}\psi_q}{\mathrm{d}t}\right)\mathrm{j}. \tag{3.36}$$

The other induced voltages corresponding to damper and armature reaction and stator leakage flux linkages, are obtained by calculating the derivatives numerically in the stator reference frame. This is an easy solution but causes some numerical inaccuracy in the vector diagram. The inaccuracy does not affect the actual model behaviour, so it is not critical. Furthermore, the inaccuracy can be mitigated by decreasing the time step size. At steady state, the load-angle δ marked in the figure between the $\boldsymbol{\psi}_\mathrm{s}$ and the $\boldsymbol{\psi}_\mathrm{PM}$ is almost the same as the angle between the $\boldsymbol{u}_\mathrm{s}$ and the $\boldsymbol{e}_\mathrm{PM}$. The stator resistance causes a small deviation.

3.9 Considerations

In practice, the amount of details in the model must be appropriately limited. Otherwise, the number of input parameters may become impractical, the performance of the model may suffer too much and the risk of unexpected conflicts such as numerical errors, unsolvable algebraic loops and convergence issues may increase. This chapter briefly discusses probably the most significant simplifications of the generator model.

3.9.1 Time step

Differential equations are solved numerically step by step, which may cause very significant calculation errors if the time step is set to be too large. The selection of suitable time step is a trade-off between performance and accuracy. The highest frequency and the lowest time constant of the system can be used as a guideline. One method is to decrease the time step until no significant changes in the behaviour of the model can be observed. In Simulink®, it is possible to use a variable-step solver and specify the suitable max. step size and tolerance. The variable-step approach can significantly increase performance without losing accuracy. The default solving method in the variable-step solver of the used Simulink® version is Dormand-Prince.

3.9.2 Saturation

In ferromagnetic materials, magnetic domains that contain already perfectly aligned magnetic dipole moments, tend to align with an external magnetic field allowing greatly increased magnetic field density compared to what is possible in vacuum. In the virgin state of the material, the magnetic domains cancel each other on average when viewed from outside the object. The realignment of the domains depends on the external field strength, temperature and mechanical disturbance. Increasing the magnetic field density by increasing the external field strength becomes more and more difficult when approaching the point where all the domains are aligned, after which the added external field magnetizes only air, which has almost a negligible effect. This is called saturation and from the modelling point view this means that the inductances should actually be dependent on the currents. Furthermore, the saturation as a phenomenon contradicts one of the main principles of the two-axis theory that is the decoupling of direct and quadrature axes. In order to accurately present the saturation of a machine, the effect of cross-saturation usually cannot be neglected. The cross-saturation can be interpreted so that the d-axis currents saturate the q-axis inductances and

vice versa. It should be noted that the cross-saturation characteristics are quite machine specific and can be somewhat unpredictable without FEA results.

Starting point for implementing saturation in the model could be neglecting the effect on leakage inductances and considering only the magnetizing inductances because the flux path from which the leakage inductances are derived include more air, so they are not as heavily affected by the saturation. For a steady state operation, the static magnetizing inductances $L_{\mathrm{md,q}}$ could be updated based on the operating point and a look-up-table created from inductance surfaces $L_{\mathrm{md}} = f(i_{\mathrm{md}}, i_{\mathrm{mq}})$ and $L_{\mathrm{mq}} = f(i_{\mathrm{md}}, i_{\mathrm{mq}})$ computed with FEM. Also, the PM flux linkage ψ_{PM} should be adjusted accordingly to the L_{md} because the virtual PM current i_{PM} remains constant. According to the reference (Kaukonen J., 1999), new dynamic inductance parameters and differential equations are needed for transient operation. The air gap flux linkage differentials with the new parameters in that case are given as follows:

$$\frac{\mathrm{d}\psi_{\mathrm{md}}}{\mathrm{d}t} = L_{\mathrm{Md}} \frac{\mathrm{d}i_{\mathrm{md}}}{\mathrm{d}t} + L_{\mathrm{dq}} \frac{\mathrm{d}i_{\mathrm{mq}}}{\mathrm{d}t}, \tag{3.37}$$

$$\frac{\mathrm{d}\psi_{\mathrm{mq}}}{\mathrm{d}t} = L_{\mathrm{Mq}} \frac{\mathrm{d}i_{\mathrm{mq}}}{\mathrm{d}t} + L_{\mathrm{qd}} \frac{\mathrm{d}i_{\mathrm{md}}}{\mathrm{d}t}, \tag{3.38}$$

$$L_{\mathrm{Md}} = L_{\mathrm{md}}^{\mathrm{d}} \cos^2(\gamma) + L_{\mathrm{md}} \sin^2(\gamma), \tag{3.39}$$

$$L_{\mathrm{Mq}} = L_{\mathrm{mq}}^{\mathrm{d}} \sin^2(\gamma) + L_{\mathrm{mq}} \cos^2(\gamma), \tag{3.40}$$

$$L_{\mathrm{dq}} = (L_{\mathrm{md}}^{\mathrm{d}} - L_{\mathrm{md}}) \sin(\gamma) \cos(\gamma), \tag{3.41}$$

$$L_{\mathrm{qd}} = (L_{\mathrm{mq}}^{\mathrm{d}} - L_{\mathrm{mq}}) \sin(\gamma) \cos(\gamma), \tag{3.42}$$

where $L_{\mathrm{Md,q}}$ are the magnetizing inductances including an incremental inductance change during a transient, $L_{\mathrm{dq,qd}}$ are the cross-coupling inductances, $L_{\mathrm{md,q}}^{\mathrm{d}}$ are the tangent slope dynamic magnetising inductances from a $(i_{\mathrm{m}}, \psi_{\mathbf{m}})$ magnetizing curve and γ is the angle between $\boldsymbol{i}_{\mathrm{m}}$ and the d-axis (Kaukonen J., 1999).

3.9.3 Iron losses

In order to obtain more accurate efficiency numbers with the model, the iron losses should be taken into account. The iron losses usually refer to the losses in the stator core. However, from the perspective of more accurate thermal modelling, for example, losses of the similar type in the permanent magnets should also be evaluated.

It seems to be quite common to neglect the iron losses in synchronous machine models. The reason for this is that the iron losses in DOL SMs are typically small in comparison to the copper losses and the fluctuation is relatively small because of the almost constant frequency. Also, the iron losses as a phenomenon is not very well compatible with the two-axis theory. It is not completely clear what would be the best way to implement the iron losses to the dynamics. An equivalent iron loss resistance could be used. Another possible simple approach could be calculating the iron losses separately with some variant of Bertotti's loss model based on the operating point and adding the result as an equivalent virtual friction to the mechanical model.

3.9.4 Harmonics

The harmonic distortion in DOL generators is typically not one of the main concerns at least from the stability point of view, especially when short pitching and skewing are used to cancel the most significant harmonic frequencies. However, one possible starting point for including harmonic frequencies to the model is shown in Figure 3.7.

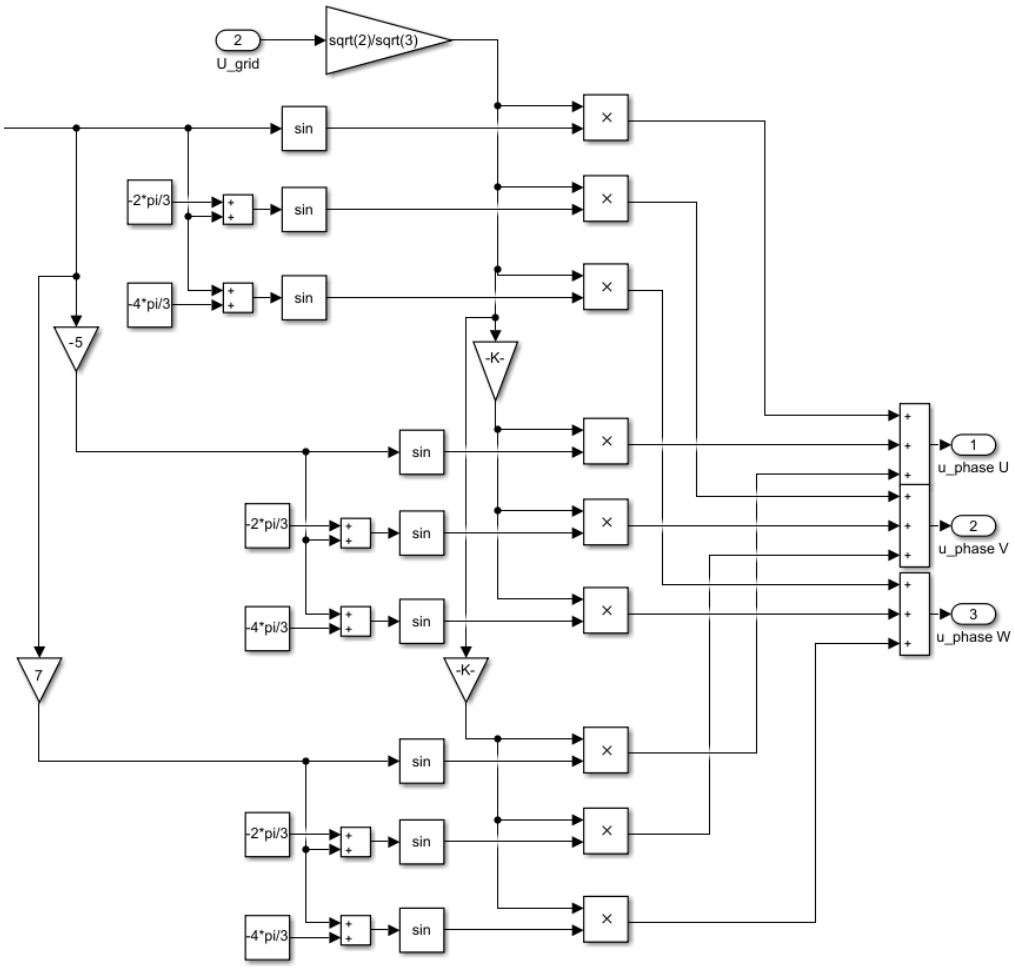

Figure 3.7 Possible approach to modelling the effect of harmonics.

By simply summing the harmonics to the grid voltage reference, the effect passes down all the way to the electromagnetic torque creating torque ripple. This could enable interesting demonstrations with the two-mass model. However, the reliability of this approach might be a bit questionable. At least one concern is that the effect of stray capacitances become increasingly more significant with higher frequencies. The harmonic distortion in the current should become accordingly scaled based on the inductances, but this is not tested or studied in this thesis any further.

4. SIMULATION AND DISCUSSION

In this chapter, the model is validated, and the main results of this thesis are presented.

4.1 Model validation

The model is validated by comparing the simulated current waveform to the measured current waveform obtained from a real-world incident. In addition, figures of maximum current as a function of phase angle difference in grid connection, active power reduction with decreasing frequency and constant turbine torque, torque as a function of load-angle at different $L_\mathrm{d}/L_\mathrm{q}$ ratios and reactive power as a function of active power in a rigid network are produced with the model to see that the curves match the expected typical behaviour.

4.1.1 Grid connection with a phase opposition

In the incident, a PMSG was reportedly connected to a grid with a phase difference of 180 degrees between the grid voltage and the induced emf. This is a quite extreme transient event because the momentary voltage across the stator resistance is at maximum with a given rotational speed. The reported machine parameters are shown in Table 4.1.

Table 4.1 Reported parameters of the PMSG that was connected with a phase difference of 180 degrees.

Quantity	SI unit value	Per unit value
Rated active power P_n	600 kW	
Rated frequency f_n	50 Hz	
Rated rotational speed	300 rpm	
PM induced voltage (line-to-line) E_PM	430 V	
Rated current I_n	890 A	
DC resistance R_s	3.642 mΩ	0.0140
d-axis synchronous inductance L_d	345 µH	0.4177
q-axis synchronous inductance L_q	360 µH	0.4359
Sustained short-circuit current i_ssc	3077 A	
Sub-transient short circuit current i_s''	8235 A	
Sub-transient reactance X_d''	0.030 Ω	0.1156
Sub-transient time constant τ_d''	0.05 s	
Damper winding reactance referred to stator	0.081 Ω	0.3122
Damper winding resistance referred to stator	8.97 mΩ	0.0346
Generator moment of inertia J	157 kgm^2	

The given parameter list is not entirely complete and directly compatible for the created model. The stator leakage inductance and separate damper winding parameters for the d and q axes are not available. Also, it seems that the i_ssc is a peak value rather than rms value considering the d-axis total inductance can be approximated (R_s neglected) as

$$L_\mathrm{d} \approx \frac{\frac{E_\mathrm{PM}}{\sqrt{3}}}{\omega_\mathrm{s}\frac{i_\mathrm{ssc,peak}}{\sqrt{2}}} = \frac{\frac{430\ \mathrm{V}}{\sqrt{3}}}{2{\cdot}\pi{\cdot}50\ \mathrm{Hz}\cdot\frac{3077\ \mathrm{A}}{\sqrt{2}}} = 363\ \mu\mathrm{H}. \tag{4.1}$$

If the reported i_ssc was rms value, the L_d would contradict too much. On the other hand, the X_d'' seems to correspond to the i_s'' as follows

$$L_\mathrm{d}'' = \frac{X_\mathrm{d}''}{\omega_\mathrm{s}} \approx \frac{\frac{E_\mathrm{PM}}{\sqrt{3}}}{\omega_\mathrm{s} i_\mathrm{s}''} = \frac{\frac{430\ \mathrm{V}}{\sqrt{3}}}{2{\cdot}\pi{\cdot}50\ \mathrm{Hz}\cdot 8235\ \mathrm{A}} = \frac{0.0301\ \Omega}{2{\cdot}\pi{\cdot}50\ \mathrm{Hz}} = 95.86\ \mu\mathrm{H}. \tag{4.2}$$

Some manipulation and possibly trial and error are required in order to reproduce the grid connection incident. The problem is that the parameters listed correspond to the test and the conditions under which they were determined. The accuracy of the same parameters in different situations vary. Moreover, the error margins of the parameters are unknown. For example, if a sudden short-circuit test were used, it is not clear whether temperature corrections were made and whether the slight speed fluctuation in the test were taken into account.

According to the reference (Kinnunen J., 2007), the sub-transient inductances of the model can be expressed as a series connection of stator leakage and parallel connection of magnetizing and damper leakage inductances:

$$L_\mathrm{d}'' = L_{\mathrm{s}\sigma} + \frac{L_\mathrm{md} L_{\mathrm{D}\sigma}}{L_\mathrm{md} + L_{\mathrm{D}\sigma}}, \tag{4.3}$$

$$L_\mathrm{q}'' = L_{\mathrm{s}\sigma} + \frac{L_\mathrm{mq} L_{\mathrm{Q}\sigma}}{L_\mathrm{mq} + L_{\mathrm{Q}\sigma}}, \tag{4.4}$$

where $L_\mathrm{md} = L_\mathrm{d} - L_{\mathrm{s}\sigma}$, $L_\mathrm{mq} = L_\mathrm{q} - L_{\mathrm{s}\sigma}$, $L_{\mathrm{D}\sigma} = L_\mathrm{D} - L_\mathrm{md}$ and $L_{\mathrm{Q}\sigma} = L_\mathrm{Q} - L_\mathrm{mq}$. The sub-transient time constants can be calculated as the ratio of inductance to resistance in a closed-circuit stator winding:

$$\tau_\mathrm{d}'' = \frac{1}{R_\mathrm{D}}\left(\frac{L_\mathrm{md} L_{\mathrm{s}\sigma}}{L_\mathrm{md} + L_{\mathrm{s}\sigma}} + L_{\mathrm{D}\sigma}\right), \tag{4.5}$$

$$\tau_\mathrm{q}'' = \frac{1}{R_\mathrm{Q}}\left(\frac{L_\mathrm{mq} L_{\mathrm{s}\sigma}}{L_\mathrm{mq} + L_{\mathrm{s}\sigma}} + L_{\mathrm{Q}\sigma}\right). \tag{4.6}$$

The damper winding inductances are calculated from the listed damper winding reactance with a 50 Hz frequency

$$L_\mathrm{D,Q} = \frac{0.081\ \Omega}{2\pi{\cdot}50\ \mathrm{Hz}} = 258\ \mu\mathrm{H}. \tag{4.7}$$

If the stator leakage is solved from (4.3), it is obtained that $L_{s\sigma} = 91.37\ \mu H$, $L_{md} = 253.63\ \mu H$, $L_{mq} = 268.63\ \mu H$, $L_{D\sigma} = 258\ \mu H - 253.63\ \mu H = 4.20\ \mu H$ and $L_{Q\sigma} = 258\ \mu H - 268.63\ \mu H = -10.80\ \mu H$. As the $L_{D\sigma}$ is quite small and the $L_{Q\sigma}$ becomes negative, in this case the damper winding total inductances are set equal to the magnetizing inductances, i.e. $L_{D\sigma} = L_{Q\sigma} = 0$. This might be a bit coarse assumption, but must suffice because no more detailed information is available and using the sub-transient constant equation also produce negative inductances. Now it is obtained that $L_{s\sigma} = L''_d = \frac{0.030\ \Omega}{2 \cdot \pi \cdot 50} = 95.49\ \mu H$, $L_{md} = 345\ \mu H - 95.49\ \mu H = 249.51\ \mu H$, $L_{mq} = 360\ \mu H - 95.49\ \mu H = 264.51\ \mu H$.

Without further information the same damper winding resistance could be used on the d and q axes, but according to the manufacturer, the d-axis damper winding resistance is most likely higher that the q-axis resistance. Based on a brief testing in which the damper winding resistances were varied around the initial value $R_{D,Q} = 8.97\ m\Omega$ while comparing the recorded and simulated waveforms, the resistances were set to $R_Q = 8.97\ m\Omega$ and $R_D = 9.60\ m\Omega$. The calculated time constants according to (4.5) and (4.6) are then $\tau''_d = 0.0072$ s, which differs from the listed value quite a lot, and $\tau''_q = 0.0078$ s. With regard to the stator resistance, skin and proximity effects make the AC-resistance larger than the DC-resistance. The significancy of these effects depend on the frequency, the conductors used and their arrangement. In this case, the effect is assumed negligible, i.e. the AC resistance is equal to the DC resistance.

The turbine moment of inertia in this demonstration is set to 60 % of the inertia of the generator so the total moment of inertia is $0.6 \cdot 157\ kgm^2 + 157\ kgm^2 = 251.2\ kgm^2$. The total friction is set to 3 Nms/rad. The reported grid voltage and frequency were 405 V line-to-line and 50 Hz. In the simulation the temperature is set to 20 °C because the machine is probably cool when synchronized. The recorded incident and simulation of the same case is shown in Figure 4.1.

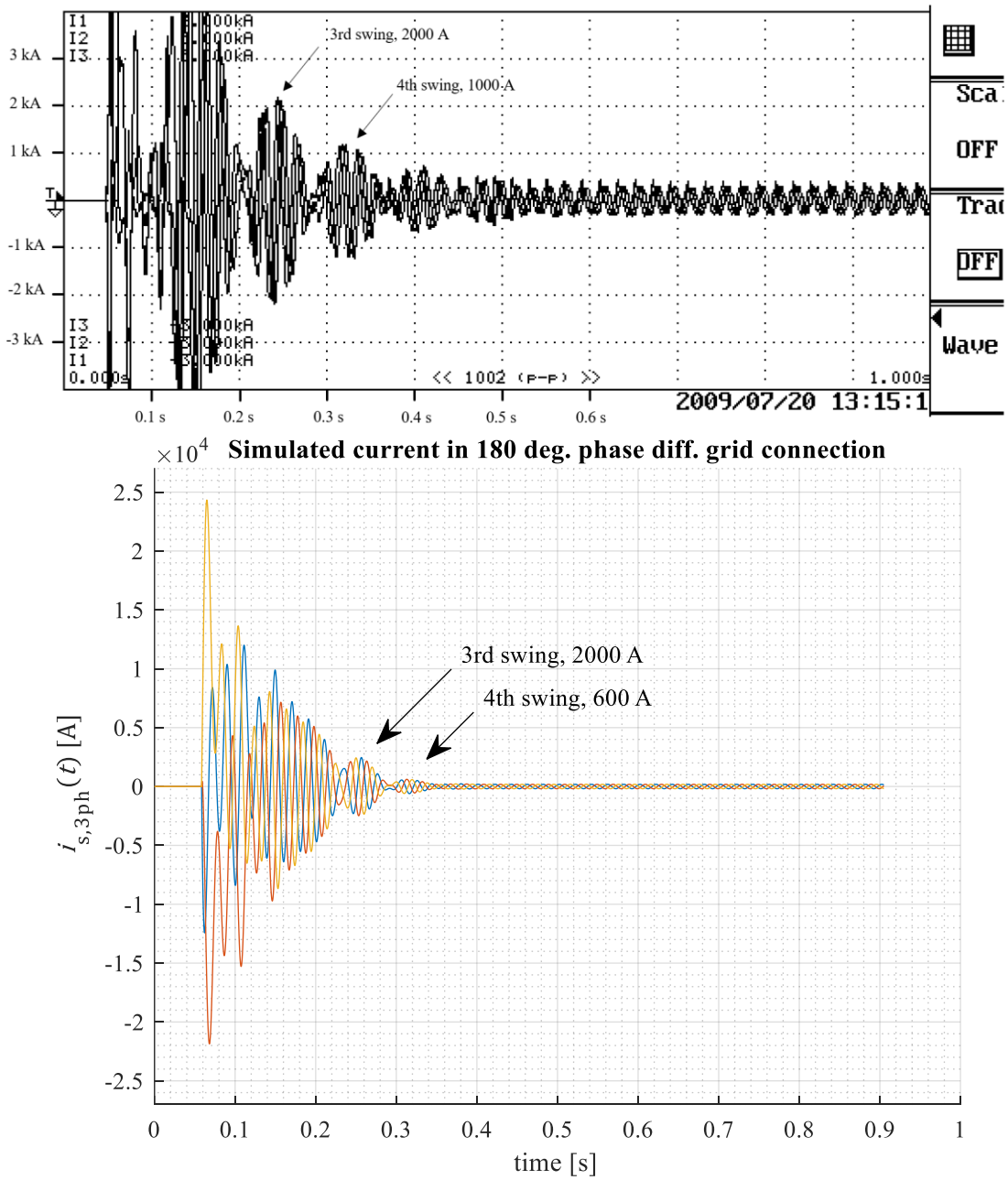

Figure 4.1 Recorded (top) and simulated PMSG grid connection with a phase difference of 180 degrees between the grid voltage and the induced emf. $L_{s\sigma} = 95.49\ \mu H$ (0.1156 pu.), $L_{md} = 249.51\ \mu H$ (0.3021 pu.), $L_{mq} = 264.51\ \mu H$ (0.3202 pu.), $L_{D\sigma} = L_{Q\sigma} = 0$, $J_{tot} = 251.2\ kgm^2$, $D_{tot} = 3\ Nms/rad$, $R_s = 0.0036\ \Omega$ (0.0140 pu.), $R_D = 9.60\ m\Omega$ (0.0370 pu.) $R_Q = 8.97\ m\Omega$ (0.0346 pu.).

It can be seen, that both the recorded and simulated current have a similar pattern where the amplitudes of the currents vary periodically. In the recorded figure the scale is limited because current probes with a rated value of 2 kA were used. Comparing the peaks in the beginning is not possible. In the simulation the first two swings are not as clearly distinguishable from each other. The simulation attenuates roughly as fast as the recorded waveform even though the calculated time constant differs from the listed value. Unfortunately,

the sudden short circuit test curves of the machine are not available, so it is not possible to verify the listed value.

Even better resemblance could likely be achieved by fine tuning the parameters, but it is not worth it with the limited available information. Also, it should be remembered that the model has simplifications. For example, the recorded waveform is distorted by the harmonics and the simulated is not. Also, saturation, temperature changes during the event and grid properties affect the waveform.

4.1.2 PMSG operation characteristics

In Figures 4.2-4.7, a few characteristic curves of a PMSG are presented. The figures are produced with the simulation tool by simply giving inputs and taking readings.

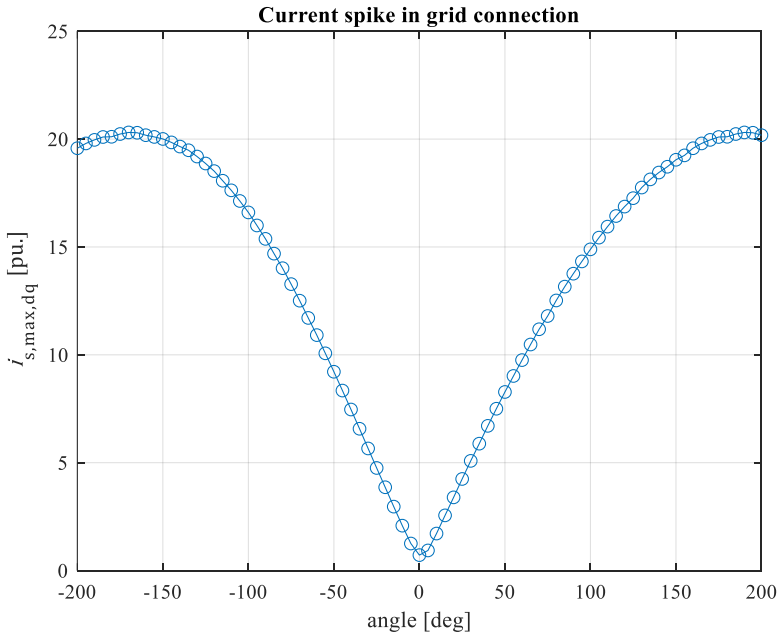

Figure 4.2 Simulated maximum current spike in grid connection with different grid voltage and emf phase difference angles. $U_{LL} = 400$ V, $E_{PM,ph} = 248$ V, $f = 50$ Hz, $p = 10$, $L_{s\sigma} = 95.49$ µH (0.1156 pu.), $L_{md} = 249.51$ µH (0.3021 pu.), $L_{mq} = 264.51$ µH (0.3202 pu.), $L_{D\sigma} = L_{Q\sigma} = 0$, $J_{tot} = 251.2$ kgm^2, $D_{tot} = 3$ Nms/rad, $R_s = 0.0036$ Ω (0.0140 pu.), $R_D = 9.60$ mΩ (0.0370 pu.) $R_Q = 8.97$ mΩ (0.0346 pu.).

It can be seen in Figure 4.2 that the higher the angular difference, the higher the current peak. With positive values the emf is leading before the connection. The highest current value is found at around 180 °, which is as expected because the instantaneous voltage across the stator resistance is the highest at that time instance. When interpreting the figure, it is important to note that the curve is not perfectly symmetrical. For example, at -50° the spike is 9.216 pu. and at 50° it is 8.279 pu. This happens because with angle values somewhat close to 0° when the emf is lagging, the modelled machine initially accelerates to match the grid

voltage and correspondingly decelerates when the emf is leading. With angle values closer to 180° the direction of the initial torque pulse is not as clear. Basically, it is decided by how the resulting current vector aligns with the stator flux linkage vector.

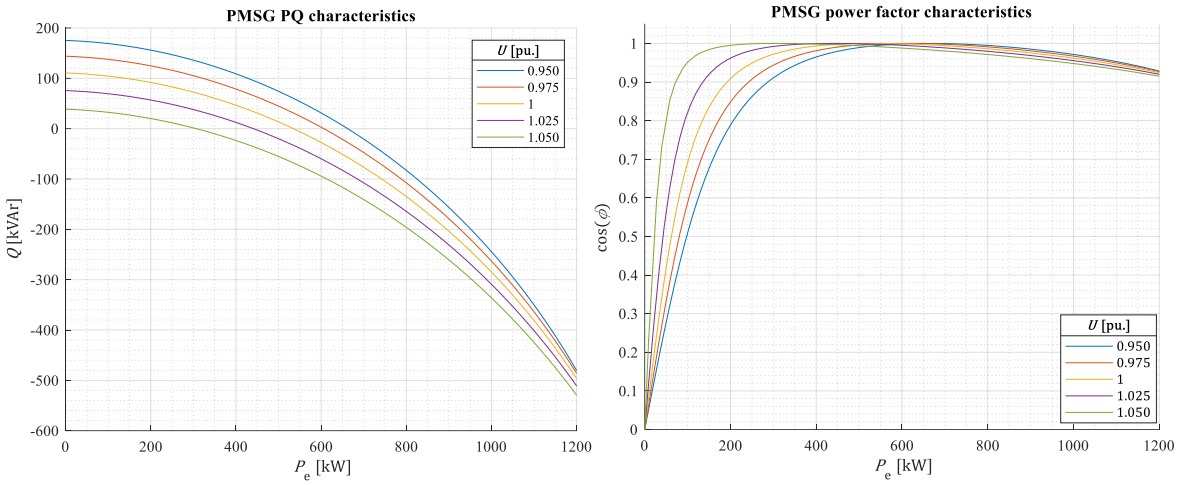

Figure 4.3 Simulated reactive power and power factor as a function active power with different grid voltage levels in rigid network. $U_{\mathrm{LL}} = \frac{\sqrt{3}u_{\mathrm{peak,ph}}}{\sqrt{2}} = 400$ V (1 pu.), $E_{\mathrm{PM,ph}} = 248$ V, $f = 50$ Hz, $p = 10$, $L_{\mathrm{s}\sigma} = 95.49$ µH (0.1156 pu.), $L_{\mathrm{md}} = 249.51$ µH (0.3021 pu.), $L_{\mathrm{mq}} = 264.51$ µH (0.3202 pu.), $L_{\mathrm{D}\sigma} = L_{\mathrm{Q}\sigma} = 0$, $J_{\mathrm{tot}} = 251.2$ kgm^2, $D_{\mathrm{tot}} = 3$ Nms/rad, $R_{\mathrm{s}} = 0.0036$ Ω (0.0140 pu.), $R_{\mathrm{D}} = 9.60$ mΩ (0.0370 pu.) $R_{\mathrm{Q}} = 8.97$ mΩ (0.0346 pu.).

The PQ and $\cos(\varphi)$ curves produced with the simulation tool in Figure 4.3 match the typical behaviour of a PMGS. The curves are similar to those in the reference (Parviainen A. et al., 2010). At low loads, the machine is overexcited and supplies some reactive power to the grid. The point $\cos(\varphi) = 1$ is found before or slightly after the rated load (600 kW) depending on the grid voltage, and after that the machine becomes under-excited. When the generator is under-excited, the current is leading the voltage and vice versa, which can be seen from the vector diagrams in Figure 3.6 and confirmed by the equation of apparent power.

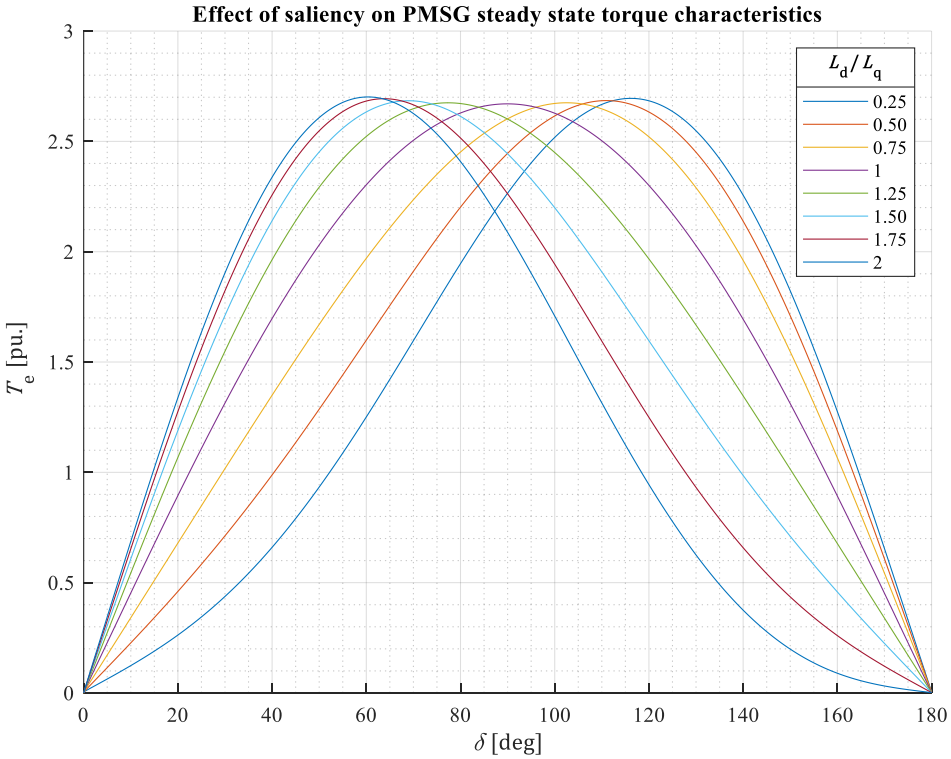

Figure 4.4 Simulated torque as a function load-angle with different inductance ratios. $U_{LL} = 400$ V, $E_{PM,ph} = 248$ V, $f = 50$ Hz, $p = 10$, $L_{s\sigma} = 95.49$ µH (0.1156 pu.), $L_{md} = 249.51$ µH (0.3021 pu.), $L_{mq} = 264.51$ µH (0.3202 pu.), $L_{D\sigma} = L_{Q\sigma} = 0$, $J_{tot} = 251.2$ kgm^2, $D_{tot} = 3$ Nms/rad, $R_s = 0.0036$ Ω (0.0140 pu.), $R_D = 9.60$ mΩ (0.0370 pu.) $R_Q = 8.97$ mΩ (0.0346 pu.).

Figure 4.4 is produced by controlling the turbine torque so that the readings could be taken when the machine is running at synchronous speed. With the simulation tool, even the unstable region can be driven quite smoothly because the turbine torque can be set as desired. Similar curves could also have been plotted by using the well-known torque equation (4.8), so the model behaves as expected here as well. The maximum steady state torque is roughly normalized by solving the inductance values with a desired ratio from the equation of the maximum torque which can be derived from the load-angle equation for synchronous machines:

$$T_e = \frac{m}{\Omega}\left(\frac{E_{PM,ph}U_{ph}}{\omega_s L_d}\sin(\delta) + \frac{U_{ph}^2(L_d - L_q)}{2\omega_s(L_q L_d)}\sin(\delta)\right), \tag{4.8}$$

where δ is the load angle and m is the number of phases (Gieras J.F. & Wing M., 1997), (Parviainen A., 2005). The sentence for maximum steady state torque is obtained by solving the δ from $\frac{\partial T_e}{\partial \delta} = 0$ and substituting the δ back to (4.8). The solution for the δ must be chosen so that the inductances become positive real numbers. This equation neglects the effect of stator resistance and therefore assumes that the grid voltage is exactly equal to the stator flux

linkage induced emf, which makes the angle between the $E_{\mathrm{PM,ph}}$ and U_{ph} the same as the angle between the ψ_{s} and ψ_{PM}. In the simulation tool, the R_{s} is not neglected and the precise value of the T_{e} would be found by replacing the U_{ph} with $E_{\mathrm{s,ph}}$ and using the corresponding angle. However, the symbolic equation for maximum steady state torque which would take the R_{s} into account would be much more complex because the $E_{\mathrm{s,ph}}$ depends on the voltage drop in the R_{s}.

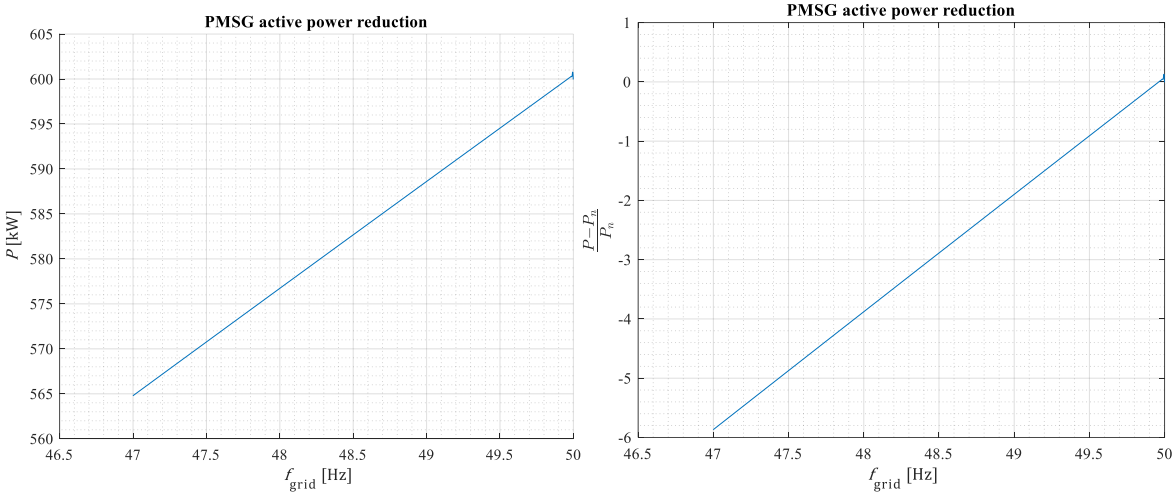

Figure 4.5 Simulated active power reduction with decreasing frequency and constant turbine torque. $U_{\mathrm{LL}} = 400\ \mathrm{V}$, $E_{\mathrm{PM,ph}} = 248\ \mathrm{V}$, $p = 10$, $L_{\mathrm{s}\sigma} = 95.49\ \mu\mathrm{H}$ (0.1156 pu.), $L_{\mathrm{md}} = 249.51\ \mu\mathrm{H}$ (0.3021 pu.), $L_{\mathrm{mq}} = 264.51\ \mu\mathrm{H}$ (0.3202 pu.), $L_{\mathrm{D}\sigma} = L_{\mathrm{Q}\sigma} = 0$, $J_{\mathrm{tot}} = 251.2\ \mathrm{kgm^2}$, $D_{\mathrm{tot}} = 3\ \mathrm{Nms/rad}$, $R_{\mathrm{s}} = 0.0036\ \Omega$ (0.0140 pu.), $R_{\mathrm{D}} = 9.60\ \mathrm{m\Omega}$ (0.0370 pu.) $R_{\mathrm{Q}} = 8.97\ \mathrm{m\Omega}$ (0.0346 pu.).

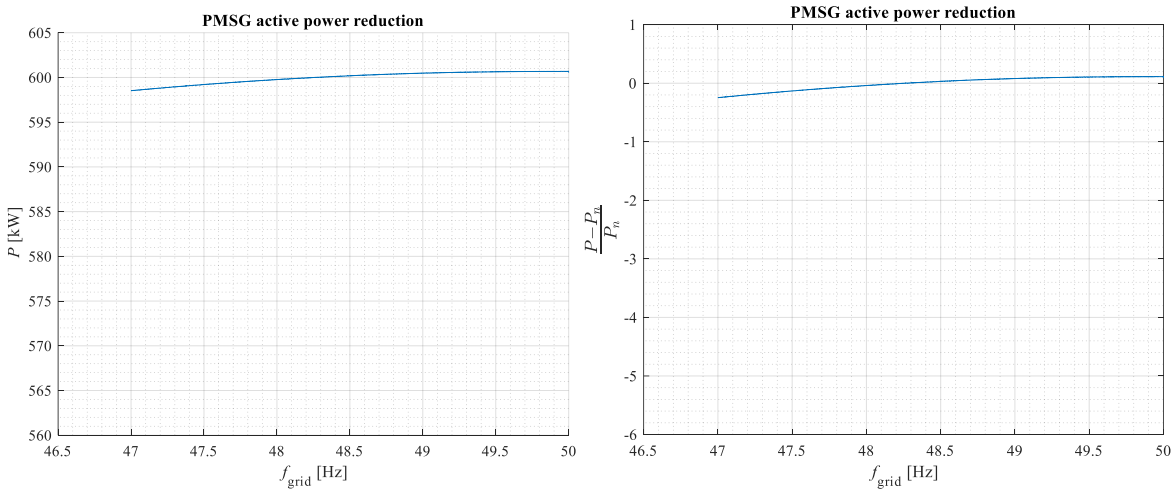

Figure 4.6 Simulated active power reduction with decreasing frequency and speed dependent turbine torque according to equation (3.27) using $\Omega_{\mathrm{run}} = 2\Omega_{\mathrm{n}}$. $U_{\mathrm{LL}} = 400\ \mathrm{V}$, $E_{\mathrm{PM,ph}} = 248\ \mathrm{V}$, $p = 10$, $L_{\mathrm{s}\sigma} = 95.49\ \mu\mathrm{H}$ (0.1156 pu.), $L_{\mathrm{md}} = 249.51\ \mu\mathrm{H}$ (0.3021 pu.), $L_{\mathrm{mq}} = 264.51\ \mu\mathrm{H}$ (0.3202 pu.), $L_{\mathrm{D}\sigma} = L_{\mathrm{Q}\sigma} = 0$, $J_{\mathrm{tot}} = 251.2\ \mathrm{kgm^2}$, $D_{\mathrm{tot}} = 3\ \mathrm{Nms/rad}$, $R_{\mathrm{s}} = 0.0036\ \Omega$ (0.0140 pu.), $R_{\mathrm{D}} = 9.60\ \mathrm{m\Omega}$ (0.0370 pu.) $R_{\mathrm{Q}} = 8.97\ \mathrm{m\Omega}$ (0.0346 pu.).

The active power reduces as expected with the decreasing frequency and constant turbine torque as shown in Figure 4.5. The reduction rate is around 2 %/Hz if the turbine torque is

constant. If the turbine torque increases with decreasing frequency accordingly to equation (3.27), the power decrease is not linear. There is necessarily no need to control the turbine at under frequencies with types A and B powerplants on behalf of the Regulation (EU) 2016/631.

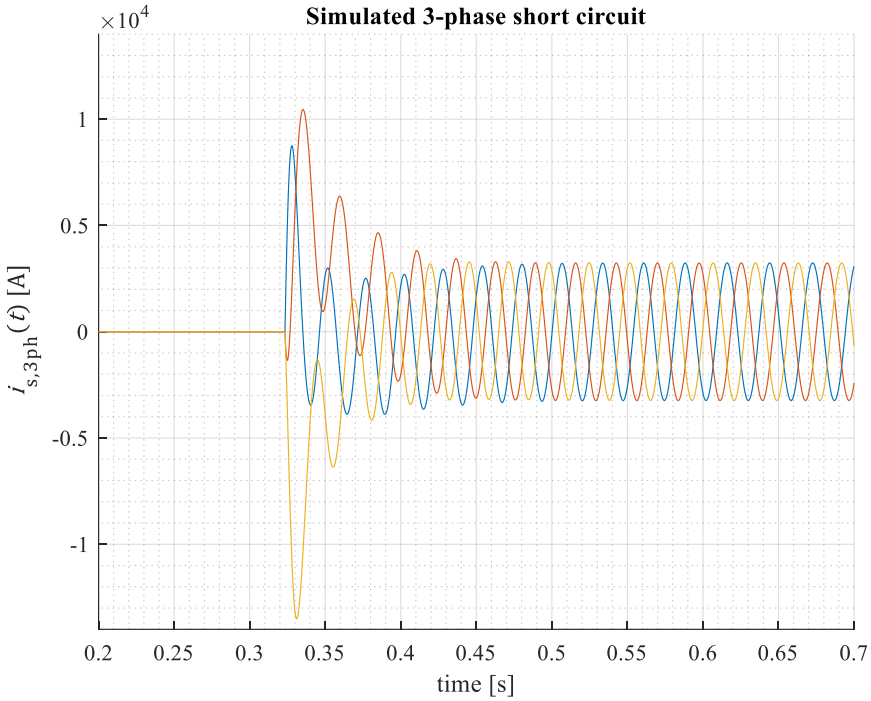

Figure 4.7 Simulated 3-phase short circuit initiated from open stator condition. $U_{\mathrm{LL}} = 0$ V, $E_{\mathrm{PM,ph}} = 248$ V, $f = 50$ Hz, $p = 10$, $L_{\mathrm{s}\sigma} = 95.49$ µH (0.1156 pu.), $L_{\mathrm{md}} = 249.51$ µH (0.3021 pu.), $L_{\mathrm{mq}} = 264.51$ µH (0.3202 pu.), $L_{\mathrm{D}\sigma} = L_{\mathrm{Q}\sigma} = 0$, $J_{\mathrm{tot}} = 251.2$ kgm^2, $D_{\mathrm{tot}} = 3$ Nms/rad, $R_{\mathrm{s}} = 0.0036$ Ω (0.0140 pu.), $R_{\mathrm{D}} = 9.60$ mΩ (0.0370 pu.) $R_{\mathrm{Q}} = 8.97$ mΩ (0.0346 pu.).

The attenuation of the three-phase short circuit current in Figure 4.7 is fast, which is somewhat typical for PMSGs because there is no field winding. The spike of the blue phase is the smallest because the short circuit was initiated when the emf of that phase was at its peak.

4.1.3 Conclusion

Based on the testing, it seems that the model works as intended. Accurate parameterization may have some challenges, but it can be argued that when the model is used to find general trends, the results are valid with acceptable uncertainty. As electrical machine design is an iterative process, the simplifications such as neglected saturation can be taken into account later in analytical design and FEA phases.

4.2 Simulation scheme

It was found out in chapter 2 that the simulations of this thesis should focus on the fault-ride-through (FRT). It was decided that a suitable approach to the problem is to produce statistical simulation data on whether the FRT is passed or not. In addition to the pass/fail tests, the synchronization time after the fault and the maximum fault duration or fault clearance time seem to be suitable performance metrics for some of the simulations.

Of course, the FRT performance is only one goal and other constraints and goals such as short circuit current, torque and induced emf quality and maximum torque must be considered when deciding on the final design target parameters.

The purpose of the simulations is to find to which parameters the performance in FRT is sensitive and to find suitable parameter ranges. The simulations are carried out as stated in the following:

- Three reference machines of different sizes (speed and power ratings) are included in the study, Table 4.2.
- Stiff shaft mechanical model is used. The total friction is set to $3\ \mathrm{Nms/rad}$ on all machines.
- The FRT profile with the most extreme values [U_{ret}, U_{clear}, U_{rec1}, U_{rec2}] = [0.05, 0.7, 0.7, 0.85], [t_{clear}, t_{rec1}, t_{rec2}, t_{rec3}] = [0.25, 0.25, 0.7, 1.5] is injected as a voltage reference when the machine is initially operating at its rated load if not stated otherwise. It should be noted that the profile is not completely realistic, but it is exactly what is required in the regulation.
- The turbine torque is kept constant during the fault. It was decided that the turbine characteristics should be modelled in detail in order to be worth considering. The characteristics likely have a notable positive effect on the performance in FRT because the decrease in torque would limit the acceleration. Therefore, keeping the torque constant can be regarded here as a worst-case scenario, but in practise must be confirmed case-by-case, as some deviations in turbine performance may appear.
- The steady-state stator and rotor temperatures at the nominal apparent power are set to $T_{\mathrm{th,n,s}} = 100\ ^{\circ}\mathrm{C}$ and $T_{\mathrm{th,n,r}} = 50\ ^{\circ}\mathrm{C}$ respectively and the no-load temperatures to $T_{\mathrm{th,0,s}} = T_{\mathrm{th,0,r}} = 20\ ^{\circ}\mathrm{C}$, even though the temperature dependencies at this level of detail are not very meaningful from the perspective of finding general trends.

- The stator AC resistance is set equal to the DC resistance on all the machines.
- The variable-step solver is used with the default method, max. step size of 0.0003 s and relative tolerance of 1e-6. Based on testing, decreasing the max. step size further with the variable-step solver did not have any meaningful effect other than loss of performance. In brute-force type simulations, wasting performance is not desirable.
- Synchronism is detected by the following conditions that must be true for 0.04 s continuously after the t_{rec3} time instance: $|slip| < 0.02$, $\left|I_{\mathrm{DQ,pu.}}\right| < 0.01$, $\left|\frac{\mathrm{d}\delta}{\mathrm{d}t}\right| < 2$. If synchronism is not detected within 4 s after the t_{rec3} or $\Omega > 3\Omega_{\mathrm{n}}$ at any time or $\Omega < 0$ at any time, the test run is deemed a failure. The multiple conditions for synchronism detection are to reduce the risk of false positive results even though using only the slip requirement would most likely work just fine. The $\Omega > 3\Omega_{\mathrm{n}}$ and $\Omega < 0$ are short cuts to speed up the simulation process.
- The FRT is tested while varying the parameters in loops. For some parameters additional reference data is gathered.
- Exceeding the load-angle values of 0…180° is allowed temporarily during the FRT.
- Because the process as a whole becomes computationally heavy, the number of nested loops for different parameters must be limited in this thesis. Truly exhaustive survey where all the relations between different parameters are inspected is not feasible. The results must also be reasonably easy to analyze and realistically exportable to the design of a machine.

Table 4.2 The reference machines used in the surveys. The parameters are based on computations by the manufacturer.

Quantity	340-250	520-600	1300-125
Rated active power P_n	340 kW	520 kW	1300 kW
Rated active power S_n	355 kVA	542 kVA	1310 kVA
Rated shaft torque T	13.5 kNm	8.6 kNm	106 kNm
Generator rotor moment of inertia J_g	169 kgm^2	25 kgm^2	2900 kgm^2
Turbine moment of inertia J_t	101 kgm^2	32 kgm^2	2560 kgm^2
Rated frequency f_n	50 Hz	60 Hz	50
Rated rotational speed n	250 rpm	600 rpm	125 rpm
Number of pole pairs p	12	6	24
Rated speed PM induced voltage (line-to-line) E_{PM}	430 V	510 V	730 V
Line-to-line grid voltage	400 V	480 V	690 V
Rated current I_n	510 A	650 A	1100 A
Temperature rise	130 (B-class)	130 (B-class)	130 (B-class)
DC resistance R_s	6.7 mΩ (0.015 pu.)	5.5 mΩ (0.013 pu.)	5 mΩ (0.014 pu.)
d-axis synchronous inductance L_d	0.8 mH (0.555 pu.)	0.86 mH (0.760 pu.)	0.55 mH (0.477 pu.)
q-axis synchronous inductance L_q	0.8 mH (0.555 pu.)	0.86 mH (0.760 pu.)	0.55 mH (0.477 pu.)
Sub-transient d-axis reactance X_d''	58.9 mΩ (0.13 pu.)	111 mΩ (0.26 pu.)	170 mΩ (0.47 pu.)*
Sub-transient d-axis time constant τ_d''	0.06 s	0.02 s	0.11 s
Damper winding d-axis resistance R_D	22.6 mΩ (0.05 pu.)	25.6 mΩ (0.06 pu.)	39.8 mΩ (0.11 pu.)
Damper winding q-axis resistance R_Q	22.6 mΩ (0.05 pu.)	25.6 mΩ (0.06 pu.)	39.8 mΩ (0.11 pu.)

Regarding the selected machines in Table 4.2, it is notable that the 520-600 is a 60 Hz machine and the other two are 50 Hz machines. The 60 Hz machine probably is not even subject to the Regulation, but that is not relevant. The machines are of type A or B depending on the installation location and they have different rated voltage, speed and power. It can be seen that the highest speed machine has a relatively high power rating, considering how much lower the moment of inertia is compared to the others.

Initially, the inductance corresponding to the X_d'' is used as the stator leakage inductance similarly as in chapter 4.1.1. Although, for the 1300-125 that assumption would make the $L_{s\sigma}$ clearly way too high causing a failure in the model already in grid connection with zero phase angle difference. Manipulating the values using equation (4.3) did not produce anything rational. Therefore, the stator leakage for that machine is set to an arbitrary value of $L_{s\sigma} = L_d/3$ initially to get the model working with that machine and allowing to proceed with the study. Having very precise initial parameters is not crucial in these simulations.

4.3 Results

In Figure 4.8 an illustration of successful and failed FRT simulation results are shown to give an idea of the event from which the parameter survey data is gathered.

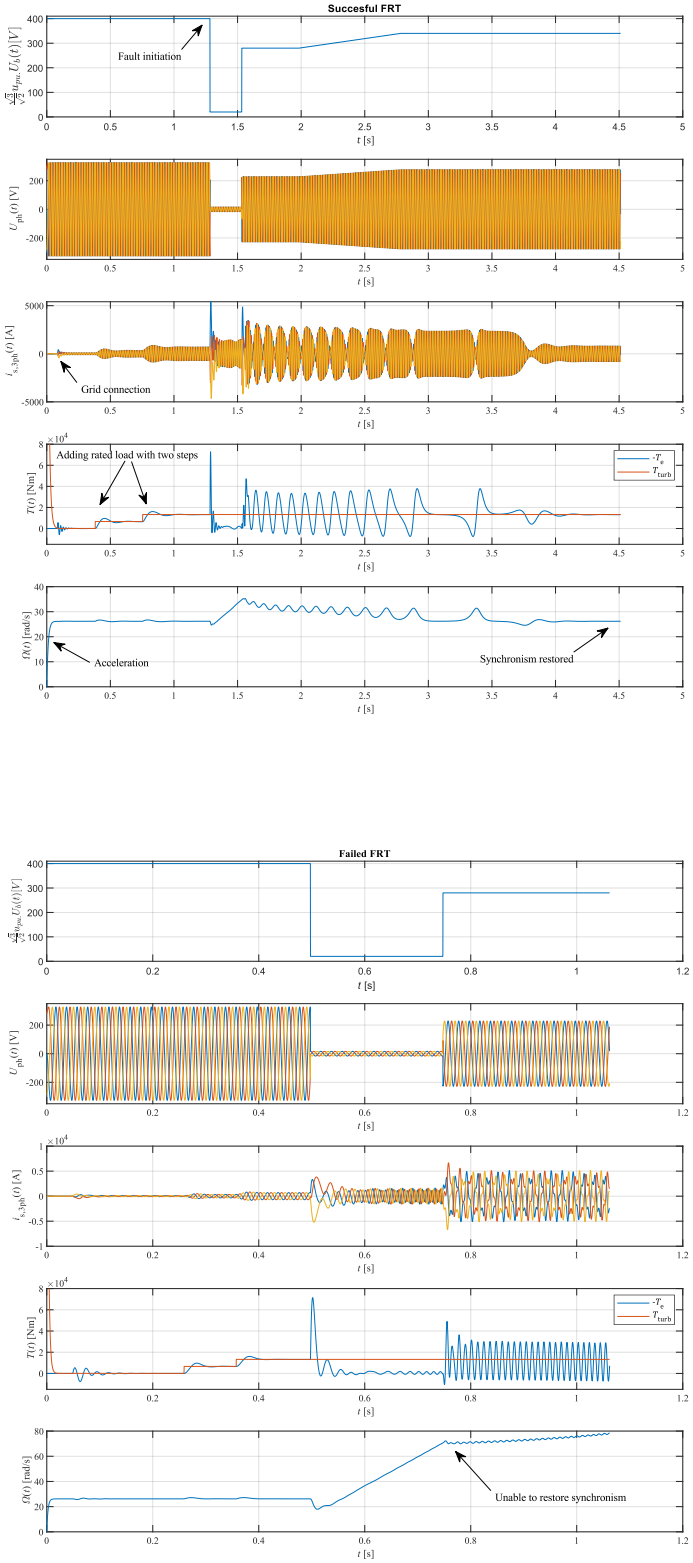

Figure 4.8 Successful (top) and failed FRT simulation. The machine used was the 340-250. To obtain the successful result, the damper winding resistances were tuned slightly. The failure in FRT was then created by cutting the total inertia until synchronism could not be restored anymore so that the speed starts to accelerate. The acceleration torque before the grid connection is unrealistic, but it does not matter since the stiff shaft model is used.

None of the machines passed the test with the initial parameters. However, at least the 340-250 was close and slight damper winding resistance tuning (from $R_{\mathrm{D,Q}} = 22.6\ \mathrm{m\Omega}\ (0.05\ \mathrm{pu.})$ to $R_{\mathrm{D,Q}} = 22.3\ \mathrm{m\Omega}\ (0.0492\ \mathrm{pu.})$) was enough to pass. This is the starting point to which the effect of varying the parameters is relatively compared in the tests. Interpretation of the results in an absolute sense easily leads to misconception.

With a DOL PMSG it seems to be difficult to achieve the FRT performance according to the regulation without a temporary pole slip. The reason for this is that the high stator current in the beginning of the fault causes a high stator leakage flux linkage, which has a great impact on the stator flux linkage orientation with respect to the permanent magnet flux linkage. The pole slip is not addressed in the Regulation. However, the relevant TSO or system operator may not allow this to happen, as is the case in Finland (Fingrid, 2018). On the other hand, as the powerplants in category A are not subject to the FRT requirement, full compliance may not be necessary. It seems to be possible to restore synchronism even in the event of a pole slip because of the damper winding if the resulting mechanical stresses and oscillations can be tolerated and there is enough confidence that detrimental resonances will not occur. It is extremely important to stress that all the results correspond to the assumption that the pole slip can be tolerated temporarily without disconnection.

Another possible type of failure is a scenario in which too high overspeed does not occur, but undamped oscillations remain, or the machine is unable to recover from asynchronous operation back to synchronism. It is important to note that the criteria for condition that is considered synchronism is somewhat arbitrary as is the time after which a test run is deemed failure if synchronism is not detected.

The maximum current value gathered during some of the tests is the current in dq-coordinate system. It is, in fact, a type of peak envelope of the three-phase current waveform, Figure 4.9. It is also consistent irrespective of the phase angles, for example in a sudden short circuit.

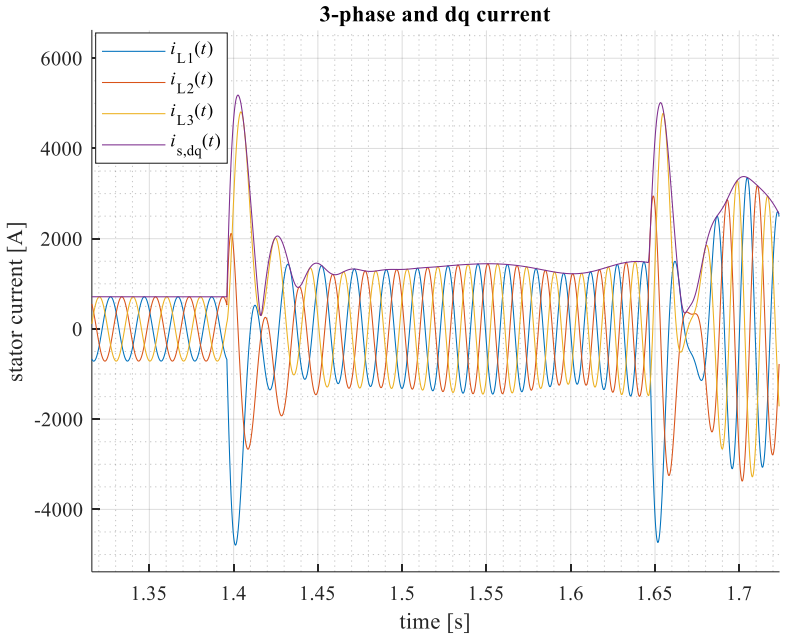

Figure 4.9 Illustration of the stator current as dq and 3-phase variables.

4.3.1 Damper winding resistances

The damper winding resistances R_{DQ} are interesting because in principle they do not affect the steady state operation point. The result of varying damper winding resistance is shown in Figure 4.10. The figures contain some unrealistic datapoints because in reality the R_D and the R_Q depend on each other to some extent. The 520-600 did not pass the test with any tested damper winding resistance values. Also, many different inertia values were tested in combination with varying the resistances without much success. However, during the testing it was inspected that the 520-600 would have eventually passed with some of the parameters if the failure timer was removed.

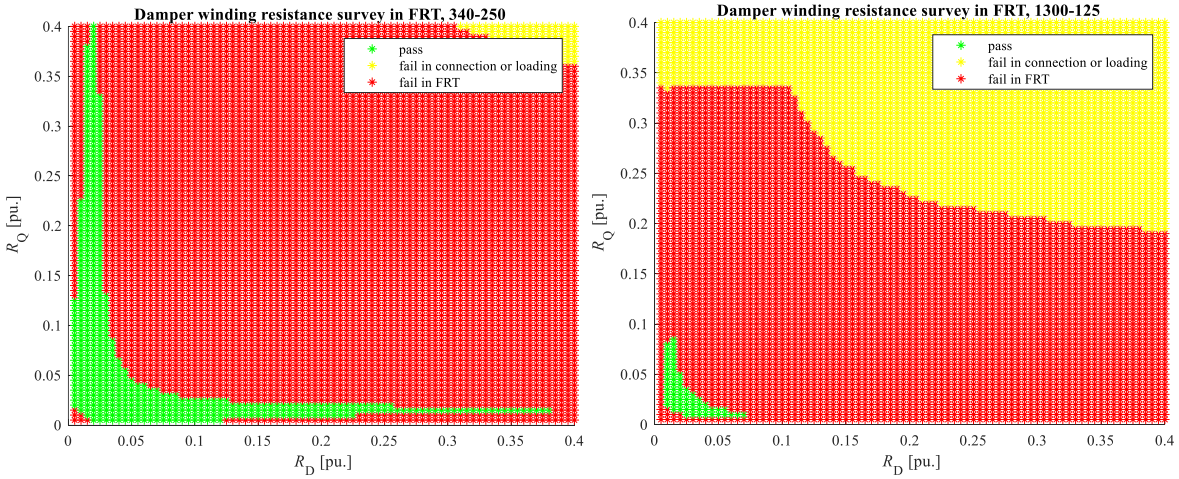

Figure 4.10 Damper winding resistance survey. The other parameters were at their initial values.

It can be seen that the damper winding resistances have a great impact on the passing of the FRT as expected. It seems that the resistances should be around 0.04 pu. or a bit smaller in

these cases. Based on the figure, a suitable ratio between the axes could be 1. Damper winding resistances are inspected further in chapter 4.3.8 and 4.3.7 alongside with the damper winding leakage inductances.

4.3.2 Saliency

Suitable inductance ratios L_d/L_q are tested with a locked $L_{s\sigma}$ and roughly normalized maximum steady state torque based on the reference machine. Another considered option was to normalize the $L_{d.}$ The saliency is interesting because the ratio can be independent of the leakage inductances in the model parameterization. Also, the choice of inductance ratio is a fundamentally significant issue in machine design as it changes the torque characteristics. Using reluctance torque may help in maintaining stability or allow lesser PM material to be used, for example. It should be noted though that saliency can negatively affect the torque and induced emf quality because in case of saliency the armature reaction caused air-gap flux density is non-sinusoidal and in such a case stator winding factors dictate the deviation from sinus back emf (Pyrhönen et al., 2014). The result of varying the inductance ratio is shown in Figure 4.11. The load-angle before the fault initiation is used as a reference. The 520-600 and the 1300-125 did not pass with any tested inductance ratios. Therefore, it can be said at least that the inductance ratio does not seem to have a major positive effect on the FRT. It is also possible that some parameters, such as the stator leakage, in the cases of the 520-600 and the 1300-125 are acting as limiting factors. Nevertheless, based on the result of the 340-250, it seems that inverse saliency is preferable compared to normal saliency in FRT which is suitable for a PMSG. This information may be considered when choosing the PM topology of a machine. The PM material has a very low permeability, and therefore embedding the magnets can cause some inverse saliency depending on the topology because the reluctance increases when some of the high permeability core material is replaced with the PM material.

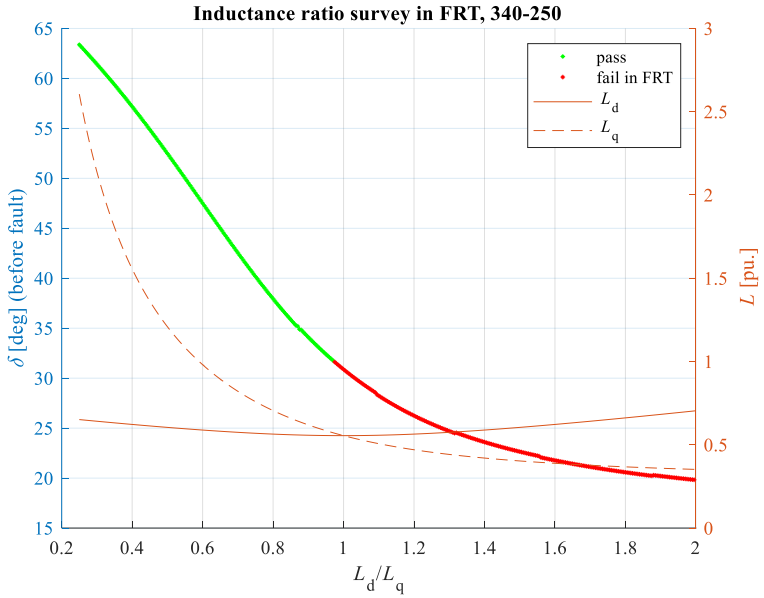

Figure 4.11 Inductance ratio survey.

This result, however, must be interpreted with caution. It is not perfectly clear how the effect of saliency should be isolated in this simulation to obtain a fair and meaningful comparison. For example, keeping the stator leakage the same with all the inductance ratios is probably not realistic and might skew the result. Some of the tested parameter configurations in Figure 4.11 may not be realistic to begin with. Furthermore, suitable resulting short circuit current value that is in practice needed for fault detection was not considered when choosing the inductance values in the test.

4.3.3 Stator resistance

In the stator resistance tests, a time elapsed between the fault initiation and the instance the synchronism conditions were met was used as a reference as it is a convenient way to present the results while providing some additional information. The data is presented in Figure 4.12 as a high-resolution bar graph.

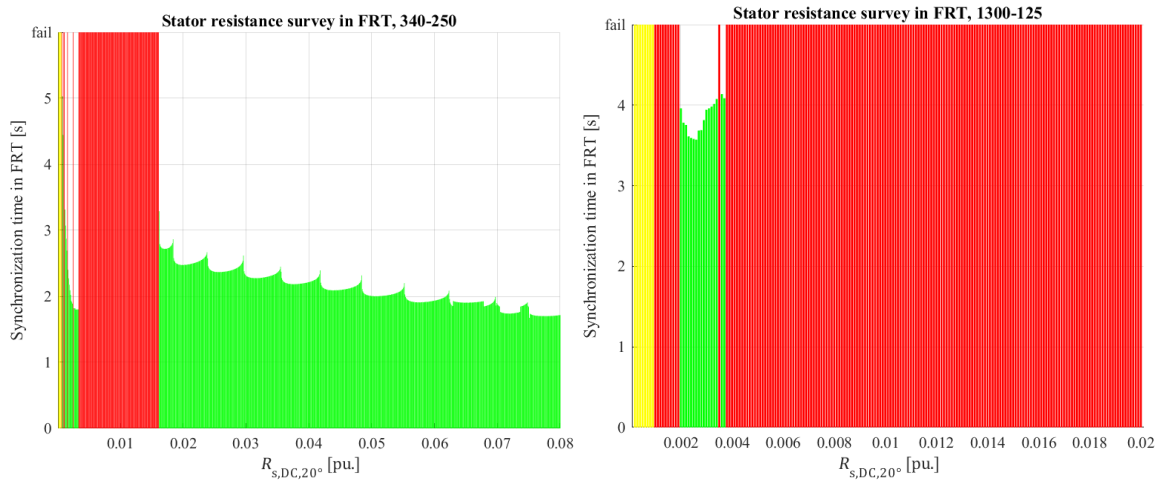

Figure 4.12 Stator resistance survey bar graphs. The other parameters were at their initial values. The figure of the 1300-125 is zoomed. After the resistance value of 0.02 pu. there were only failed test runs.

The 520-600 did not pass the test with any resistance value. The stator resistance is primarily just a loss component being the most significant source of losses in DOL PMSGs. It has some effect on the FRT but focusing on the stator resistance in the machine design when the FRT performance is considered, probably is not worthwhile. Regarding the synchronization times in the figure, the pattern comes from the interaction between the speed oscillation and the stated conditions for what is considered synchronism. In the case of the 340-250 machine, it is a bit curious that before the resistance value 0.0033 pu. the FRT is passed or failed irregularly and after that the FRT fails until the value 0.0162 pu. The conclusion regarding the stator resistance is that it can be minimized in an effort to reduce losses and the required FRT performance may be achieved by focusing on other areas of the machine.

4.3.4 Source voltage

The PM flux linkage induced source voltage E_{PM} affects the PMSG *PQ*-operating point, the maximum steady-state torque and the short circuit current. The voltage level with a given flux and rotational speed can be adjusted by the number of turns of the stator winding. The result of varying the E_{PM} while keeping the inductances fixed is shown in Figure 4.13. The power factor and the load-angle before the fault initiation is used as a reference.

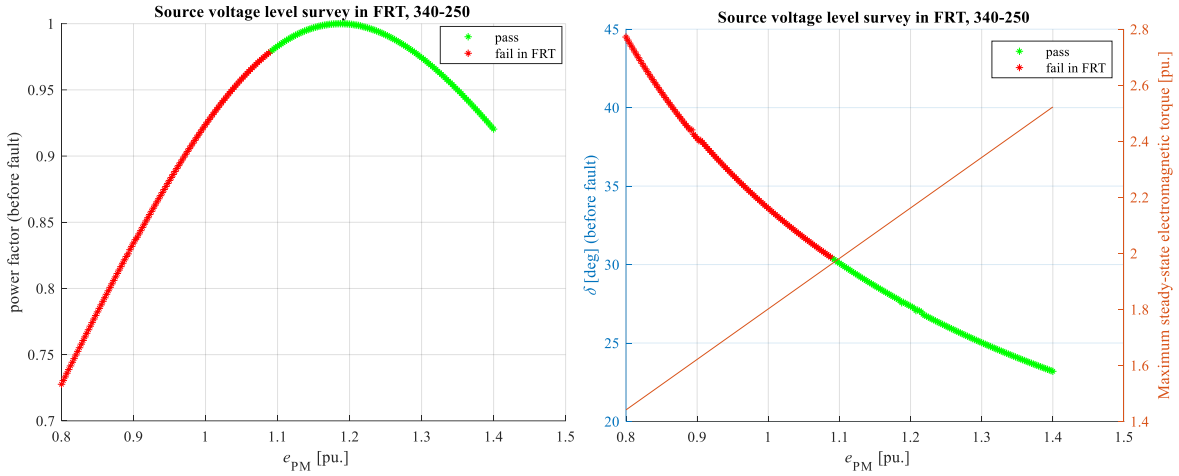

Figure 4.13 Source voltage level survey. Other parameters were at their initial values.

The 520-600 and the 1300-125 did not pass the test indicating with the result of the 340-250 that the source voltage level has only a minor effect on the FRT. The decreased load-angle before the fault is not very meaningful because the pole slip takes place in any case. The same test was also made while keeping the maximum steady-state torque fixed by increasing the total inductances while keeping a constant stator leakage and total inductance ratio. In that test run, none of the machines passed the test with any E_{PM} value (i.e no change from baseline).

The 340-250 with the initial parameters was already very close to passing the FRT, so it cannot be said that increasing the E_{PM} would have a very significant effect since it did not help with the other two machines and had no notable effect at all on the ability of passing the test when the maximum steady-state torque was normalized. Moreover, to achieve a smooth grid connection, the rated speed back-emf should be relatively close to the grid voltage level which limits the possibilities. The Finnish VJV2018 suggests that the back-emf should not deviate from the grid voltage by more than 0.05 pu. in the grid connection. However, a larger deviation may be used if agreed between the power generating facility owner and the relevant network operator (Fingrid, 2018).

4.3.5 Stator leakage inductance

The flux leakage can be often considered as a negative phenomenon in DOL machines. In converter connected machines the $L_{\mathrm{s}\sigma}$ may be beneficial in field weakening and filtering.

For the stator leakage inductance tests, maximum stator current (dq variable) and maximum electromagnetic torque in a standard sudden short circuit test were chosen as reference values

because those are heavily dependent on the stator leakage. The values were not obtained from the FRT event because a comparison between passed and failed runs was not desired. The stator leakage inductance values in the range of (0.1 … 0.8) times the total d-axis inductance were tested while keeping the total inductance fixed by tuning the magnetizing inductances accordingly. Figure 4.14 is meant to be interpreted so that a suitable target for leakage inductance value can be chosen as close as possible to the green area considering that the $i_{\mathrm{s,max}}$ and the $T_{\mathrm{e,max}}$ are not too high, for example from the perspective of mechanical integrity of the machine.

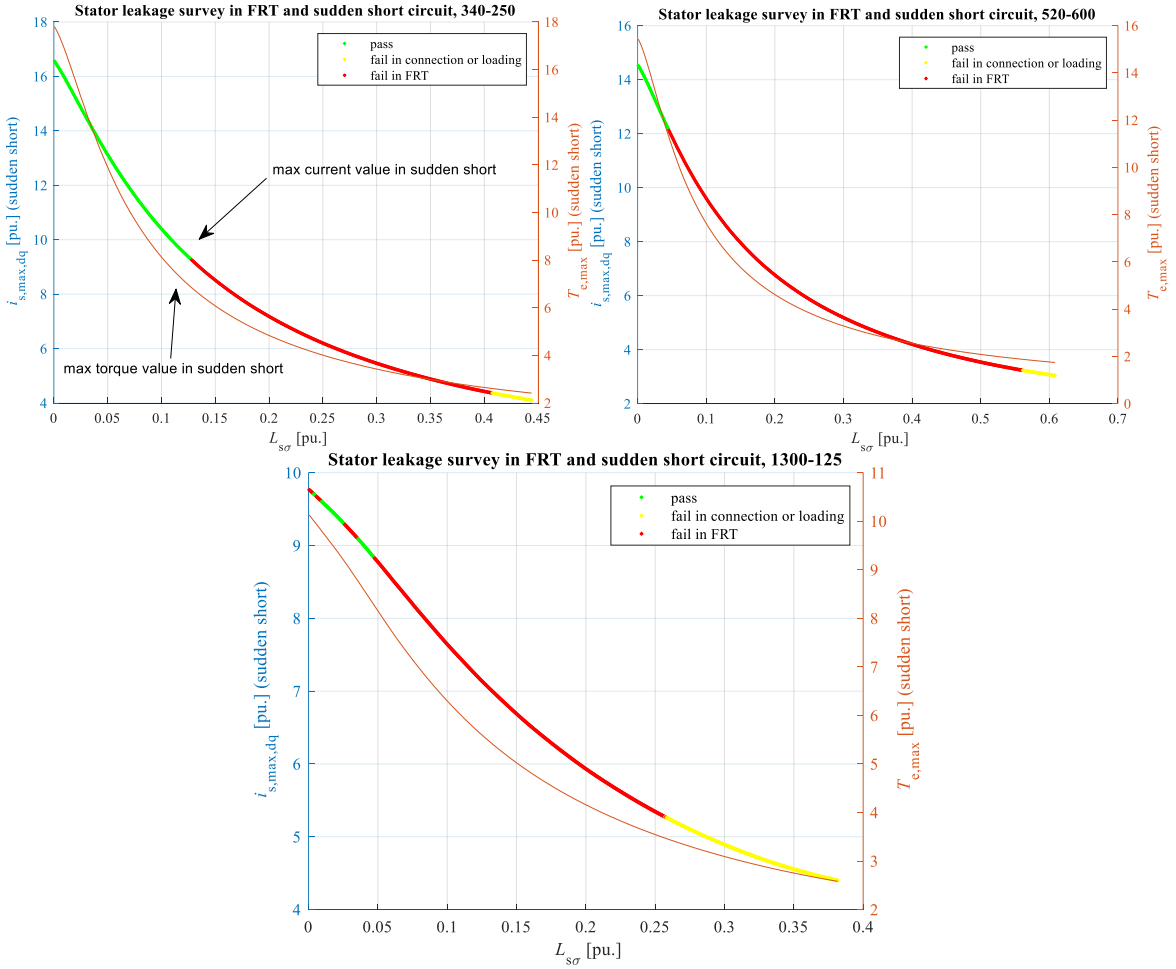

Figure 4.14 Stator leakage inductance survey.

It can be seen, that minimizing the stator leakage is beneficial for passing the FRT, although in the case of the 1300-125 there is slight inconsistency in the behaviour. This can be considered a somewhat unfavourable result because having a high stator leakage inductance is quite common in a low-speed PMSM. Also, minimizing the leakage may require fairly advanced design skills. Such a task may include, for example choosing a suitable stator topology that allows tight end windings, careful shaping of teeth and slots, choosing a suitable

PM topology and evaluating skewing and short pitching possibilities. It is very important to note though that these figures were produced by keeping the other parameters as listed initially. Minimizing the stator leakage is not necessarily mandatory, but beneficial. However, the stator leakage seems to be one of the major factors in passing the FRT.

4.3.6 Total inductances

The effect of varying the total inductances while keeping the initial L_d/L_q ratio and the $L_{s\sigma}/L_d$ ratio fixed is shown in Figure 4.15. This test attempts to find out whether it would be beneficial to oversize the maximum steady-state torque value.

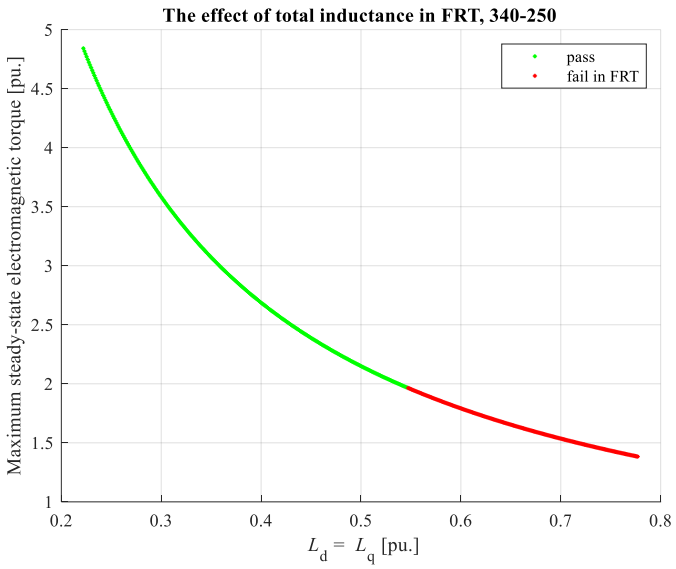

Figure 4.15 The effect of total inductances.

There was no change from baseline on the ability to pass the test in the cases of the 520-600 and the 1300-125. Decreasing the total inductances allowed the 340-250 to pass the test, but once again, it was already very close to passing in the first place. Therefore, oversizing the maximum steady-state torque because of the FRT performance does not seem a good idea.

4.3.7 Damper winding leakage inductances

In the damper winding leakage inductance simulations, the parameter step size was doubled compared to the damper winding resistance simulations to save time. The damper leakage inductance values in the range of (0 … 0.5) times the initial stator leakage inductance were tested. None of the machines passed with the initial parameters and the increased damper winding leakage did not help. It seems that the damper winding leakage is not beneficial and should likely be minimized in machine design. However, the question of does the damper winding leakage affect the suitable damper winding resistance values is too obvious to not

to be tested at all. The result of damper winding resistance survey of the 340-250 with $L_{\mathrm{D,Q\sigma}} = 0.03$ pu. is shown in Figure 4.16 in comparison with the initial test with $L_{\mathrm{D,Q\sigma}} = 0$ pu. The test indicates that the damper winding leakage is indeed harmful to the performance in FRT. It also shows that the region of suitable resistance values does not seem to shift but shrink from the edges, which is a very positive finding because designing the damper winding based on specific leakage values is not necessarily very straightforward. As long as the resistance values are carefully chosen, the resulting leakage values do not seem to matter too much.

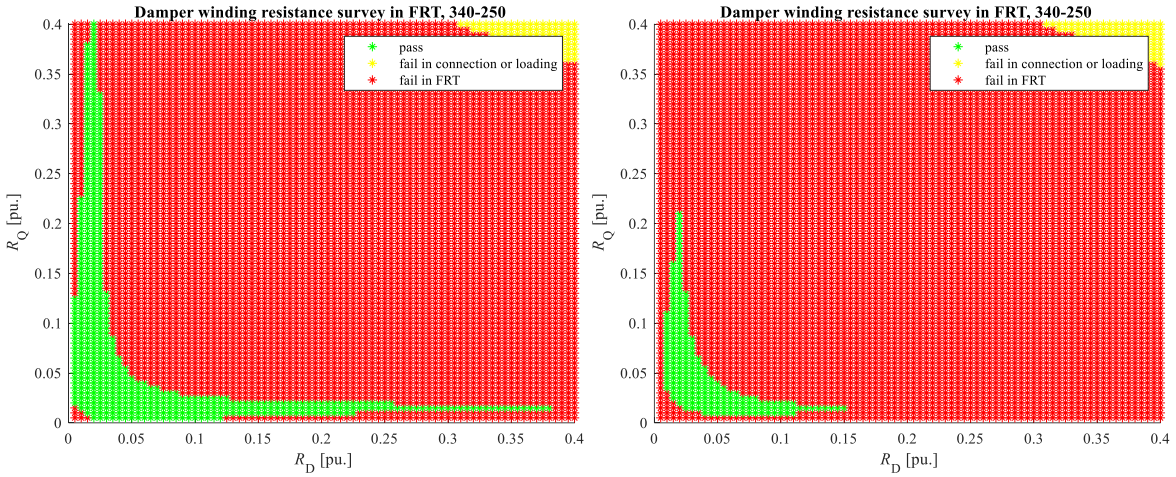

Figure 4.16 Damper winding resistance survey with $L_{\mathrm{D,Q\sigma}} = 0$ pu. (left) and $L_{\mathrm{D,Q\sigma}} = 0.03$ pu.

4.3.8 Reiterating the damper winding resistance test and combining the findings

The damper winding resistance survey is made for all the machines once again while employing the findings related to the other parameters in a suitable manner. The effect of total system inertia to the suitable damper winding resistances is inspected in the case of the machine that seems to have the most issues in passing the FRT. The source voltage levels, and the stator resistances are kept at their initial values on all the machines. The inductance ratio is set to $\frac{L_\mathrm{d}}{L_\mathrm{q}} = 0.95$ while keeping the initial maximum steady state torque on all the machines. The stator leakage inductance is set to 0.2 times the synchronous d-axis total inductance on all the machines and the damper winding leakage inductances are set to 0.1 times the stator leakage inductance. The base values are kept corresponding to the initial parameter list. The results of using these modifications are shown in Figures 4.16 - 4.18 alongside with surface plots of synchronization times elapsed in FRT viewed from above, maximum transient torque values in FRT and contour maps of synchronization times in grid connection using a phase angle difference of 0°. In the surface and contour figures, interpolation was used between the data points.

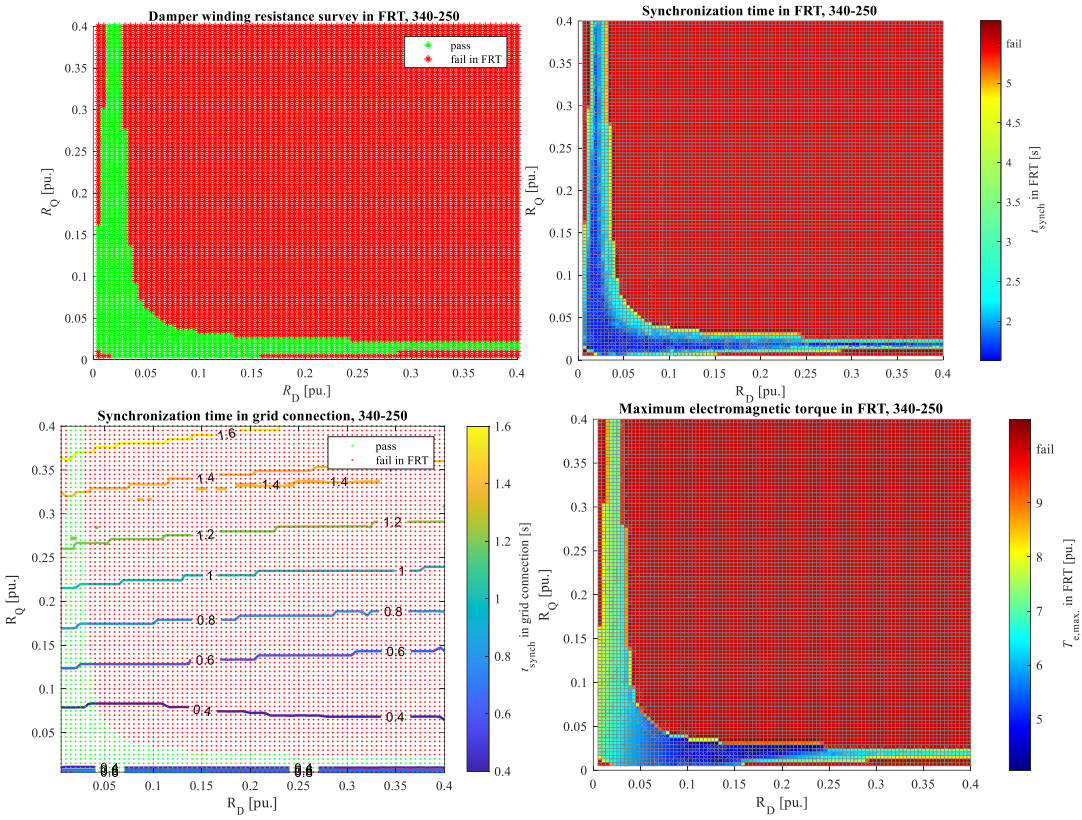

Figure 4.17 Damper winding resistance survey of the machine 340-250 with the modified parameters using the synchronization times in FRT and grid connection as performance metrics.

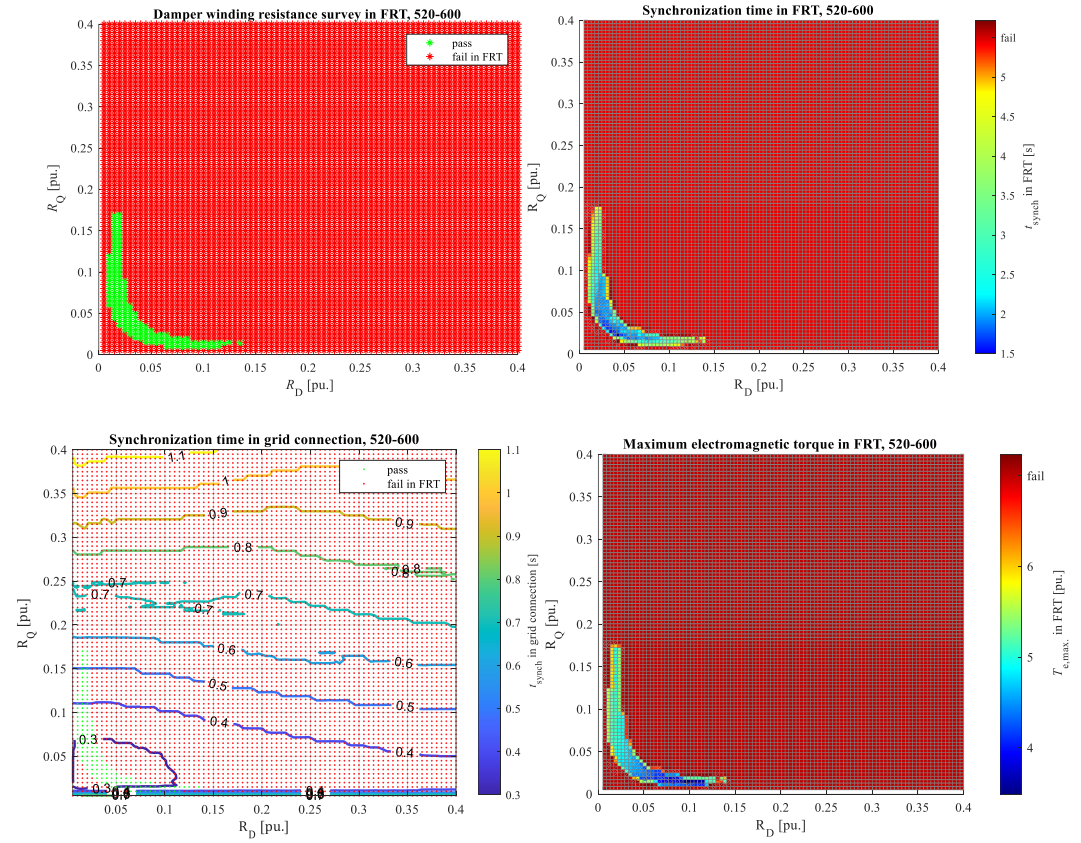

Figure 4.18 Damper winding resistance survey of the machine 520-600 with the modified parameters using the synchronization times in FRT and grid connection as performance metrics.

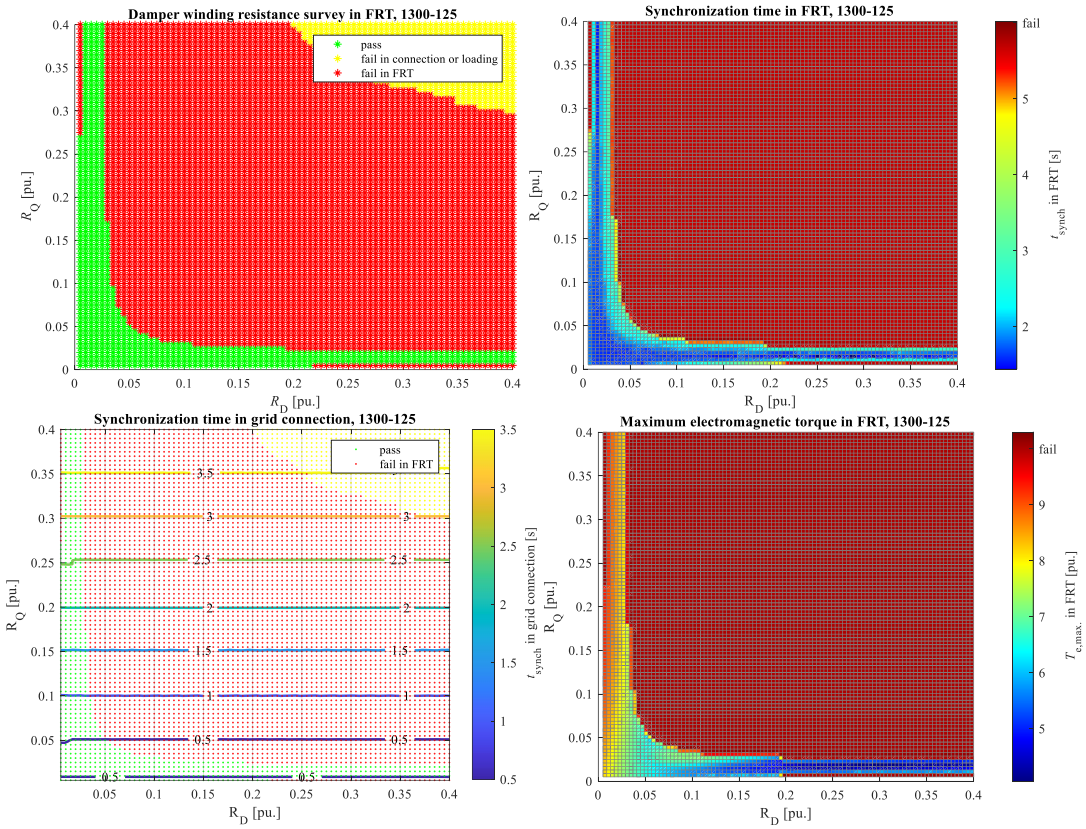

Figure 4.19 Damper winding resistance survey of the machine 1300-125 with the modified parameters using the synchronization times in FRT and grid connection as performance metrics.

Using the modified parameters, the area of suitable damper winding resistances expanded on all machines even though some damper winding leakage, which has a negative effect, was used. Now the 520-600 can pass the test but seems to still have the most difficulties. Therefore, the test is repeated with different system inertia values for that machine to see if there is a benefit. This is shown in Figure 4.20. It can be seen from the contour maps that the d-axis resistance has only a small effect on the synchronization time in grid connection. It is possible to choose the resistance values so that the FRT is passed while minimizing the synchronization time. Based on the maximum transient electromagnetic torque figures, the maximum torque can be limited by choosing a small q-axis resistance and a high d-axis resistance.

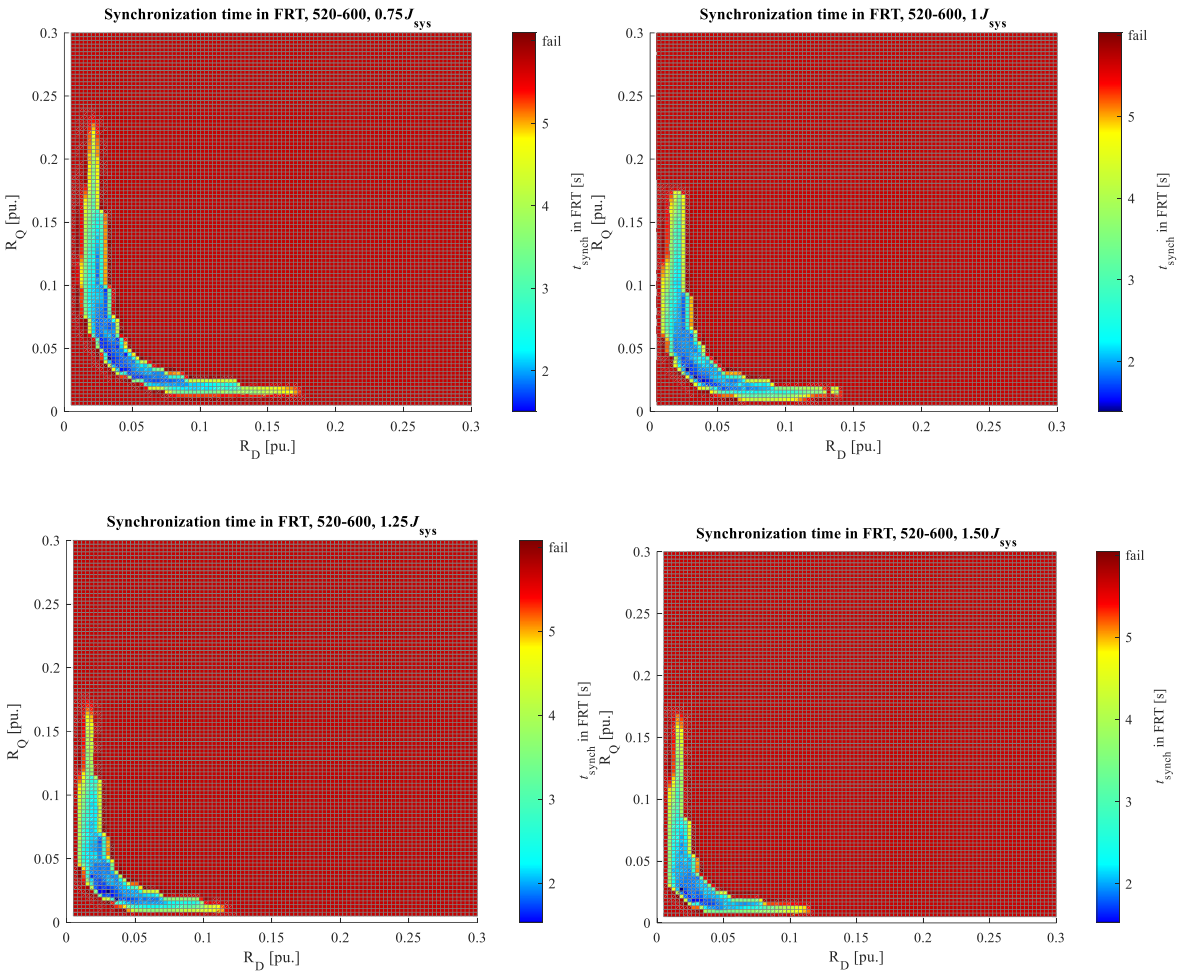

Figure 4.20 Damper winding resistance survey of the 520-600 machine with different system inertia values.

The system inertia seems to shift and slightly reshape the suitable resistance area. Lower system inertias seem to favour higher resistance values. It appears that for every electromagnetic design there is a suitable range of system inertia values and likely an optimum, as long as there are no limiting factors. Therefore, a set of simulations varying only the system inertia is made in chapter 4.3.9.

As an additional test, the maximum fault duration with different $R_{\mathrm{D,Q}}$ values using the 340-250 machine was searched. This was done by introducing a fault profile time parameter scaling factor k_{fault} and finding the maximum value for that factor at which the FRT passes. All the time parameters were multiplied by the k_{fault}, but the voltage parameters were retained as before. The maximum value for the k_{fault} was searched via a simple bracketing method which is presented as a flow chart in Appendix 2. The value $k_{\mathrm{fault}} = 1$ corresponds to the profile which was used in previous tests (the most extreme that can be required). The

bracketing is time consuming and therefore this test was done only with one machine. The result is shown in Figure 4.21.

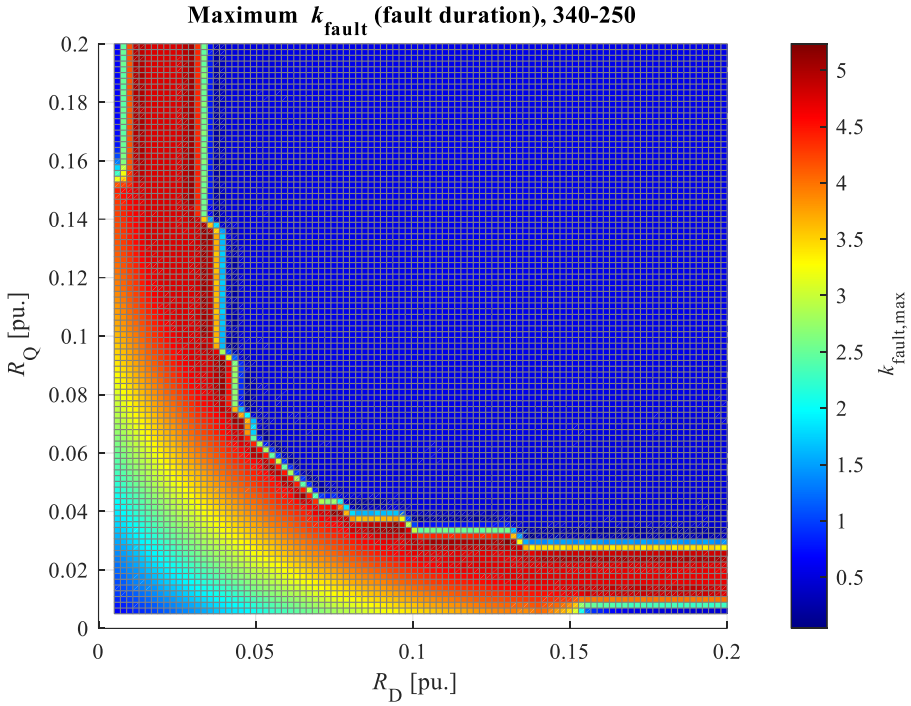

Figure 4.21 Damper winding resistance survey of the 340-250 machine using the fault time parameter scaling factor as a performance metric.

If the k_{fault} is regarded as a type of performance metric with the idea that the higher the better, it seems to be conflicting to some degree with the synchronization time in FRT. However, more than $k_{\text{fault}} = 1$ is not necessary in any case and even $k_{\text{fault}} = 0.6$ (corresponds to $t_{\text{clear}} = 0.15$ s) may be acceptable depending on what is the required fault profile. In this test it is assumed that the higher the k_{fault}, the harder the test. That is, the higher the k_{fault} the fewer parameter configurations would be able to pass, but this assumption is actually not verified. Also, it is important to remember that the result corresponds to the stated conditions for what is considered a failure or pass.

4.3.9 System inertia

Increasing inertia on the shaft will slow down the speed fluctuation. Additional inertia can be beneficial, but it can also cause oscillations to attenuate poorly and inability to recover from asynchronous operation if a pole slip takes place. System inertia values were tested in a somewhat reasonable range of (0…5) times the initial value. The results are shown in Figure 4.22. The electromagnetic parameters are as stated in chapter 4.3.8 and the damper winding resistances are chosen somewhat arbitrarily based on the previous tests as follows:

340.250 $R_{D,Q} = 0.029$ pu., 520-600 $R_{D,Q} = 0.033$ pu., 1300-125 $R_{D,Q} = 0.028$ pu. The synchronization time in FRT is used as reference data.

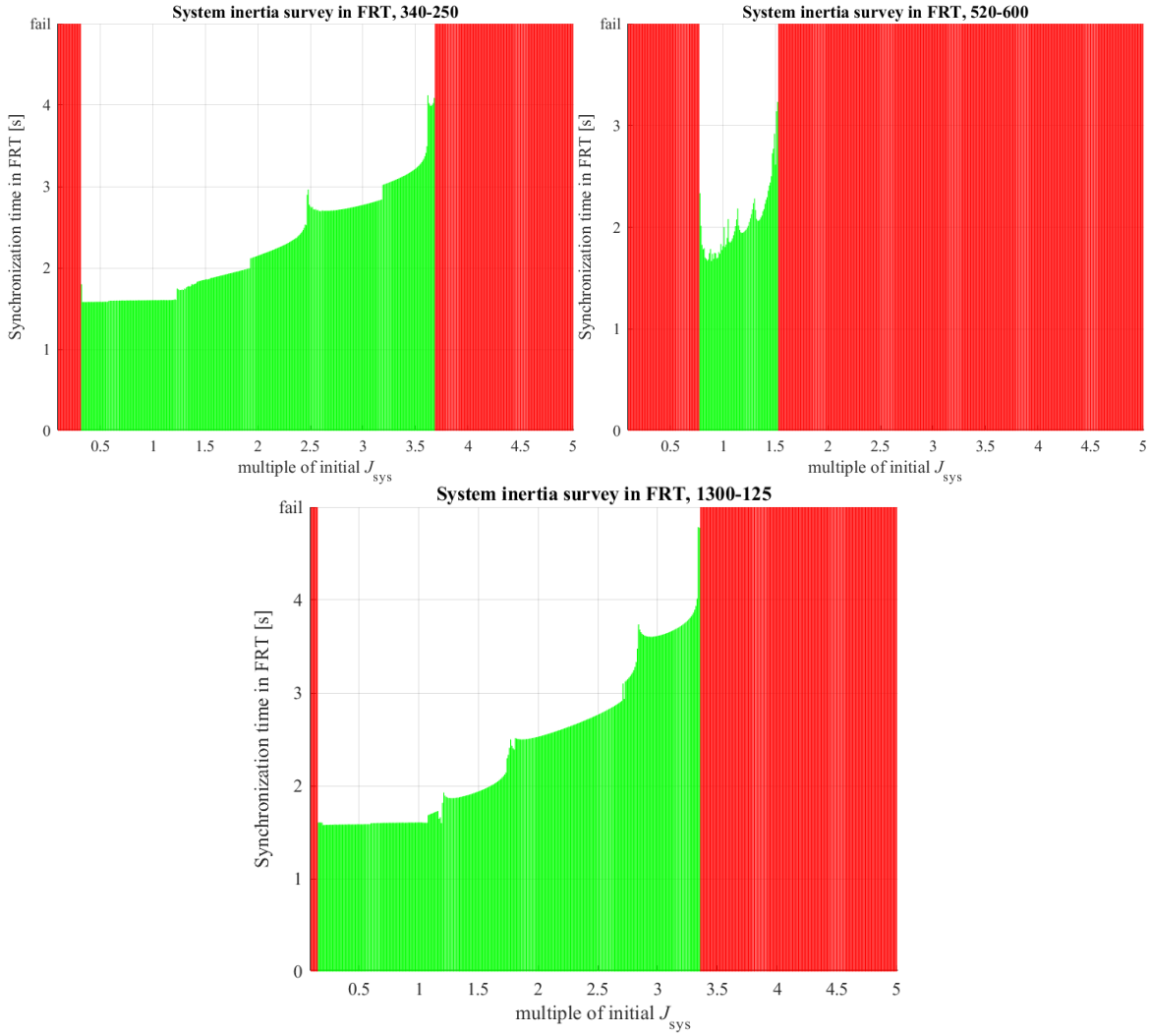

Figure 4.22 System inertia survey bar graphs.

First of all, the discontinuities in the synchronization time scaling with the J_{sys} come from the interaction between the oscillation and the stated conditions for what is considered synchronism. The result show that the electromagnetic design of a generator should match the system inertia correctly to pass the FRT.

If an existing generator is found losing synchronism frequently in similar scenarios that are considered here, adding external rotating mass to the shaft may or may not help and it should be evaluated on a case-by-case basis. Adding inertia may not be desirable because of material costs and concerns about compromising the mechanical properties of the system.

4.3.10 Time domain graphs with the modified parameters

The time domain graphs of the FRT simulations are presented in Figures 4.22-4.24 mainly to show the end result of tweaking the parameters.

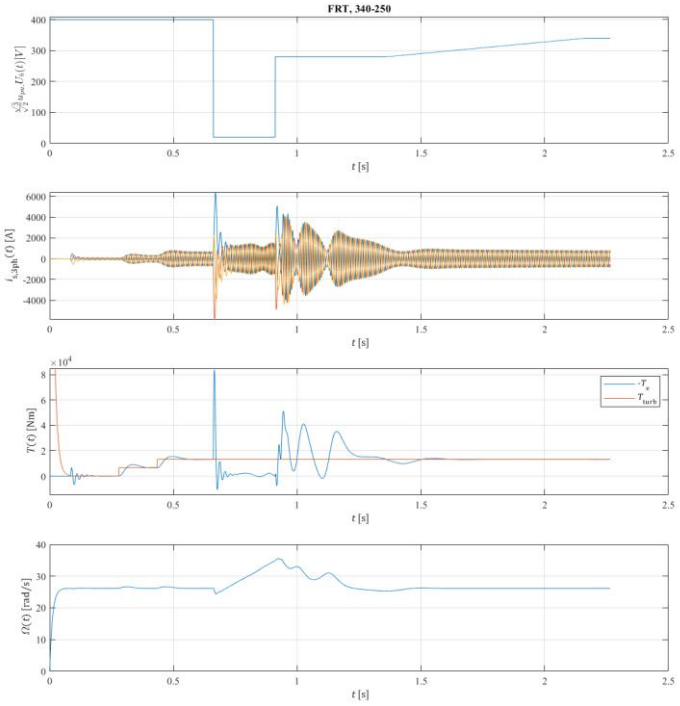

Figure 4.23 FRT simulation of the 340-250 machine with the tweaked parameters. $L_{s\sigma} = 160.17$ µH (0.111 pu.), $L_{md} = 640.69$ µH (0.445 pu.), $L_{mq} = 682.84$ µH (0.474 pu.), $L_{D\sigma} = L_{Q\sigma} = 16.02$ µH (0.0111 pu.), $R_D = R_Q = 0.0131$ Ω (0.0290 pu.).

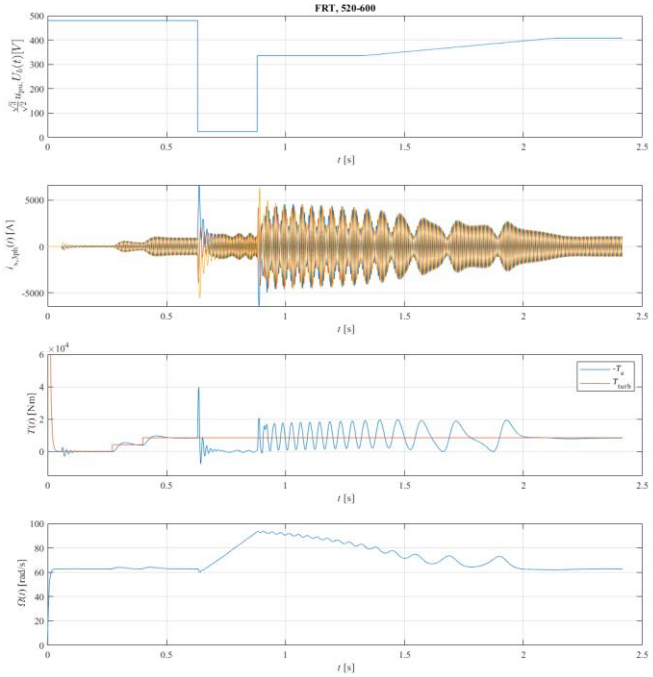

Figure 4.24 FRT simulation of the 520-600 machine with the tweaked parameters. $L_{s\sigma} = 172.19$ µH (0.1523 pu.), $L_{md} = 860.95$ µH (0.6090 pu.), $L_{mq} = 906.26$ µH (0.6491 pu.), $L_{D\sigma} = L_{Q\sigma} = 17.22$ µH (0.0152 pu.), $R_D = R_Q = 0.0141$ Ω (0.0330 pu.).

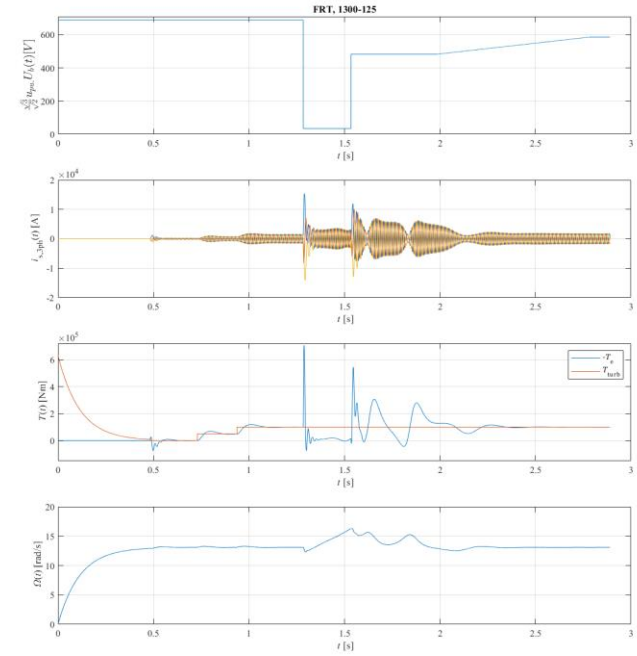

Figure 4.25 FRT simulation of the 1300-125 machine with the tweaked parameters. $L_{s\sigma} = 110.12$ µH (0.0955 pu.), $L_{md} = 440.49$ µH (0.3821 pu.), $L_{mq} = 469.47$ µH (0.4073 pu.), $L_{D\sigma} = L_{Q\sigma} = 11.01$ µH (0.0096 pu.), $R_D = R_Q = 0.0101$ Ω (0.0280 pu.).

Now all the machines pass the test and the oscillations of the 340-250 are improved in comparison with Figure 4.8. Based on the observations during the parameter surveys, the oscillation of the 520-600 could be reduced if desired, by fine tuning the parameters further. The oscillations may cause harmful mechanical stresses, and it should be evaluated whether they can be tolerated or not.

5. SUMMARY AND CONCLUSIONS

The role of hydropower and DOL PMSGs in hydropower was evaluated with a conclusion that the importance of hydropower is likely to remain or become even more emphasized in the near future because renewable power is heavily desired and the uneven production of emerging PV solar power and wind power must be counterbalanced. Also, the synchronous inertia the DOL generators provide is a desirable feature. The PM technology in hydropower generators is primarily used to maximize efficiency. The growth of hydropower may come from the modernization of existing power plants or from new installations, although the installation potential of new power plants, at least in Europe is diminishing in general.

In the overview of the Regulation (EU) 2016/631 focusing on the DOL generators, it was found out that the voltage control requirements limit the practical usability of DOL PMSGs to power plant category B and below. For an already successful PMSG design, the most interesting issue in the Regulation was identified to be the fault-ride-through requirement which states that generators in categories B, C or D should be capable of remaining connected and retaining synchronism in a specific type of fault. It was argued that the FRT capability would be beneficial also in category A. Therefore, it was decided that the simulations of this thesis should focus on the FRT performance.

A suitable simulation tool for a DOL PMSG was created using MATLAB® and Simulink®, documented, validated and demonstrated in detail. The two-axis theory and lumped parameter model were used as a basis. Saturation, iron losses and harmonics were neglected, but discussed. Regarding the mechanics, a two-mass model and simple stiff shaft model were introduced. Temperature dependences of resistance parameters and PM flux linkage were considered in steady state operation. The validation was carried out by comparing a measured current waveform with a simulated one in the case where a grid connection was made in phase opposition. In addition, many characteristic figures of a PMGS were produced with the simulation tool to see that the model performs as expected. It was noted that the accurate parameterization of the model may have some difficulties, at least with industrial machines, for which a detailed list of parameters is usually not available. Also, keeping the inductances as constants (neglecting saturation) is likely to cause a significant error in some situations. To improve simulation accuracy, there shall be available detailed inductance planes as a

function of current derived through FEA. It was still concluded that the general trends found using the tool should be within acceptable uncertainty.

The approach chosen for the simulations was to gather statistical data with different sets of parameters on whether the FRT is passed or not. Three reference machines of different sizes were selected for the study and suitable ranges for the parameters were searched and the sensitivity of the performance to the parameters was evaluated.

As a result, it was found out that synchronism can be restored with a DOL PMSG in a FRT event. However, it seemed very difficult to operate without a temporary pole slip. Therefore, the simulations were carried out with an assumption that a temporary pole slip can be allowed. It was found out that in that case a designer should aim to minimize the stator and damper winding leakage inductances and focus on carefully choosing the damper winding resistances to improve the probability of being able to restore synchronism in FRT with a DOL PMSG. Inverse saliency may be beneficial, but this should be studied in more detail. The source voltage level can be decided mainly based on the desired rated operating point. Oversizing the maximum steady-state electromagnetic torque does not seem to have a notable benefit. The stator resistance has some, but not a particularly clear, effect on the FRT and it may be minimized in an effort to minimize losses. The damper winding leakage reduces the pool of suitable damper winding resistance values, but this is not an issue as long as the resistances are selected from the centre of the region of suitable values of the $(R_{\mathrm{D}}, R_{\mathrm{Q}})$ map. The optimal damper winding resistances for FRT seem to be close to optimal also for synchronization performance in grid connection. The maximum transient torque can be limited by having a relatively small q-axis resistance and relatively high d-axis resistance. There was some evidence of a trend that the lower the system inertia is the higher damper winding resistances are required. However, to verify this, more results with different machines are needed. Finally, it was found out that increasing system inertia by adding external mass to the shaft may or may not help in passing the FRT depending on the electromagnetic design in the case where a pole slip takes place. Therefore, it is advisable to take the resulting total inertia into account in the electromagnetic design, if possible, and adding external inertia may be considered as a last resort if the generator is found to have unacceptably poor ability to retain synchronism in the faults that must be cleared according to the FRT requirements.

As a suggestion for future work, the simulation tool could be developed further by including a dynamic thermal model, more detailed grid model, for example for island operation simulations, characteristics of transformers, detailed water and turbine dynamics and some of the other simplifications that were mentioned. Also, it would be desirable to have more comparisons between measurements and simulations. Especially, real measurement data from a fault-ride-through event would be very useful. With regard to the simulations of this thesis, the findings give some basis to proceed with finite element analysis and analytical design or mechanical stress analysis of a water turbine DOL PMSG system. In the case pole slip phenomena is not accepted to happen, one shall investigate further solutions to overcome this issue.

In addition, some of the simulations of this thesis were merely demonstrative in nature, and to obtain a full picture on the effects of a certain parameter, probably more detailed simulations should be carried out. One of the ideas of this thesis was to search trends independent or dependent of machine size. However, the three machines included in this thesis were not enough to allow to state much about it. To find such results, many more different machines should be included, and then perhaps it would be possible to make meaningful comparisons using per unit values on whether the FRT passes or not to truly identify the trends.

REFERENCES

The European Commission, "Commission Regulation (EU) 2016/631 of 14 April 2016 establishing a network code on requirements for grid connection of generators", Official Journal of the European Union, Brussels, April 2016.

Chown G., Wright J., van Heerden R., Coker M., "System inertia and Rate of Change of Frequency (RoCoF) with increasing non-synchronous renewable energy penetration", 8th CIGRE Southern Africa Regional Conference, Cape Town, Africa, Nov. 2017.

Corà E., "Hydropower Technologies The State-of-the-Art", Hydropower Europe, WP4-DlRp-02, March 2020

Fingrid, "Voimalaitosten järjestelmätekniset vaatimukset VJV2018 ", Nov. 2018.

Freschi F. and Repetto, M., "Natural Choice of Integration Surface for Maxwell Stress Tensor Computation", IEEE Transactions on Magnetics, vol. 49, NO. 5, May. 2013.

Gieras J.F. & Wing M., (1997), *Permanent Magnet Motor Technology – Design and Applications*. New York: Marcel Dekker Inc.

Hydropower Europe (2020), *Hydropower in Europe*. [Online document]. [Accessed 13.5.2020]. Available at https://hydropower-europe.eu/about-hydropower-europe/hydropower-energy/.

IEA (2019), *World Energy Outlook 2019*, IEA, Paris. [Online document]. [Accessed 17.4.2020]. Available at https://www.iea.org/reports/world-energy-outlook-2019.

IEEE (2011), *IEEE Guide for the Application of Turbine Governing Systems for Hydroelectric Generating Units*, IEEE Power & Energy Society, Std 1207TM-2011, New York, June 2011.

Kamiev K., (2013), *Design and testing of an armature-reaction-compensated permanent magnet synchronous generator for island operation*, Acta Universitatis Lappeenrantaensis 539, Diss. Lappeenranta University of Technology ISBN: 978-952-265-485-4.

Kaukonen J., (1999), *Salient Pole Synchronous Machine Modelling in an Industrial Direct Torque Controlled Drive Application*, Acta Universitatis Lappeenrantaensis 77, Diss. Lappeenranta University of Technology ISBN: 951-764-305-5.

Kim J., Wright J., Jo I., Park J., Shin Y., Chung J., "Theoretical method of selecting number of buckets for the design and verification of a Pelton turbine", Journal of Hydraulic Research, Sept. 2017.

Kinnunen J., (2007), *Direct-on-line axial flux permanent magnet synchronous generator static and dynamic performance*, Acta Universitatis Lappeenrantaensis 284, Diss. Lappeenranta University of Technology ISBN: 978-952-214-470-6.

Kirkpatric J., “Hydrogenerator design manual”, Electrical and Mechanical Engineering Division, Bureau of Reclamation Denver Office, Technical report, Denver, Colorado, April 1992.

Korhonen J., (2012), *Active inverter output filtering methods*, Acta Universitatis Lappeenrantaensis 482, Diss. Lappeenranta University of Technology ISBN: 978-952-265-285-0

Koritarov V., Veselka T., Gasper J., Bethke B., Botterud A., Wang,J., Mahalik M., Zhou Z., Milostan C., Feltes J., Kazachkov Y., Guo T., Liu G., Trouille B., Donalek P., King K., Ela E., Kirby B., Krad I. and Gevorgian V., “Modeling and Analysis of Value of Advanced Pumped Storage Hydropower in the United States”, Argonne National Laboratory Report ANL/DIS-14/7, Argonne, Illinois, June 2014.

Krause P., Wasynczuk O., O’Connell T., Hasan M., “Tesla’s Contribution to Electric Machine Analysis”, IEEE Transactions on energy conversion, vol. 32, NO. 2, JUNE 2017.

Neorem magnets Oy, “Datasheet: Neorem 576a”. [Online document]. [Accessed 11.9.2020]. Available at https://neorem.fi/wp-content/uploads/2019/04/hysteresis-graph-576a.pdf

Parviainen A., (2005), *Design of axial-flux permanent-magnet low-speed machines and performance comparison between radial-flux and axial-flux machines*, Acta Universitatis Lappeenrantaensis 209, Diss. Lappeenranta University of Technology ISBN: 952-214-030-9.

Parviainen A., Lindh T., Nerg J., “Direct-On-Line Permanent-Magnet Generators for Small Hydropower”, Proceedings of Hidroenergia, 2010.

Peltoniemi P., “Compensating the rotating mass kinetic energy in grids including high shares of renewable”, 2017 19th European Conference on Power Electronics and Applications (EPE'17 ECCE Europe), Warsaw, Poland, Sept. 2017.

Peltoniemi P., “Grid Connection of Renewable Power Plants”, (2020), Lecture material at LUT at the course Electrical Engineering in Wind and Solar Power Systems.

Pyrhönen J., Jokinen, T. & Hrabovcovà V., (2014), *Design of Rotating Electrical Machines*. Chichester: Wiley. John Wiley & Sons, ISBN: 978-1-118-58157-5.

Rincón R., Pavas A., Mojica-Nava E., “Long-term voltage stability analysis and network topology in power systems”, 2016 IEEE PES Innovative Smart Grid Technologies Conference Europe (ISGT-Europe), Ljubljana, 2016, pp. 1-6, doi: 10.1109/ISGTEurope.2016.7856237.

Saarakkala S., Hinkkanen M., “Identification of Two-Mass Mechanical Systems Using Torque Excitation: Design and Experimental Evaluation”, IEEE Transactions on industry applications, vol. 51, NO. 5, Oct. 2015.

Wu D., Zhu Z., “Design Tradeoff Between Cogging Torque and Torque Ripple in Fractional Slot Surface-Mounted Permanent Magnet Machines”, IEEE Transactions on Magnetics, vol. 51, NO. 11, Nov. 2015.

Woodson H. and Melcher J. Electromechanical Dynamics. 3 vols. (Massachusetts Institute of Technology: MIT OpenCourseWare). http://ocw.mit.edu [Accessed 29.5.2020]. Jan. 1968. License: Creative Commons Attribution-NonCommercial-Share Alike.

Zaidi A. and Cheng Q., “An Approximation Solution of the Swing Equation Using Particle Swarm Optimization”, 2018 IEEE Conference on Technologies for Sustainability (Sus-Tech), Long Beach, CA, USA, March. 2018.

Appendix 1. Main parts of the simulation model

The main parts of the model are shown in Figures 1. and 2. Data logging and monitoring blocks are not shown for better clarity. Parameter initialization, data processing and the commands for looped simulations are done in a Matlab®-script. In specific long looped simulations to increase performance, it is worth removing all the functionalities that are not absolutely necessary.

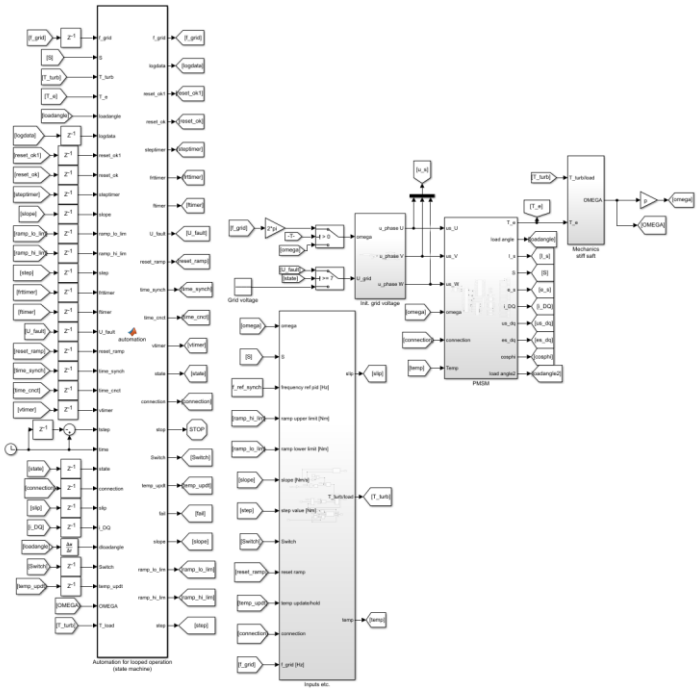

Figure 1. Main view.

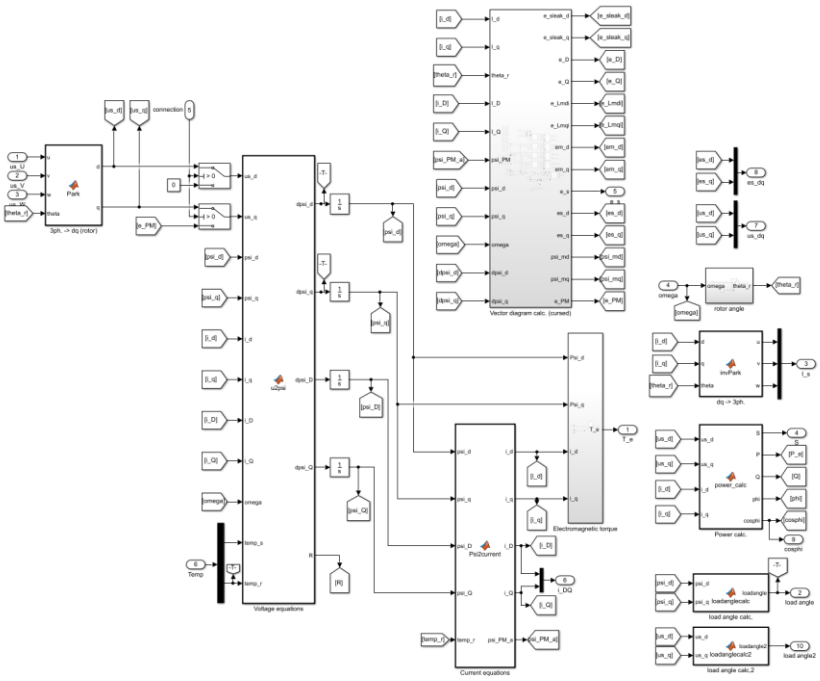

Figure 2. Inside of the PMSM block

Appendix 2. Bracketing routine used in a simulation

The bracketing routine used to find the maximum value for the fault profile time parameter scaling factor is shown in Figure 1. The factor was introduced as a type of performance metric in a fault-ride-through simulation. The method is simple and reliable, but of course time consuming.

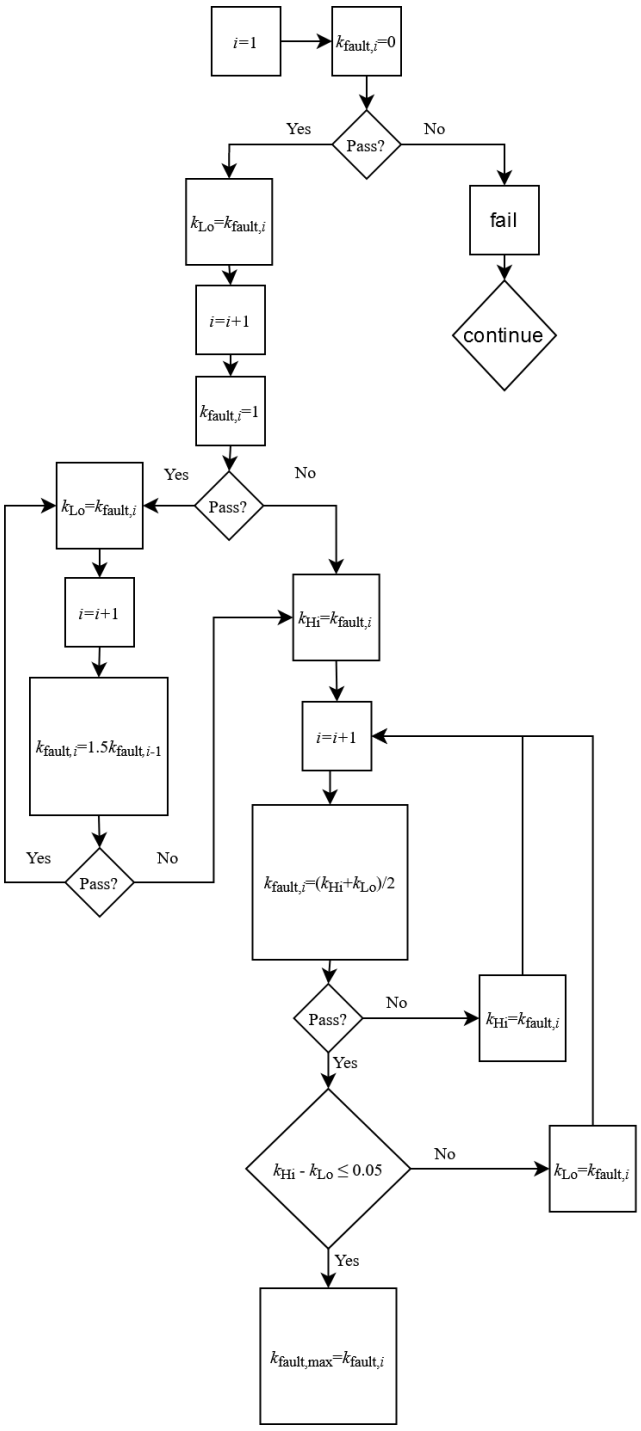

Figure 1. The bracketing routine.